IMPROVEMENTS IN PROCESSING AND STRETCHABILITY OF SUPER GAS BARRIER MULTILAYER THIN FILMS

A Dissertation

by

FANGMING XIANG

Submitted to the Office of Graduate and Professional Studies of
Texas A&M University
in partial fulfillment of the requirements for the degree of

DOCTOR OF PHILOSOPHY

Chair of Committee,	Jaime C. Grunlan
Committee Members,	Hong Liang
	Jodie Lutkenhaus
	Xinghang Zhang
Head of Department,	Andreas A. Polycarpou

May 2015

Major Subject: Mechanical Engineering

ABSTRACT

Polymeric materials with gas barrier equivalent to metalized plastics have become increasingly important for food packaging, electronic device encapsulation, and vacuum insulation. Early attempts to develop alternative gas barrier materials have focused on thick (>10 μm) polymer/clay composites produced using physical mixing, but only limited improvement was achieved due to aggregation and random orientation of clay platelets. Layer-by-layer (LbL) assembly is a simple yet powerful bottom-up fabrication technique, which allows assembly of thin films with designed microstructure under ambient conditions. These multilayer thin films have many desirable properties: mechanical flexibility, transparency, and impermeability. This dissertation sought to further improve the processing and properties of high gas barrier thin films produced using LbL assembly.

The influence of deposition time on gas barrier of polymer/clay multilayer thin films composed of polyethylenimine (PEI), poly(acrylic acid) (PAA), and clay was investigated. Multilple PEI/PAA bilayers (BL) were deposited between clay layers to construct multilayer assemblies with quadlayer (QL), hexalayer (HL), and octalayer (OL) sequences. Regardless of film structure, polymer/clay multilayer thin films prepared using shorter dipping time were thicker and exhibited better gas barrier than samples prepared using longer dipping time in the first few layers. This seemingly counterintuitive result was explained by considering desorption of previously deposited

polymers between clay layers. Reduced deposition time helped to retain more polymer between clay sheets, leading to larger clay spacing and better gas barrier.

In an effort to expand the applications and improve the throughput of layer-by-layer assembly, spray-assisted deposition of PEI/PAA bilayers was investigated. The influences of spraying time, spraying pressure, and flow rate on thickness, roughness, and gas barrier were evaluated. Spraying time was determined to be the most important parameter. A 7-bilayer PEI/PAA thin film assembled using optimized spraying parameters exhibited better gas barrier than a dip-coated multilayer prepared using the same deposition time for each layer. These findings pave the way for using the LbL technique commercially, where fast and continuous deposition of high performance thin films on large substrates is needed.

Finally, the first example of super stretchy gas barrier was developed by combining polyacrylic acid and poly(ethylene oxide) (PEO). Oxygen transmission rate (OTR) of 1.58 mm thick natural rubber was reduced by an order of magnitude after deposition of a 20 BL PAA/PEO assembly. More importantly, no cracking was observed on the PAA/PEO coating after 100% strain. A 5X improvement in gas barrier was retained after this extreme stretching. Additionally, the effect of assembling condition on the permeability of PAA/PEO multilayer thin films was investigated. By setting the assembling pH at 2.75, the negative impacts of PAA ionization and COOH dimer formation could be minimized, leading to a 50% reduction in oxygen permeability. This unique combination of elasticity and gas barrier makes the PAA/PEO assembly an ideal candidate for improving the barrier of elastomeric materials.

DEDICATION

I dedicate this dissertation to my wife, dad, mom, grandpa, and grandma. Thank you for keeping me happy and motivated throughout my graduate study.

ACKNOWLEDGEMENTS

First and foremost, I would like to express my gratitude to my advisor, Dr. Jaime Grunlan, for his academic guidance, financial support, and enthusiastic encouragement throughout this research. I feel truly privileged to work in this great research group. I would like to thank my committee members, Dr. Hong Liang, Dr. Jodie Lutkenhaus, Dr. Xinghang Zhang for taking time out of their busy schedules to serve on my Ph.D. committee and for their valuable suggestions. I appreciate the assistance of Dr. Micah Green, and Dr. Oren Regev (of Ben-Gurion University of the Negev) for their investment in my research.

I would like to thank the group members of the Polymer NanoComposites Lab for being great friends and coworkers. The help of my outstanding undergraduate assistants, Justin Sawyer, Sarah Ward, and Tara Givens, is highly appreciated. Thanks also go to former and current graduate students of the Polymer Nanocomposites Lab, Dr. You-Hao Yang, Dr. Galina Laufer, Dr. Gregory Moriarty, Bart Stevens, Ping Tzeng, David Hagen, Kevin Holder, Tyler Guin, Blake Teipel, Merid Haile, Yixuan Song, Ryan Smith, Morgan Plummer, Taylor Smith, Dr. Marcus Leistner, Dr. Chungyeon Cho, and Dr. Debabrata Patra. A special thanks to Dr. Morgan Priolo for being a great mentor.

Thanks also go to my friends and colleagues and the department faculty and staff for making my time at Texas A&M University a great experience. Hanging out with Joseph Sargent and Pingjia Ming was the best pastime that I had in College Station. Additionally, I want to thank Dorsa Parviz for being a great collaborator, Dr.

Mohammad Naraghi for teaching the most interesting course, and Dr. Wilson Serem (of the Materials Characterization Facility at Texas A&M University) for AFM measurement.

Finally, thanks to my dad, mom, grandpa, and grandma for their encouragement and to my wife for her patience and love.

NOMENCLATURE

AFM	Atomic Force Microscopy
ASTM	American Society for Testing and Materials
BL	Bilayer
EVOH	Ethylene Vinyl Alcohol
HL	Hexalayer
H-Bond	Hydrogen Bonding
LAP	Laponite
LbL	Layer-by-Layer
MMT	Montmorillonite
OTR	Oxygen Transmission Rate
OL	Octalayer
PAA	Poly(acrylic acid)
PAAM	Polyacrylamide
PAH	Poly(allyl amine hydrochloride)
PANI	Polyaniline
PDAD	Poly(diallyldimethylammonium)
PECVD	Plasma-Enhanced Chemical Vapor Deposition
PEI	Branched Polyethylenimine
PEO	Poly(ethylene oxide)
PET	Poly(ethylene terephthalate)

PHEA	Poly(2-hydroxyethyl acrylate)
PMAA	Poly(methacrylic acid)
PNIPAAM	Poly(N-isopropyl acrylamide)
PP	Polypropylene
PSS	Poly(styrene sulfonate)
PVCL	Poly(N-vinylcaprolactam)
PVD	Physical Vapor Deposition
PVME	Poly(vinyl methyl ether)
PVP	Polyvinylpyrrolidone
QCM	Quartz Crystal Microbalance
QL	Quadlayer
RH	Relative Humidity
SEM	Scanning Electron Microscopy
TEM	Transmission Electron Microscopy
VMT	Vermiculite

TABLE OF CONTENTS

Page

LIST OF FIGURES

FIGURE Page

FIGURE Page

FIGURE Page

FIGURE Page

FIGURE Page

FIGURE Page

LIST OF TABLES

TABLE Page

CHAPTER I

INTRODUCTION

1.1 Background

Gas barrier materials are widely used in multiple applications, such as food packaging, photovoltaic device encapsulation, vacuum insulation, and organic light emitting diode protection.[1-3] Food packaging is of one of the most important applications, not only due to the amount of gas barrier material consumed but because of the number of consumers that are affected. Among the numerous options for food packing, polymers are the most commonly used due to light weight, low cost, and ease of processing.[1] Despite being advantageous in these aforementioned aspects, the application of polymer-based packaging materials is limited by their relatively low gas barrier.[4] Many studies have been conducted to improve the gas barrier of polymeric material through filler incorporation or thin film deposition. Filler incorporation involves adding another component with better gas barrier into the original polymer matrix.[5-8] The most popular fillers are clay platelets, which are ~1 nm thick disc-shaped nanoparticles with aspect ratios up to several thousands.[9] In order to fully utilize the gas barrier of clay platelets, these gas impermeable fillers need to be fully exfoliated and aligned perpendicular to the diffusion direction.[10] These aligned platelets can effectively reduce gas permeation by forcing gas molecules to travel along a zigzag shaped diffusion path. Theoretical calculations suggest an extended diffusion path, consisting of parallel clay platelets, can lead to several orders of magnitude reduction in gas

permeation.[10] Until recently, this potential was never realized in conventional polymer composites due to aggregation and random orientation of platelets.[5, 11-12] Moreover, polymer/clay composites prepared using mechanical mixing usually leads to undesirable changes in optical (opaqueness) and mechanical (stiffening) properties,[13-15] leaving these materials deficient for many applications. Optical and/or mechanical properties of polymer substrates can be left almost intact with thin film deposition.[16] This surface coating technique involves deposition of metal, or metal-oxide (such as SiO_x, or Al_yO_z), or a combination of polymer and metal-oxide layers.[3] Despite showing exceptional gas barrier, these thin films require complicated and expensive fabrication processes. Alternatively, layer-by-layer (LbL) assembly technique has shown numerous advantages over all of the above mentioned gas barrier technologies.

Layer-by-layer assembly uses the complementary interactions between species to deposit materials one layer at a time.[17-19] A typical multilayer thin film, constructed through alternate deposition of positively (polycations) and negatively-charged polyelectrolytes (polyanions), is shown in Figure 1. 1. In this process, a negatively-charged substrate is initially dipped into a solution with polycations, which are deposited through electrostatic attractions. This substrate is then taken out of the solution, rinsed with water to remove excess material, and then dried with air. Since polycations have multiple positive charges along their loopy backbones, not all of the charges are coupled with negative charges on the substrate, leaving unbounded charge on the surface.[20] These excess positive charge reverses the total surface charge, allowing this substrate to be electrostatically bound with negatively charge of the polyanion in the following

deposition step. This phenomenon, where the surface charge is reversed at the end of a deposition step, is essential for all electrostatically bonded layer-by-layer assembly (known as "charge over-compensation").[18] Each cationic and anionic pair shown in the schematic of a typical multilayer assembly (Figure 1.1b) is called as a bilayer (BL). This alternative deposition procedure can be repeated many times until the desired number of bilayers is reached. Similar to SiO_x deposition, layer-by-layer assembled multilayers do alter the optical and mechanical properties of the underlying polymer substrate. Moreover, the LbL technique provides several other advantages over traditional surface deposition techniques.

Layer-by-layer assembly is highly versatile. Any components with complementary interactions (such as electrostatic bonding,[17, 21] hydrogen bonding,[22-23] hydrophobic interaction,[24] charge-transfer interaction[25-26]) can be used for alternating deposition. The wide selection of usable components allows numerous desirable properties to be imparted to the final assembly. For example, by using non-metallic components, such as polymer and clay, a transparent and microwavable gas barrier assembly can be obtained.[27] Another example involves pH-sensitive multilayer assemblies that are fabricated using poly(acrylic acid).[28] An electrochromic multilayer assembly has been produced, utilizing the redox property of polyaniline.[29] In addition to versatility, LbL assembly is also very simple. Most LbL assemblies are deposited with water-based solutions under ambient condition.[30-32] Most importantly, LbL assembly is a bottom-up approach, which allows precise control of nanoscale film structure.[33] It is for

these reasons that multifunctional LbL assemblies, with well controlled morphology, can be obtained.[34]

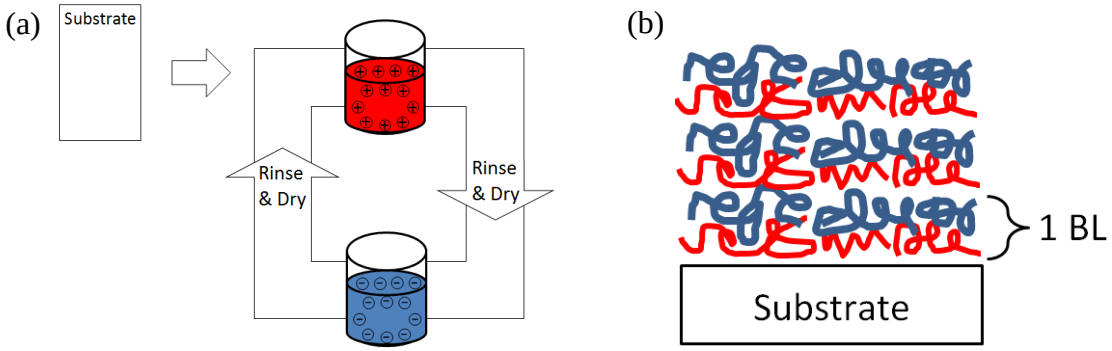

Figure 1.1. Schematic of the layer-by-layer assembly processes, using positively-charged (red) and negatively-charged (blue) polyelectrolytes (a). An over-simplified schematic illustration of the resulting multilayer thin film is also shown (b).

1.2 Objectives and Dissertation Outline

Layer-by-layer assembled multilayer thin films have been shown to exhibit exceptional gas barrier,[16] unmatched by other commercially available gas barrier thin films (e.g. ethylene vinyl alcohol [EVOH] and SiO_x).[35] This bottom-up technique allows single clay nanoplatelets to be deposited in a highly oriented manner. The resultanting structure, with parallel clay alignment, can dramatically diminish gas permeation by extending the diffusion path of gas molecules.[36] Equally remarkable improvement in gas barrier can be achieved without using impermeable clay platelets.[37] The gas barrier of all-polymer LbL assemblies originates from the numerous electrostatic crosslinks between oppositely charged polyelectrolytes, which densifies polymer chains to suppress gas diffusion.[37] Despite showing great potential, LbL assembly has not widely been used

in commercial scale manufacturing, largely due to the relatively slow deposition process. In an effort to make this powerful technology more commercially appealing, the influence of various deposition parameters (time, flow rate, pressure, etc.) on gas barrier of LbL assemblies have been studied. Super stretchy gas barrier multilayer thin films further extend the application of LbL assembly to elastic substrates.

Chapter II provides a brief review of conventional gas barrier techniques and layer-by-layer assembly. The first part describes the gas barrier of polymer composites, including all-polymer blends and polymer/platelet composites. The second part reviews existing surface deposition techniques, such as metal or metal-oxide thin film coatings, fabricated using physical vapor deposition. The third part of this chapter covers the basics of LbL assembly, with special emphasis given to electrostatically bonded assembly, spray-assisted deposition, and hydrogen-bonded LbL assembly.

Chapter III examines the influence of deposition time on gas barrier of multilayer thin films composed of polyethylenimine (PEI), poly(acrylic acid) (PAA), and clay. Shorter dipping time was found to result in thicker polymer/clay multilayer assemblies with better gas barrier (for the first few layers). This seemingly counterintuitive finding is explained using the unique growth mechanism of the polymer segment (PEI/PAA bilayers) between clay layers. The reduced deposition time suppresses desorption of previously deposited polyelectrolytes, leading to more material retention and larger clay spacing. This more open structure allows gas molecules to travel perpendicularly to the diffusion direction between clay layers, further elongating the diffusion path. The

universality of this method is further confirmed by the use of different film compositions and different clay types.

Chapter IV investigates spray-assisted assembly as a means to fabricate PEI/PAA multilayer thin films with super gas barrier. Thickness, roughness, and gas barrier were evaluated with varying spraying time, spraying pressure, and flow rates. A film coated using optimized spraying parameters was compared with a dip-coated sample prepared using the same deposition times. Surprisingly, the spray-coated sample had larger film thickness and better gas barrier, which originated from the enhanced material retention through expedited evaporation and rapid drainage of excess polymer solution.

Chapter V describes a super stretchy gas barrier multilayer assembly. Hydrogen bond donating PAA and hydrogen bond accepting poly(ethylene oxide) (PEO) were alternately deposited on natural rubber. A 20 BL, 367-nm thick PAA/PEO coating was found to reduce the OTR of a 1.58 mm thick natural rubber sheet by one order of magnitude. More interestingly, a 5X improvement in gas barrier was retained after 100% strain. This ability to maintain gas barrier after stretching is explained with the help of scanning electron microscope (SEM) images, which show evenly distributed plastic deformation instead of cracking. A conceptual model is provided to correlate the changes in surface morphology and gas barrier of stretched samples.

Chapter VI provides some conclusions for this work and points out opportunity for future research. This dissertation investigated the influence of processing conditions, including LbL deposition time and technique, on the gas barrier of multilayer thin films. Additionally, a new super stretchy gas barrier assembly was developed. The structure-

property relationships revealed in these studies will be of great value to current and future researchers. In an effort to utilize the excellent gas barrier of graphene sheets, layer-by-layer assembly of stabilized graphene will be investigated. The utility of stretchy gas barrier will be improved if cyclic stretching can be endured. A new recipe that shows no sign of plastic deformation with stretching will be needed. The possibility of using electrostatically bonded stretchy multilayer thin film as polymer electrolyte will also be verified.

CHAPTER II

LITERATURE REVIEW

Gas barrier materials can be used for multiple applications, such as food packaging, liquid crystal display and photovoltaic module encapsulation, vacuum insulating, and organic light emitting diode protection, as shown in Figure 2.1.[3] The development of new gas barrier materials for food packaging is very important, because the only way to feed more population with less land is to reduce food waste. Even in the United States, which employs modern farming, transportation, and storage techniques, it is estimated that up to 40 percent of the food produced is wasted every year.[38] The most effective method to reduce food waste is to cook/process fresh produce and then encapsulate with packaging before selling to consumers. Traditionally, glass and metal were used as the gas barrier for food packaging due to their exceptional gas barrier properties, but they are relatively heavy and expensive, making them less appealing to the modern food industry that wants to reduce shipping and manufacturing cost. In contrast, polymers are better suited for modern packaging needs due to light weight, low cost, ease of processing and formability.[1] Pure polymers, such as polyethylene terephthalate (PET) and polypropylene (PP), are widely used to make soft drink bottles and milk jugs, but their barrier does not meet the standards for other important applications, such as alcoholic beverages.[2] In an effort to expand the application of polymeric packaging materials, high-barrier fillers are often added to a polymer matrix to improve properties (see Section 2.1).[5, 39-40] Unfortunately, only limited improvement

in gas barrier has been achieved using this approach due to aggregation and random alignment of fillers. Furthermore, the incorporation of fillers usually leads to corresponding changes in optical and/or mechanical behavior, rendering these composites unsuitable for certain applications. The need to obtain materials with well-controlled structure, and to maintain the desirable properties of the polymer substrates, has driven research toward thin film deposition technologies. Various thin film deposition techniques are described in Section 2.2.[3, 41-42] Despite showing good gas barrier properties, these techniques often require vacuum environments and involve complex fabrication procedures, making industrial use of these technologies very difficult. A simple surface coating technique that is capable of controlling microstructure in order to improve gas barrier is highly desirable. Layer-by-layer assembly is the technology for this purpose, as described in Section 2.3. The combination of versatility and high performance makes LbL assembly ideal for super gas barrier thin film fabrication.

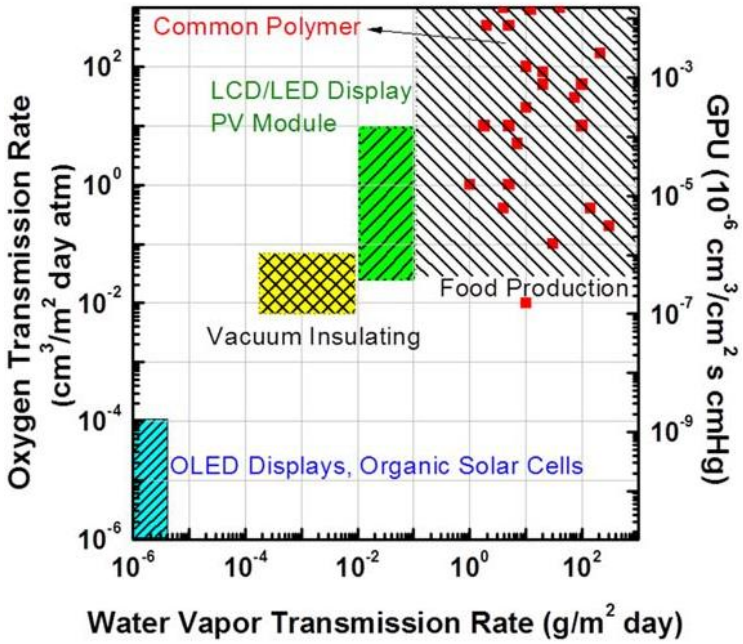

Figure 2.1. OTR, water vapor transmission rate (WVTR), and of conventional polymeric barrier films and the requirements for various applications. (1 GPU (gas permeation unit) = 10^{-6} cm^3 (STP) cm^{-2} s^{-1} $cmHg^{-1}$).[43]

2.1 Polymer Composites

2.1.1 Polymer Blends

The difference between oxygen permeability of dissimilar polymers can be as high as six orders of magnitude.[44] One of the simplest methods used to improve the gas barrier of a permeable polymer is to add another polymer with better gas barrier.[6] The resulting mixtures are usually immiscible due to the different chemical structures of these components, with the added polymer usually existing as a dispersed phase.[45] Gas molecules is more likely to diffuse within the more permeable polymer matrix instead of the less permeable dispersed domains, so gas permeation can be suppressed by increasing the tortuosity of the diffusion path,[46] as shown in Figure 2.2. It can be seen

that the permeability of the polymer blends decreases with increasing aspect ratio of dispersed domains, which correlate well with experimental observation. For polymer blends, there are two possible methods to obtain an elongated disperse phase.[39]

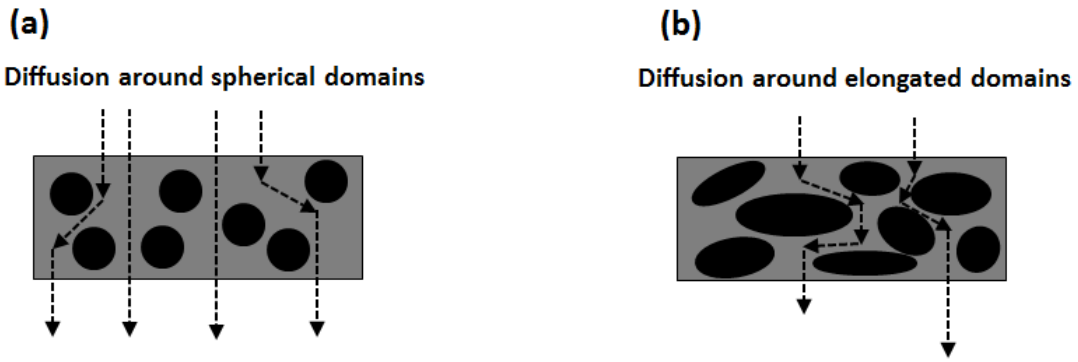

Figure 2.2. Diffusion of gas molecule through polymer blends with spherical (a) and elongated (b) dispersed domains.

The first method involves post-mix drawing. The dispersed phase most often exists as spherical domains to minimize interfacial interactions.[45] Stretching the polymer blend at elevated temperature elongates the dispersion, creating high aspect ratio domains perpendicular to the direction of permeation. As can be seen in Figure 2.3a, EVOH exists as spherical dispersed phase within a PP matrix before stretching.[47] These spherical domains transform into an elliptical shape after drawing, and their aspect ratio can be increased with greater draw ratio. A relationship can be established between drawing and gas barrier, with the largest draw ratio leading to the largest reduction in permeability, as shown in Figure 2.4d.

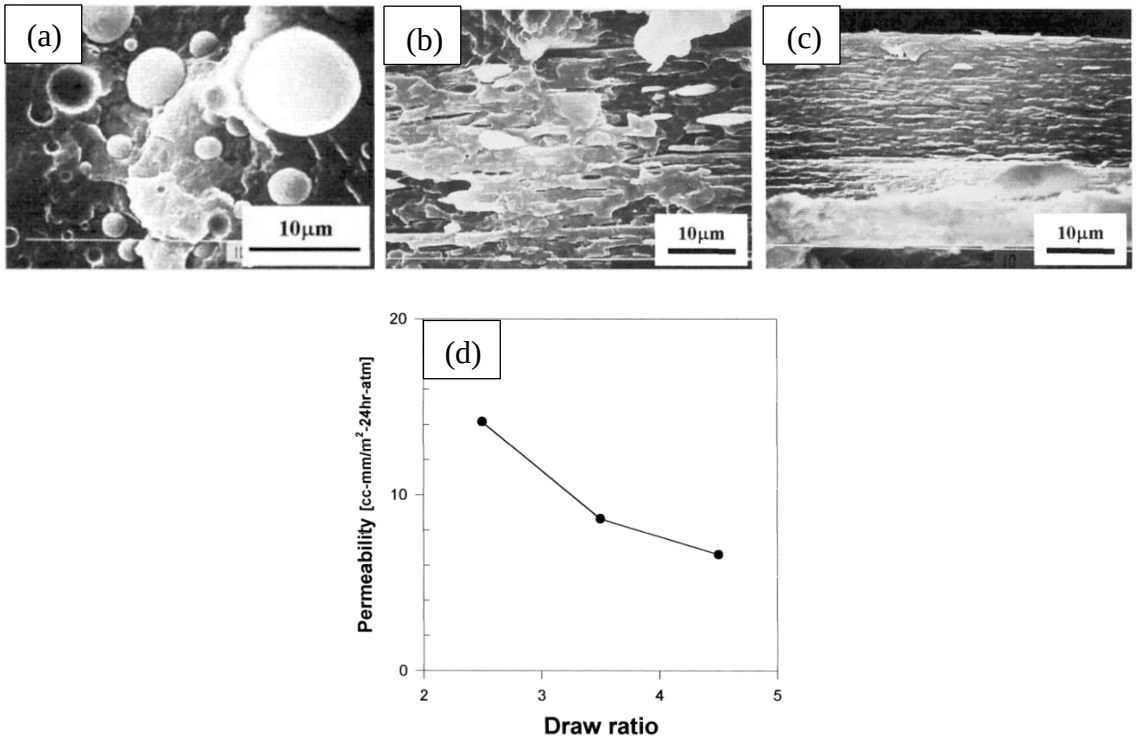

Figure 2.3. Morphology (a, b, c) and permeability (d) of PP/EVOH blends with different draw ratios: 0 (a), 2.5 × 2.5 (b), and 4.5 × 4.5 (c).[47]

Besides post-mix drawing, layer-multiplying coextrusion can also be used to improve gas barrier of polymer blends. When a crystalline or semi-crystalline polymer crystallizes in a confined two-dimensional space, they can form impermeable single crystals that greatly enhance the gas barrier of the polymer blend. The ability of semi-crystalline PEO to improve gas barrier was studied using multilayer polymer blends of poly(ethylene-co-acrylic acid) EAA and PEO.[48] The thickness of the PEO layer was reduced by repeating the coextrusion process. For an EAA/PEO film with 90/10 composition, the nominal PEO layer thickness was reduced to 20 nm after ten repeating coextrusions. As can be seen in Figure 2.4a, PEO layers crystallized as a single crystal

within the nanolayers. These impermeable PEO two-dimensional single crystals increase the diffusion path of gas molecules, leading to improved gas barrier, as shown in Figure 2.4b.

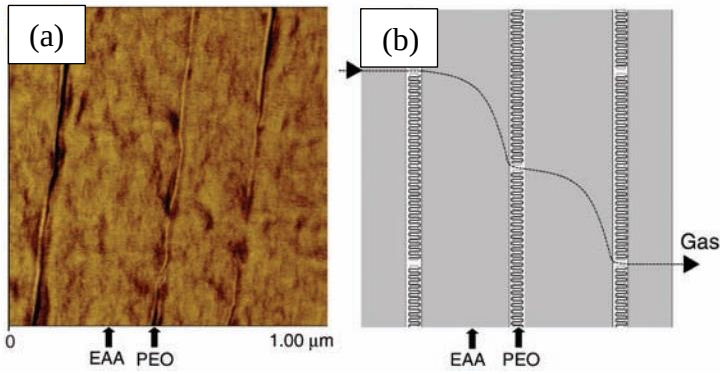

Figure 2.4. A high-resolution image showing PEO layers crystallized as single, large lamellae in a coextruded EAA/PEO assembly with 1025 alternating layers (a). A schematic showing the gas diffusion pathway within this assembly (b).[48]

Despite showing some positive results, polymer blends fails to receive as much attention as polymer/clay composites in the gas barrier community,[7, 46, 49-50] because clay platelets are more impermeable and less expensive than polymer fillers. Clay platelets also have very high aspect ratio (up to several thousands), thus eliminating the need to increase filler aspect ratio through post-mix elongation. It should be noted that other disc-shaped fillers, such as graphene/graphene oxide or boron nitride sheets can also be used as gas barrier filler.[51]

2.1.2 Polymer/Platelet Composites

Unlike polymer blends, the dispersion and exfoliation of inorganic clay platelets within a polymer matrix is very difficult.[52-54] One of the most common methods to improve the affinity between polymer and clay is by modifying the clay surface with organic cations (typically quaternary alkylammonium ions) to prepare "organoclay".[55] These modified clay platelets can be fully exfoliated and distribute homogeneously within polymer matrix due to enhanced affinity and the intense shear force within twin screw extruder.[13] The exfoliation of organoclay involves three major steps: organoclay particle breakup, clay tactoid breakup, and platelet exfoliation (Fig. 2.5a-c). A transmission electron microscope (TEM) image of a typical nylon 6/organoclay nanocomposite (Fig. 2.5d) shows that organoclay can be exfoliated as single platelets and dispersed evenly within the polymer matrix.

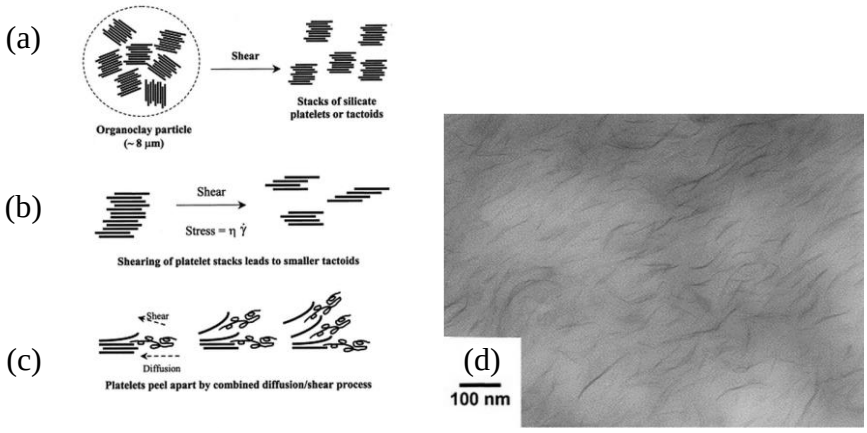

Figure 2.5. Stepwise mechanism of clay exfoliation in the melt compounding of polymer/organoclay nanocomposites (a-c). TEM image of a typical nylon 6/organoclay nanocomposite (d).[13]

Although clay platelets are virtually impermeable to any gas, the addition of clay in polymer composites only leads to marginal improvement in gas barrier due to random alignment of exfoliated clay.[5, 11-12] In order to fully realize the potential of clay as gas barrier filler, clay platelets need to be aligned perpendicular to the diffusion direction, forcing permeating gas molecules to travel between the impermeable clay platelets, as shown in Figure 2.6.[10, 46]

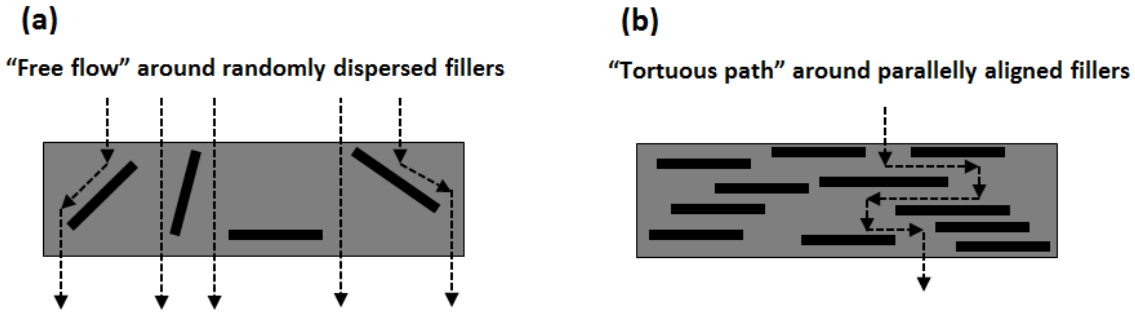

Figure 2.6. Diffusion of gas molecule through polymer composites with randomly aligned fillers (a), and parallel fillers (b). Dashed lines indicate the diffusion paths.

The alignment of clay is very difficult to control during the melt-blending process, due to the Brownian motion of clay platelets within molten polymer, but there are other options to improve the alignment of filler within polymer matrix. When plate-like zirconium phosphate (ZrP) nanoplatelets are mixed with epoxy, the level of filler alignment increases with filler concentration, as shown in Figure 2.7.[56] At low concentration, the nanoplatelets are randomly aligned due to Brownian motion of these particles. As filler concentration increases, the neighboring blocks will begin to repel each other and consequently assemble in an orderly fashion to minimize the total free

energy of the composite. The parallel packing of the nanoplatelets is accompanied by good transparency. This nanocomposite also exhibits a shear-thinning behavior, which lower energy for processing. Unfortunately, the ZrP platelets need to be dispersed in acetone, making the dispersion process more complicated and dangerous than water-based dispersion of clay platelets. Furthermore, this technology is only successful in epoxy, which is too rigid and brittle to be used for food packaging. In order to overcome the aforementioned disadvantages of these polymer composites, thin film deposition approach has been employed to improve the gas barrier of polymer substrates.

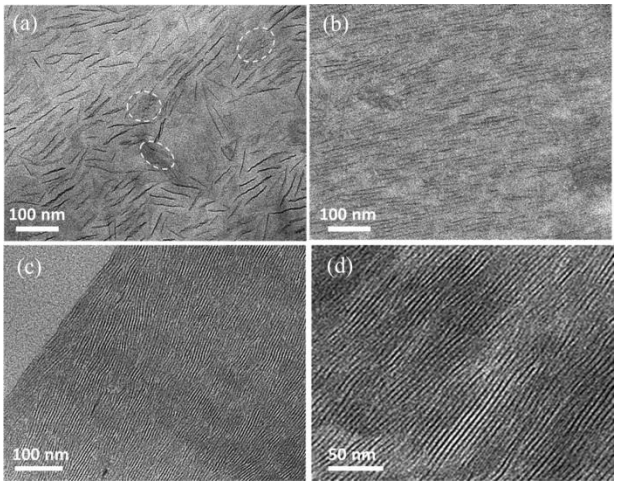

Figure 2.7. TEM images of epoxy/zirconium phosphate (ZrP) nanocomposites with various ZrP concentrations: (a) 1.7, (b) 3.4, and (c, d) 8.2 vol %.[56]

2.2 Thin Film Gas Barrier

2.2.1 Thin Metal Films

Metallic thin films can be deposited on various non-metallic substrates. The earliest example of this technique involved coating a glass surface with metallic silver to produce a mirror.[26] This technique has evolved since its debut in 1835.[14] Nowadays, the most commonly used thin metal deposition method is vacuum metallizing.[57] This technique involves heating a metal to its boiling point, and then immediately vaporizing the liquid metal. Upon condensation, a thin layer of metal (about 10-100 nm) can be deposited on polymeric substrates. This approach is highly effective with, a very thin layer of metal reducing the permeability relative to the polymer substrate by three orders of magnitude.[58] Metalized plastics are widely used in food packaging, electronics encapsulation, and decorative coating.[42] Despite being highly effective in improving gas barrier, the application of metalized plastics is restricted by some inherent drawbacks, such as microvavability, opaqueness, and recyclability. In an effort to overcome these issues, thin metal-oxide coatings have been introduced.

2.2.2 Thin Metal-Oxide Films

Metal-oxide thin films were initially developed for their exceptional dielectric properties,[59] only later being used for gas barrier applications.[60-62] These films are commonly produced using plasma-enhanced chemical vapor deposition (PECVD) or physical vapor deposition (PVD).[2] Metal-oxide coated polymers can be used as alternatives to metalized plastics due to water-repellancy, retortablility,

microwaveablility and gas barrier.[2] These desirable properties also make these films very effective for protecting food from moisture ingress or aroma loss.

It is interesting to note that although bulk metal-oxides (SiO_x or Al_yO_z) are virtually impermeable to any gas due to their high density, thin film gas barrier is significantly compromised. Only 1 to 3 orders of magnitude reduction in OTR can be achieved by metal-oxide thin film deposition, regardless of the type of polymer substrate. This level of improvement in gas barrier is very similar to that of metallic thin films. Further characterization reveals that the formation of defects (e.g. pinholes) during PVD process prevents both metallic and metal-oxide thin films from realizing their full gas barrier potential. As shown in Figure 2.8, the increase in defect density scales logarithmically with the OTR of coated PET films.[63] Increasing the thickness of the coating can help to improve gas barrier, but the increase of processing time and cost makes this impractical. Alternatively, the concept of multilayers is employed.

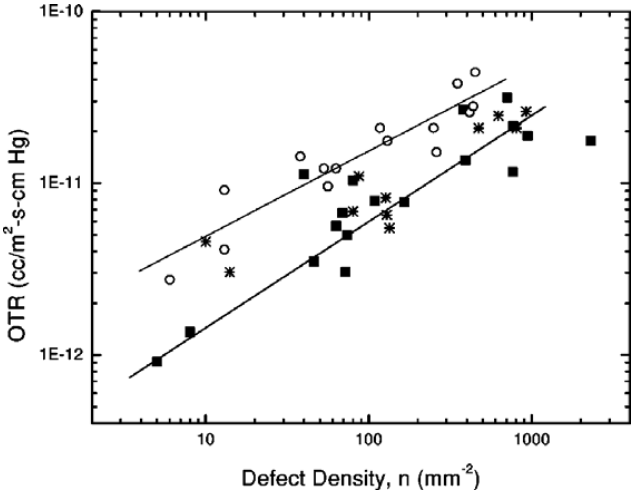

Figure 2.8. Oxygen transmission rate as a function of defect density for Al (○), SiO_x (*), and SiN (■) coated PET films.[63]

2.2.3 Super Gas Barrier Multilayers

Due to the presence of defects, single layer metal-oxide deposition only leads to limited enhancement in gas barrier. In an effort to produce transparent barrier films that meet the requirements of flexible organic light-emitting diodes (OLED), a multilayed structure was prepared.[35] An example of this approach is a thin film produced using Vitex technology,[64] which has alternating layers of Al_2O_3 and polyacrylate, shown in Figure 2.9. Within this multilayer structure, polyacrylate layers act as a binder to smooth surface, reduce mechanical damage, and increase thermal stability of the nucleation surface. The high density Al_2O_3 layers provide the gas barrier. Defects in each Al_2O_3 layer become decoupled if enough alternating Al_2O_3 layers are deposited, thereby suppressing the negative impact of pinholes. When the thickness of the organic layer is reduced to the same average size of pinholes in the inorganic layer, significantly improved gas barrier can be achieved due to the formation of a tortuous diffusion path. These multilayer thin films feature exceptional water vapor barrier, with WVTR as low as 10^{-6} g/m^2/day, matching the requirement for OLED. Even though Vitex multilayer shows great potential due to its exceptional barrier and flexibility, its manufacturability remains questionable.[3] An alternative method to fabricate multilayer structures is through layer-by-layer assembly, which is the focus of this dissertation.

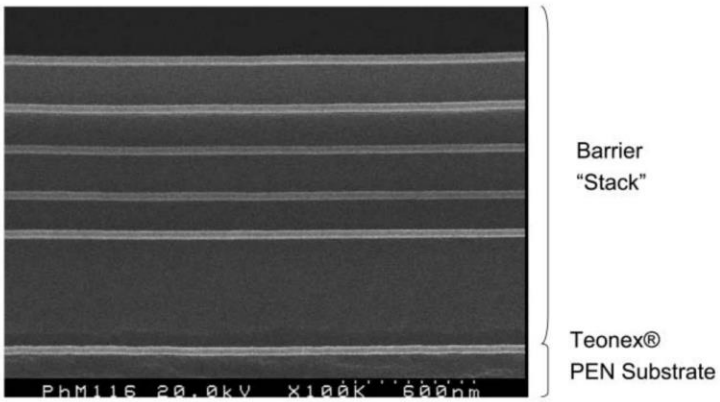

Figure 2.9. A schematic illustration and corresponding cross-sectional image of a multilayer thin film produced using Vitex technology. [7]

2.3 Layer-by-Layer Assembly

Layer-by-layer assembly is a simple (ambient deposition using aqueous solutions) yet powerful (super gas barrier, fire retardant, etc.) method that utilizes the complementary interactions between species to deposit material one nanolayer at a time.[16] LbL deposition technique was developed nearly 50 years ago, when Iler showed that positively charged bohemite fibrils and negatively charged colloidal silica could be layered step-by-step to build thin films, as shown in Figure 2.10.[20, 65] Based on this discovery, Iler further proposed that a wide range of charged materials could be incorporated like this, as long as the charge reversal was satisfied after each deposition step. The importance of this discovery was left unrecognized until 1991, when Hong and Decher made the first polyelectrolyte multilayer using oppositely charged polymers.[17] A later discovery by Decher and coworkers showed the stratified structure of poly(styrene sulfonate) (PSS)/poly(allylamine hydrochloride) (PAH) multilayers (Fig. 2.11), proving

for the first time that layer-by-layer assembly could be used to control film architectures at nanoscale.[66]

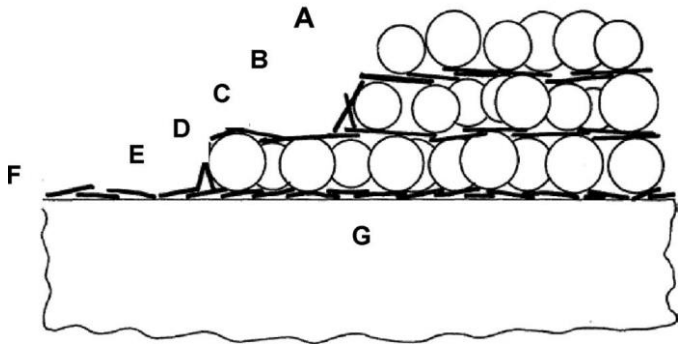

Figure 2.10. Schematic of a multilayer thin film composed of silica particles (A, C, and E) and boehmite fibrils (B, D, F) on a silica substrate (G).[65]

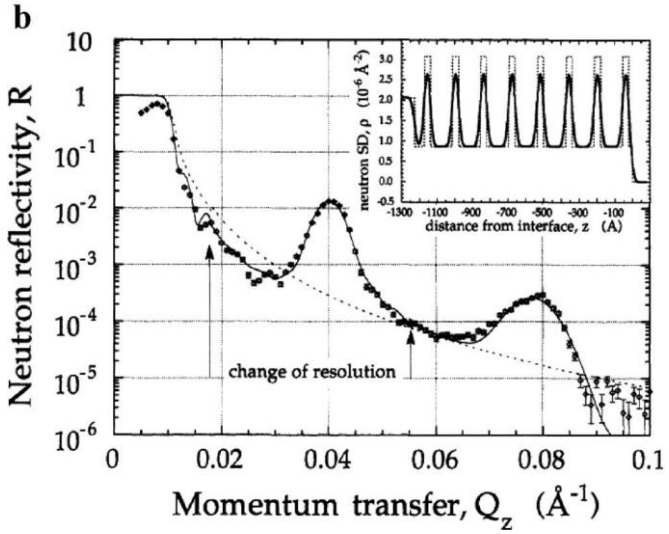

Figure 2.11. Neutron reflectivity as a function of the momentum transfer for PAH/PSS multilayer. The insert represents the deuterium profile of the film that is calculated from the neutron reflectivity curve.[66]

Most LbL assemblies are made following the schematic shown in Figure 1.1. A negatively charged substrate is initially dipped into a solution of positively charged material for a given amount of time (from a few seconds to tens of minutes).[67-68] With the first layer deposited, the surface charge is reversed due to over compensation of charge. This positively charged substrate is then rinsed with deionized water to remove loosely bound material, and then immersed into another solution with negatively charged materials. Every deposited cationic and anionic pair is known as a bilayer, and this assembling procedure can be repeated as many times as needed to obtain a thin film with many layers. Although the assembling scheme is highly similar among different multilayer thin films, the resultant films are highly tailorable due to the multiple assembling techniques, components, and interactions that are available. The diversity of LbL assembly enables it to be used for applications, such as antimicrobial,[69-70] drug delivery,[71-73] gas barrier,[74-76] and flame retardant.[77-79]

2.3.1 Electrostatic Layer-by-Layer Assembly

As mentioned earlier, multiple interactions can be used to fabricate multilayer thin films, such as electrostatic,[80] hydrophobic interaction,[24] hydrogen bonding,[81] charge-transfer,[25] host-guest interaction,[82] coordination chemistry,[83] and covalent bonding.[84] Electrostatic interaction is the most common, because it is the first and is by far the most explored assembly mechanism.[85] Electrostatically bonded LbL films were successfully used in many applications, such as gas barrier,[37] fire-retardant,[79] gas separation[86], superhydrophobicity,[87] drug delivery,[88] electrochromic,[29] and antifogging[89]. Figure 2.12a shows the schematic of a typical multilayer thin film assembled with

positively charged PEI and negatively charged montmorillonite (MMT) clay platelets. This schematic correlates well with the cross-sectional TEM image of the PEI/MMT multilayer thin film (Fig. 2.12b).

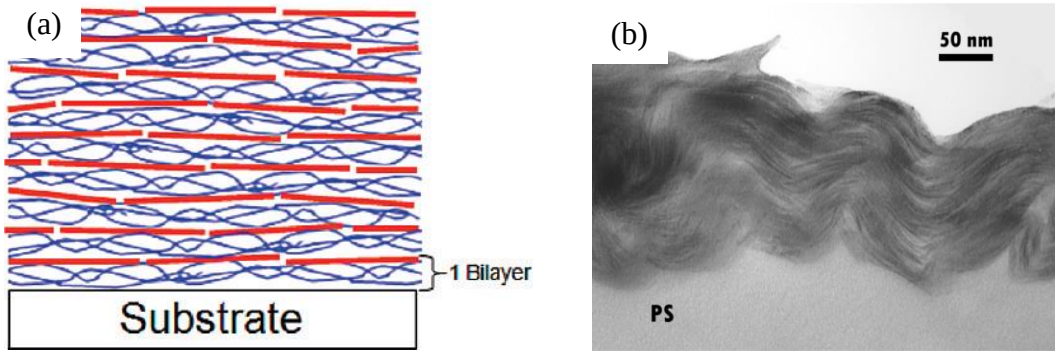

Figure 2.12. Schematic of PEI/MMT bilayers (a). TEM image of 40-bilayer PEI/MMT thin film (b).[90]

The properties of LbL films are closely related to their thickness and density.[78] So it is crucial to understand the growth mechanism of LbL assemblies before discussing how properties can be improved using structure-property relationships. The growth of LbL assemblies can be categorized into three major types, linear, exponential, or a combination of linear and exponential growth. Most multilayer thin films with linear growth are based on strong polyelectrolyte pairs, such as poly(styrene sulfonate) and poly(allylamine hydrochloride). These assemblies grow linearly in mass and film thickness as a function of layers deposited (Fig. 2.13a).[33] Exponential growth can be observed if at least one weak polyelectrolyte is used for the assembly. Typical exponential growing polyelectrolyte pairs includes poly(L-lysine) and hyaluronic acid,[91]

chitosan and hyaluronic acid,[92] and polyethylenimine and poly(acrylic acid).[37] It is widely accepted that the diffusion of weak polyelectrolytes "in-and-out" of multilayer thin films during the assembling process (as shown in Figure 2.14) results in more mass and thickness increment than in linear growing multilayers. With more layers added, exponential growth eventually transforms into linear growth, as can be seen between 5 and 7 BL in Figure 2.14b. It should be noted that this transformed linear growth is still based on the preceding exponential growth, and thus capable of adding much more mass and thickness than the strong polyelectrolytes.

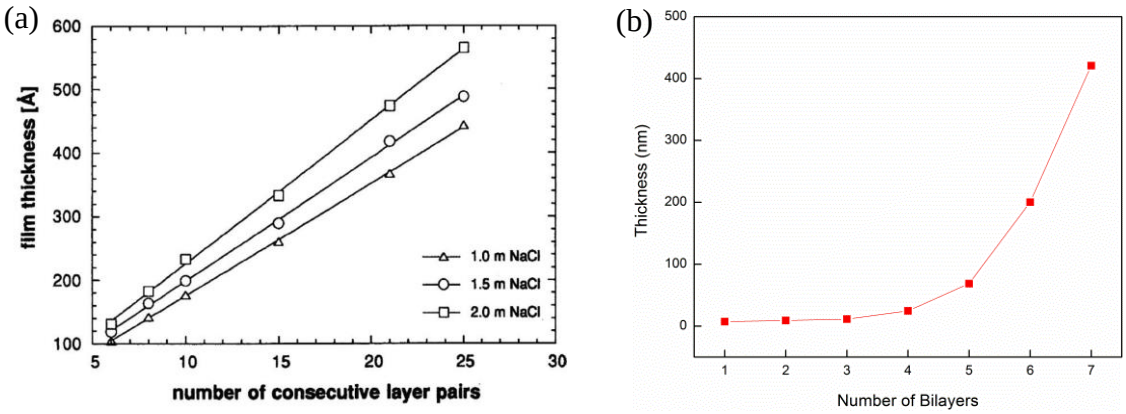

Figure 2.13. Thickness of PSS/PAH as a function of layers (a),[33] and PEI/PAA multilayer thin films as a function of bilayers deposited (b).

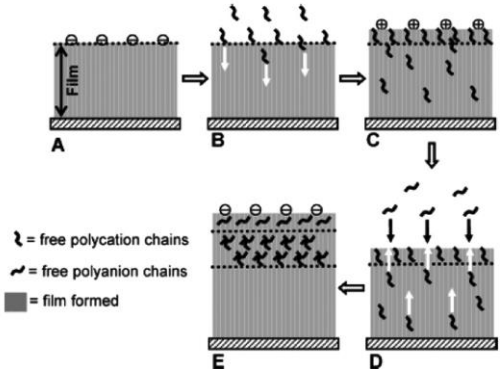

Figure 2.14. Schematic of the "in-and-out" mechanism, which is responsible for the exponential growth in LbL assemblies. [49]

According to the "in-and-out" model, the electrostatic crosslinks between oppositely charged weak polyelectrolytes are not permanent. As a comparison, crosslinks are considered "frozen" between strong polyelectrolytes.[67] These temporary crosslinks allow weak polyelectrolytes to diffuse in and out of multilayer thin films during the assembling process. Although polyelectrolytes can diffuse into the entire multilayer thin film with relative ease, an energetic barrier will prevent these absorbed polyelectrolytes from being completely desorbed when they travel outwards to combine with oppositely charged components (as shown in Figure 2.14 d and e).[20] The amount of desorbed polyelectrolyte is negligible when exponential growth is fully developed, because the material added on the surface through complexion largely outweighs the amount of desorbed material during the same time frame. This polyelectrolyte desorption is very evident at the early stage of the assembling process, when the multilayer film is relatively thin and constitutes only a few layers.[93-95] At this initial stage, the thickness of multilayer thin films depends on the both complexation and

desorption of polyelectrolytes. By controlling the assembling time, the extent of desorption can be regulated, resulting in thicker multilayer assemblies with better properties.[96]

2.3.2 Spray-Assisted Deposition of Electrostatic Bonded Layer-by-Layer Assembly

The flexibility of layer-by-layer assembly is shown not only by the range of available components and interactions, but also through the wide selection of assembling methods. Multilayer thin films can be assembled using dipping,[97] spraying,[98] spinning,[99] and a combination of spraying & spinning.[100] Dip-assisted assembly was the earliest invented and most widely used alternative method for multilayer thin film deposition. In an effort to reduce the processing time, spray-assisted LbL assembly was introduced by Ciba Vision in 1999.[101] Similar to dip coating, most spray-assisted LbL assemblies are fabricated by alternate spray coating of water-based solutions with oppositely charged components. As shown in Figure 2.15a, a typical spraying process involves deposition of polycation solution (bottle 1), spray rinsing with DI water (bottle 2) to wash off excess polycation, spray deposition of polyanion solution (bottle 3), and spray rinsing with DI water (bottle 4) to rinse excess polyanion. Apart from this similarity, spray coating differs from dip coating in two major aspects. First, it is possible to deposit oppositely charged material simultaneously through simultaneous spray coating of interacting species (SSCIS). As shown in Figure 2.15b, SSCIS can further reduce the processing time and simplify the assembling process.[102] Secondly, it is possible to deposit inorganic salt multilayer thin films.[103]

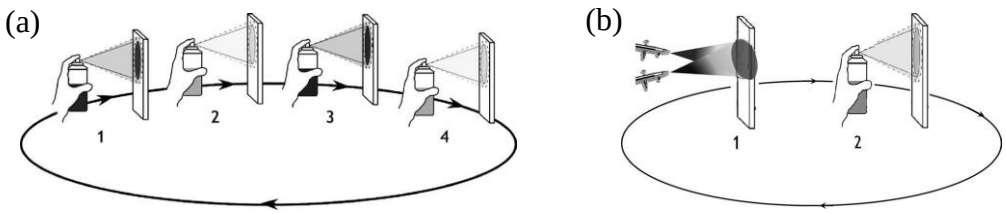

Figure 2. 15. Schematic of a conventional spray-assisted layer-by-layer deposition (a), and simultaneous spray coating of interacting species (b).[20]

There is not a consensus on the minimum time needed for the deposition of each layer. The conventional deposition time used for dip-assisted assembly is in the range of 5-20 min.[104] The introduction of spray-assisted assemblies shows that high-quality films can also be made without using very long deposition time. Spray-coated films were found to be slightly thinner or of equal thickness to that of dip-coated films.[105-106] For instance, when 10 s deposition time was used, spray-coated poly(diallyldimethylammonium) (PDDA)/PSS bilayers exhibited similar thickness to that of the same dip-coated films, as shown in Figure 2.16.[105] Moreover, the sprayed films also exhibit similar or slightly larger surface roughness than dipped films.[98, 107]

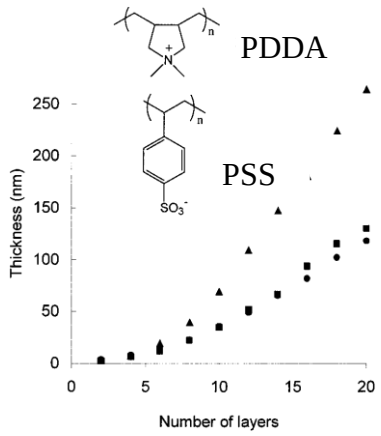

Figure 2.16. Thickness of PDDA/PSS bilayers as a function of number of layers deposited on sprayed (circles) and dip-coated (squares) silicon wafers. Results for a dip-coated sample with 5 min of contact time are also shown (triangles).[105]

Most importantly, the spray-assisted coating technique allows industrial-scale application of LbL assembly using existing apparatus. The roll-to-roll immersion coater (miniature version of industrial scale roll-to-roll coater) shown in Figure 2.17a could be easily modified to perform continuous roll-to-roll spray coating.[108] Compared with conventional dip coating, the short deposition time makes spray coating more time efficient, meeting the requirements for high throughput industrial manufacturing. Moreover, spray coating can also be used to apply multilayer thin films on substrates that are unsuitable for dip coating, such as large objects, complex shapes, or absorbent substrates (as shown in Figure 2.17b).[109]

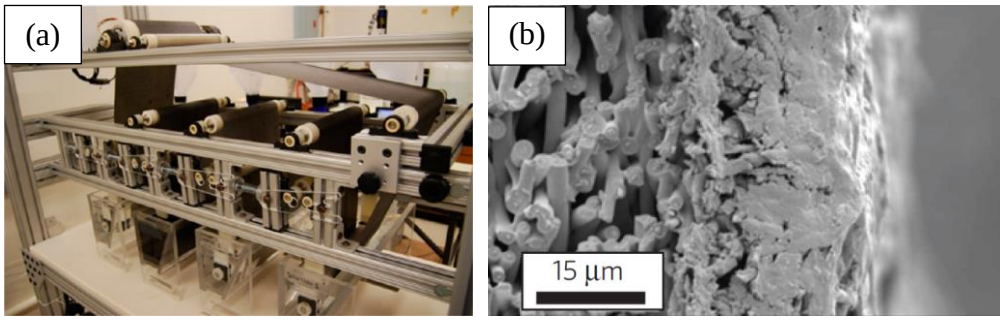

Figure 2. 17. Image of a roll-to-roll continuous immersion coating system (a).[108] Cross-section image of a spray coated nylon 6,6 mat.[109]

It is interesting to note that electrostatically-bonded multilayer thin films tend to exhibit exceptional gas barrier regardless of composition (clay or polymer) and deposition method (dipping or spraying). The low gas permeability of these multilayer thin films originates from the strong bond strength of electrostatic interaction and the high crosslinking density between components.[37] These factors also restrict the mobility of polymer chains, leading to rigid and brittle thin films (such as PEI/PAA bilayers).[110] Fortunately, the versatility of LbL assembly allows us to choose weaker bonding (i.e., hydrogen bond) and softer components (e.g., PEO) to make stretchy multilayer thin films that can be used on elastomeric substrates.

2.3.3 Hydrogen-Bonded Layer-by-Layer Assembly

Hydrogen-bonded (H-bonded) LbL assembly is a relatively new area of research.[111] Since its invention nearly two decades ago,[22] numerous studies have been conducted to develop H-bonded assemblies with interesting properties for various biomedical and engineering applications.[112-114] Hydrogen bonded assemblies differ from

their electrostatically bonded counterparts in the following aspects. First, H-bonded assemblies are responsive to neutral pH, which makes them ideal for in-vivo drug delivery applications.[115] Second, hydrogen bonding allow certain non-ionic polymers with desirable properties to be incorporated using layer-by-layer assembly. For instance, poly(N-isopropyl acrylamide) (PNIPAM) can be assembled with PAA to impart temperature-sensitivity to the final assembly.[116] Another example of a H-bond assembly involves the PAA/PEO bilayers. The addition of low T_g PEO helps to reduce the glass transition temperature of the entire assembly to a value lower than room temperature, allowing the resultant PAA/PEO bilayers to be elastomeric (Fig. 2.18).[114] Moreover, PAA/PEO assemblies can be used as proton exchange membranes[117] and electrochromic devices.[29]

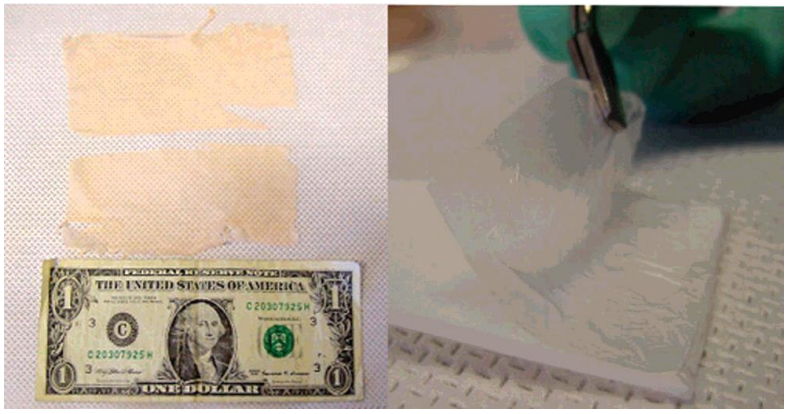

Figure 2.18. 100-bilayer PEO/PAA assembled at pH 2.5 on a Teflon substrate. This clear and flexible assembly can be peeled off as a stretchy free-standing film.[114]

Similar to electrostatically-bonded assemblies, the selection of components for hydrogen-bonded multilayers is virtually endless. Any material with H-bond donating groups can be paired with another material with H-bond accepting groups to build H-bonded multilayer films. Polyacids, such as PAA and poly(methacrylic acid) [PMAA] are the most commonly used H-bond donating polymers. Other neutral polymers, such as PEO, PNIPAM, and polyvinylpyrrolidone (PVP) can be used as H-bond accepting components. It should be noted that the assembly of hydrogen-bonded bilayers requires both components to be electrically neutral, which is why polyacids are assembled at low pH. The chemical structures of common polymers used in H-bonded LbL are shown in Figure 2.19.

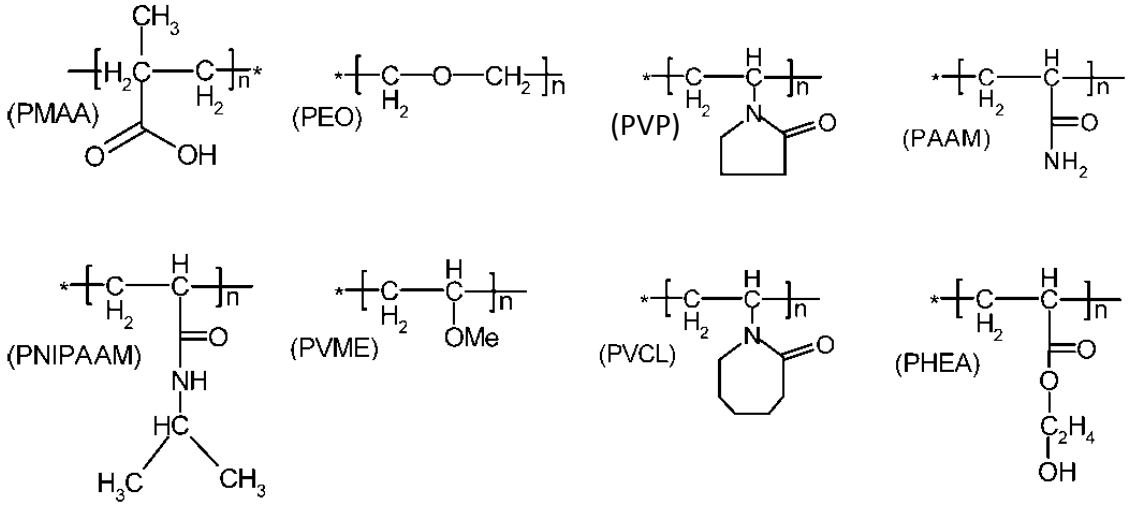

Figure 2.19. Chemical structures of common polymers involved in hydrogen bonded layer-by-layer assembly.[115] PMAA, PEO, PVP, polyacrylamide (PAAM), poly(N-isopropyl acrylamide) (PNIPAAM), poly(vinyl methyl ether) (PVME), poly(N-vinylcaprolactam) (PVCL), and poly(2-hydroxyethyl acrylate) (PHEA).

Hydrogen bonds can be categorized as strong (14-40 kcal), moderate (4-14 kcal), and weak (<4 kcal).[118] Moderate H-bonds are ubiquitous in nature, and all H-bonding interactions involved in LbL assembly fall into this category. The bond strength depends on the strength of both donor and acceptor. The strength of some common H-bond donors and acceptors are: P−OH > N−H > C−OH > O_wH > N(H)H (for H-bond donors) and O═P > O_w >C−O−C (for H-bond acceptors). Similar to the influence of charge density on multilayer thin films structure, the strength of H-bond determines the level of stratification of the final assembly. Previous reports indicate that a small difference in bond strength is enough to cause a dramatic difference in film structure.[119] Since the pyrrolidone groups on PVP are stronger H-bond acceptors than the ether groups found on PEO, when both polymers were couple with PMAA, the H-bonding with PVP is going to be stronger than that found in PEO/PMAA. The stronger H-bonding creates a stratified PVP/PMAA multilayer, as shown in Figure 2.20, while the H-bonding between PEO and PMAA is too weak to suppress polymer interdiffusion, leading to a homogeneous film structure.

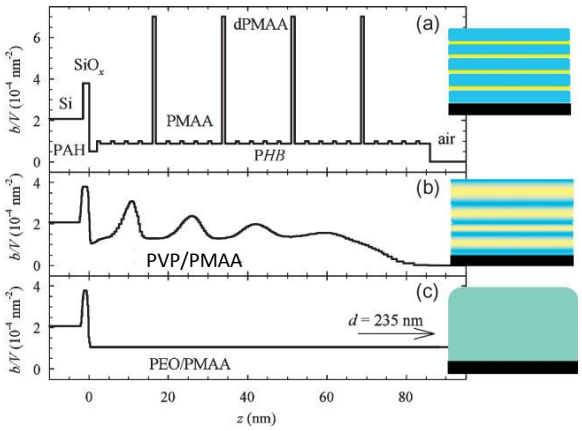

Figure 2.20. Neutron reflectivity profiles and schematic diagrams for hydrogen bonded multilayers assuming perfect layering (a), and the actual structure of PVP/PMAA bilayers (b) and PEO/PMAA bilayers (c).[119]

Regardless of bond strength, the thickness of H-bonded assemblies decreases as the deposition pH approaches a critical value, where the assembly process is completely suppressed due to deprotonation of the H-bond donor. For example, the thickness of PAA/PEO bilayers remains nearly constant when pH is increased from 2 to 2.5, as shown in Figure 2.21. A noticeable decrease in film thickness occurs as PAA begins to deprotonate beyond pH 2.5, and there is no deposition at pH 3.5 (critical pH) or higher. It should be noted that this critical pH does not correspond to the pH value where H-bond donors are totally deprotonated. In the case of PAA/PEO bilayers, only ~5% PAA is protonated at pH 3.5,[112] but, the electrostatic repulsion generated by those deprotonated carboxylic acid groups is enough to stop the film from growing completely. Moreover, the critical assembling pH is controlled by the strength of hydrogen bonding, and its value shifts to higher pH if stronger bonding is involved. For example, the critical assembling pH for PAA/PVP is 4.0, which is higher than that of

PAA/PEO (3.5).[115] It should be noted that pH-sensitive components remain sensitive to environmental pH after assembly. The pH value where dissolution of hydrogen-bonded assembly happens is known as the critical dissolution pH. This ability to dissociate at a designated pH is widely used to make H-bonded multilayers for drug-delivery applications.[71]

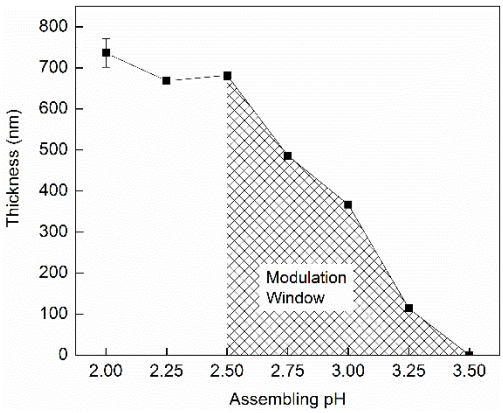

Figure 2.21. Thickness of 20-bilayer PAA/PEO thin films as a function of assembling pH.

H-bonded multilayers can be made to expand/dissociate at neutral/bodily pH by selecting appropriate polymer pairs. On the contrary, due to the high bond strength and crosslink density, electrostatically bonded films can be dissolved only under very acidic or basic conditions, making them less useful for drug delivery applications at neutral/bodily pH. The ability of H-bonded LbL films to expand/dissociate near bodily pH is critical for controlled release of drugs within human body. Two common strategies can be used to load and then deliver active compounds.[81] The first approach involves

loading the active compound by assembling it with another component. In other words, the active component is incorporated as a part of the H-bonded assembly. Figure 2.22a shows a schematic of the inclusion of a water-insoluble functional molecule, bis-triazine (DTA), using a hydrogen-bonded assembly.[120] This film is then dissociated at a designated pH to release DTA. A second method involves using a H-bonded capsule to load and then deliver the active compound (Fig. 2.22b).[111] In other words, the drug is contained within a capsule rather than being part of the capsule. The loading process occurs by putting this capsule into a solution with active compound. Because the capsule is designed to expand at the solution pH, the drug will be able to diffuse into the expanded capsule to complete the loading process. The environmental pH is then changed to shrink the capsule in order to prevent the loss of active compound during transportation. Upon arriving at the correct location, with a preset unloading pH, the capsule will again become dilated and release the active compound.

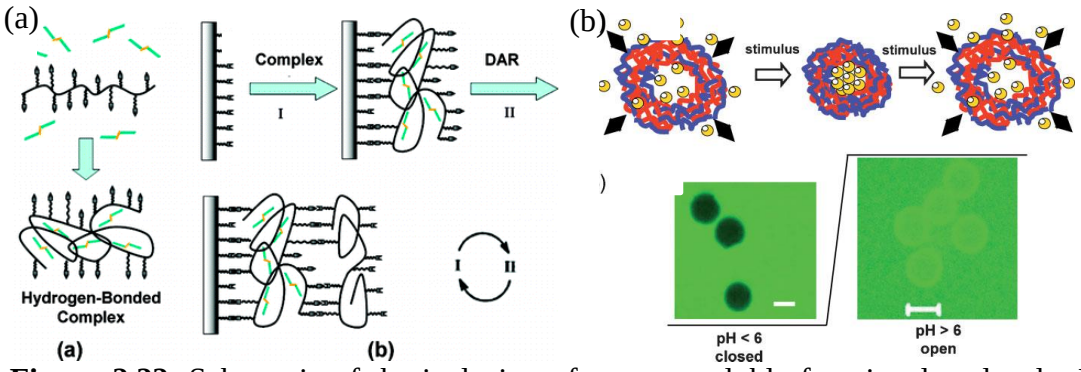

Figure 2.22. Schematic of the inclusion of a water-soluble functional molecule, DTA, within the hydrogen bonded assembly (a).[120] Schematic of encapsulation and release of substances to and from the pH-sensitive capsules, and corresponding fluorescence images (b).[111]

CHAPTER III

IMPROVING GAS BARRIER OF CLAY-POLYMER THIN FILMS USING SHORTER DEPOSITION TIMES*

3.1 Introduction

Clay continues to receive significant attention for its ability to impart mechanical reinforcement,[121-123] gas barrier,[124-126] and even flame retardant characteristics to polymers.[127-130] Conventional clay-polymer composites obtained via melt or solution mixing generally exhibit only modest improvement in gas barrier due to insufficient exfoliating and aligning of inorganic nanoplatelets within the organic polymer matrix.[8, 131] In order to prevent aggregation, clay concentration rarely exceeds 10 wt% in traditional clay-polymer composites.[50, 132-133] Numerous attempts have been made to improve clay exfoliation in polymer matrices, including in-situ polymerization and clay functionalization,[134-136] but the improvement in gas barrier is still limited by insufficient clay alignment.[5, 11-12] Shear force can be applied to align clay platelets in molten polymer, but Brownian motion of clay platelets (and relaxation of the polymer matrix during solidification) prevents high levels of clay alignment.[132, 137-138] A relatively simple method for achieving high clay concentration and alignment is to prepare polymer/clay nanocomposites using the layer-by-layer (LbL) assembly technique.[90, 125]

*Reprinted with permission from Xiang, F. M.; Tzeng, P.; Sawyer, J. S.; Regev, O.; Grunlan, J. C., Improving the Gas Barrier Property of Clay−Polymer Multilayer Thin Films Using Shorter Deposition Times. *ACS Appl. Mater. Interf.* **2014**, *6*, 6040-6048**.**

A typical bilayer (BL) polymer/clay assembly can be constructed by alternately assembling negatively charged platelets with a positively charged polyelectrolyte.[90] Upon deposition of a few BLs, a 'nanobrick wall' structure with high clay alignment is produced. This structure exhibits remarkable tortuosity for diffusing gas molecules, giving these clay-polymer thin films super oxygen barrier that rivals SiO_x or metal oxide coated films.[35, 139] Improvement in polymer-clay nanobrick walls have been made by switching from BL to quadlayer (QL) recipes, which consist three layers of oppositely charged polyelectrolytes between each clay layer,[16] and also by increasing nanoplatelet aspect ratio.[125, 140] For example, it takes 24 BL of branched polyethylenimine (PEI) and montmorillonite (MMT) clay (48 individual layers) to achieve an undetectable oxygen transmission rate (OTR < 0.005 $cm^3/(m^2 \cdot day \cdot atm)$),[141] while four PEI/poly(acrylic acid) (PAA)/PEI/MMT QL (16 individual layers) can provide the same level of performance.[16] Further analysis revealed that this improvement in gas barrier originated from a more open nanobrick wall structure. According to a tortuous path model developed by Cussler, instead of following a staircase-like pattern between highly aligned clay layers, gas molecules wiggle laterally while traveling parallel to the diffusion direction (between the clay layers).[10] Greater clay spacing in the QL film provides more room for gas molecule wiggling, leading to a prolonged diffusion length and improved gas barrier. Despite the success of adding polyelectrolyte layers to transform bilayers to quadlayers, inserting even more polyelectrolyte layers between clay layers may dilute clay concentration and consequently diminish the gas barrier of

these films. With a given clay type, an alternative route to optimize this nanobrick wall structure involves altering the deposition time used to deposit the polyelectrolyte layers.

A wide range of assertions have been made on the deposition time needed to form a layer (from seconds to hours).[18, 142-144] The general consensus has been "the longer the better" because the adsorption of polyelectrolyte in each deposition step was typically considered to be an irreversible process involving kinetically "frozen" crosslinks at (or near) the liquid-solid interface.[67, 104, 145] Moreover, it was generally accepted that a pronounced change in the adsorbed amount occurs within the first 10 min (or even faster), and a maximum adsorption time of 20 min is needed for saturation (i.e., to reach equilibrium).[146-148] Based on these assumptions, typical literature deposition times for LbL assembly are set between 5 and 20 min.[149-151] The work presented in this chapter demonstrates that shorter dipping time actually leads to thicker clay-polymer films, with increased clay spacing and improved gas barrier. Application of shorter dipping time during assembly enables clay-polymer LbL films with larger thickness and better gas barrier to be manufactured using less time and fewer layers. These results suggest that 5 s exposure times are better for LbL films prepared with weak polyelectrolytes and clay platelets. The universality of this discovery may prove to be of great importance as these multifunctional thin films move toward commercialization in a variety of arenas (e.g., protection of electronics, food packaging and flame retardant treatments)[1, 78, 152].

3.2 Experimental Section

3.2.1 Materials

Laponite (LAP) (Laponite RD) and sodium montmorillonite (MMT) (Cloisite NA^+) clays were purchased from Southern Clay (Gonzales, TX) and used as received. Vermiculite (VMT) (Microlite 963++) clay dispersion was supplied by Specialty Vermiculite Corp. (Cambridge, MA). PEI (M_w = 25000 g/mol) and PAA (M_w = 100000 g/mol) were purchased from Sigma-Aldrich (Milwaukee, WI) and used as received. A 1 wt% VMT solution was prepared using 18.2 MΩ deionized water, by rolling for 24 h and then allowing for sedimentation of insoluble fractions for another 24 h. All the other solutions were prepared by simply rolling for 24 h to achieve homogeneity. Prior to deposition, the pH of each PEI solution (0.1 wt% PEI) was altered to 10 using 1 M HCl, and the pH of PAA solutions (0.2 wt% PAA) was altered to 4 using 1 M NaOH. All clay solutions were used at their unaltered pH (1 wt% for VMT, MMT and LAP).

3.2.2 Substrates

Poly(ethylene terephthalate) (PET) film with a thickness of 179 μm (ST505, DuPont-Teijin) was purchased from Tekra (New Berlin, WI) and used as the substrate for OTR testing and TEM imaging. PET films were rinsed with deionized water and methanol just prior to deposition. Cleaned PET substrates were dried and then treated with a BD-20C corona treater (Electro-Technic Products Inc., Chicago, IL). Corona treatment improves adhesion of the first polyelectrolyte layer by oxidizing the film surface.[153] Single side polished silicon wafers were purchased from University Wafer (South Boston, MA) and used to monitor the change in film thickness via ellipsometry.

Silicon wafers were cut to 10 × 2 cm strips, and then cleaned with piranha solution for 30 min, rinsed with deionized water, acetone, and deionized water again, and dried with filtered air prior to deposition. ***Caution!*** *Piranha solution reacts violently with organic materials and needs to be handled properly*. Polished Ti/Au crystals with a resonance frequency of 5 MHz were purchased from Maxtek (Cypress, CA) and used to monitor mass deposition using a quartz crystal microbalance (QCM).

3.2.3 Layer-by-Layer Deposition

The overall layer-by-layer deposition processes for QL, hexalayer (HL) and octalayer (OL) are illustrated in Figure 3.1. Treated substrates were dipped in the PEI solution for 5 min, rinsed with deionized water, and dried with filtered air. This procedure was followed by an identical dipping, rinsing, and drying procedure in the PAA solution. After this initial bilayer was deposited, different numbers of layers were added to make QL, HL or OL films using the same rinsing and drying conditions. This procedure was repeated until the desired number of layers was achieved. In order to study the influence of dipping time on the properties of these films, the dipping time in polyelectrolyte solutions was set at either 5 s or 1 min, while the dipping time of clay suspensions remained at 1 min. All thin films were prepared using home-built robotic dipping systems.[153-154]

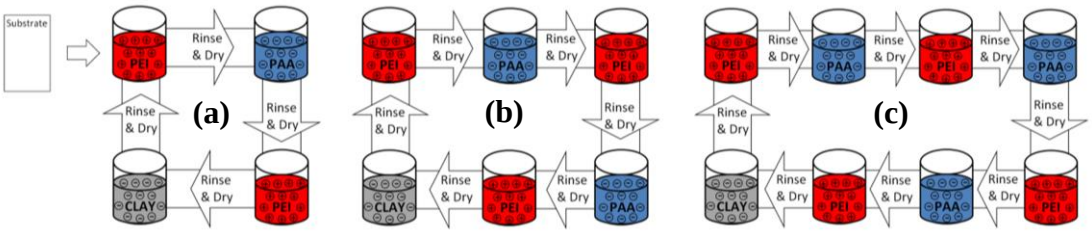

Figure 3.1. Illustration of the LbL assembly processes for quadlayer (a), hexalayer (b), and octalayer (c) films.

3.2.4 Film Characterization

Film thickness was measured (on silicon wafers) using an alpha-SE ellipsometer (J.A. Woollam Co., Inc., Lincoln, NE). Films with thickness above 1000 nm, or films too hazy for the ellipsometer, were measured with a P-6 profilometer (KLA-Tencor, Milpitas, CA). Regardless of the measurement method used, average film thickness was the average of three measurements. Mass of these multilayer films were measured at each quadlayer with a quartz crystal microbalance (QCM) (Inficon, East Syracuse, NY) having a frequency range of 3.8-6 MHz. QCM crystals were cleaned in a PDC-32G plasma cleaner (Harrick Plasma, Ithaca, NY) for 5 min at 10.5 W prior to deposition, and then inserted in a holder and dipped into the corresponding solutions. After each deposition, the crystal was rinsed and dried and then left on the microbalance to stabilize for 5 min. Oxygen transmission rate measurements were performed by MOCON (Minneapolis, MN) using an Oxtran 2/21 ML oxygen permeability instrument (in accordance with ASTM Standard D-3985) at 23 °C and at 0% relative humidity (RH).

3.2.5 Microtomy and TEM Imaging

LbL assemblies were deposited on PET film, coated with carbon, embedded in Epofix (EMS, Hatfield, PA) resin overnight, and microtomed (Leica Ultracut UCT, Leica, Inc., Germany) to 90 nm thick sections using a Ultra 45° diamond knife (Diatome, Hatfield, PA, 1mm/s). Thin sections were floated onto water and picked up by 300 mesh copper grids (Ted Pella). The grids were imaged using a Tecnai G2 F20 FE-TEM (FEI, Hillsboro, OR) at an accelerating voltage of 200kV and analyzed using Digital Micrograph software 3.0.

3.3 Results and Discussion

3.3.1 Influence of Exposure Time on Film Growth and Oxygen Barrier

The influence of exposure time on the growth of all-polymer PEI/PAA bilayer films is shown in Figure 3.2a. Both growth curves have exponential and linear growth regions, but there are remarkable differences in thickness. The film prepared using 5 s exposures grows faster in the exponential growth region and exhibits an earlier transition to linear growth (after 3 BL). In contrast, the film prepared with 1 min dips grows more slowly in the exponential growth zone. It takes 5 BL to transition to linear growth with this longer exposure time. At the end of exponential growth, both films are thick enough to allow maximum polyelectrolyte interdiffusion, which dominates the linear growth of these films. Consequently, films prepared using 1 min dipping eventually become thicker (at 7 BL) than their 5 s counterparts due to longer interdiffusion time. The thickness of an 8 BL film prepared with 1 min dipping (675 nm) is much greater than

that made with 5 s dips (455 nm), and this is directly reflected in the gas barrier behavior of these films. As shown in Figure 3.2b, undetectable OTR (<0.005 $cm^3/(m^2 \cdot day \cdot atm)$) is achieved for an 8 BL PEI/PAA film prepared with 1 min dipping,[37] while the thinner film made with 5 s dips has an OTR of 0.093 $cm^3/(m^2 \cdot day \cdot atm)$. Although shorter dipping time appears to require more layers to achieve high oxygen barrier in all-polymer systems, it can be ideal for clay-polymer assemblies. The addition of clay suppresses polyelectrolyte interdiffusion and thus delays the transition to linear growth, which keeps films prepared with 5 s dips thicker for more deposited layers.

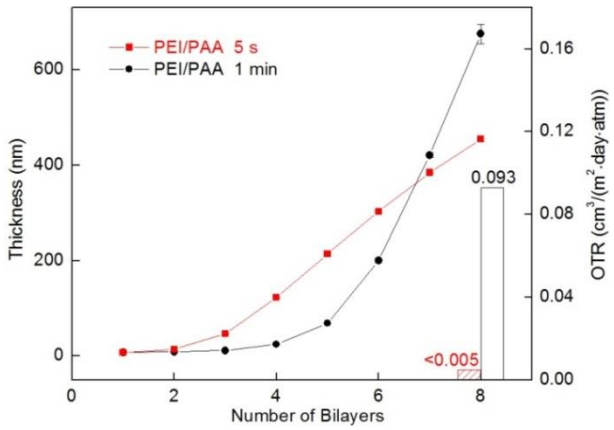

Figure 3.2. Film thickness as a function of bilayers for PEI/PAA films made with 1 min and 5 s exposure times. The OTR of 8 BL PEI/PAA film with 1 min (from Ref. 37) and 5 s dipping time is also shown.

As can be seen in Figure 3.3, shorter dipping time yields thicker clay-polymer films for the initial layers deposited and the addition of clay effectively postpones the overtaking in film thickness. In the case of PEI/PAA/PEI/MMT quadlayers, it takes 4 QL with 1 minute dipping to achieve an undetectable OTR,[16] but the 5 s films remain

thicker until 9 QL. It is the same situation for $(PEI/PAA)_2PEI$/MMT HL films. It takes 3 HL prepared with 1 minute exposure to achieve undetectable OTR (see Table 3.1), while the overtaking in thickness doesn't occur until 5 HL. Since the overtaking in thickness always happens after undetectable OTR is achieved, any 5 s films with measurable OTR are thicker than their 1 min counterparts and should exhibit better gas barrier. It is interesting to note that the overtaking in thickness also depends on polymer/clay ratio. The numbers of individual layers needed for overtaking in thickness are 14, 24, 30, and 36 for BL all-polymer film, OL, HL, and QL clay-polymer films, respectively. As the clay/polymer concentration ratio increases, there will be more clay platelets in the LbL film to block polyelectrolyte interdiffusion, leading to further postponement for longer dipping time exceeding shorter in thickness.

Table 3.1. Properties of three hexalayer films fabricated with MMT clay using different dip times.

3 HL film recipe	film thickness (nm)	OTR ($cm^3/(m^2 \cdot day \cdot atm)$)	permeability ($\times 10^{-16}$ $cm^3 \cdot cm/(cm^2 \cdot s \cdot Pa)$)	
			film[a,b]	Total[b]
$(PEI/PAA)_2PEI$/MMT 5 s	349	<0.005[b]	0.00004	0.0095
$(PEI/PAA)_2PEI$/MMT 1 min	141	<0.005	0.00001	0.0095

[a] Film permeability was decoupled from the total permeability using a previously described method. [b] The low end detection limit for an Ox Tran 2/21 L module is 0.005 $cm^3/(m^2 \cdot day \cdot atm)$.

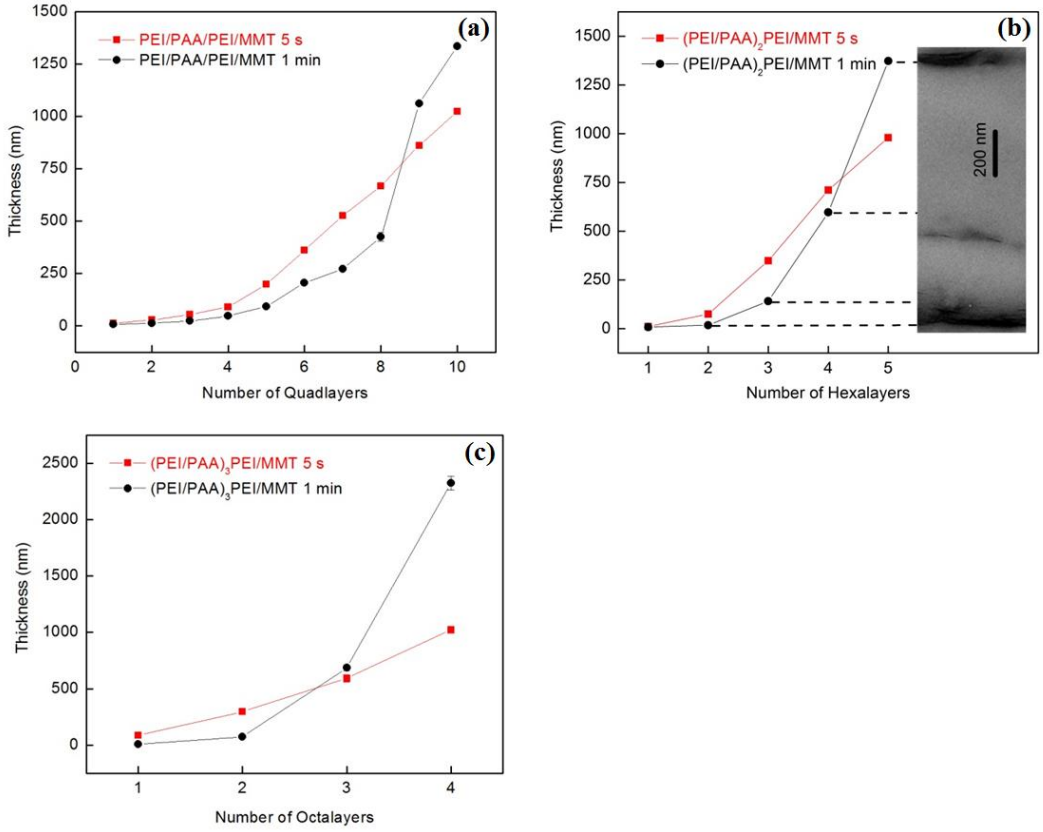

Figure 3.3. Film thickness as a function of quadlayers (a), hexalayers (b), and octalayers (c) deposited using 5 s and 1 min dipping times. Growth curve of hexalayer films, prepared using 1min dipping, is correlated to the TEM micrograph of a 5 HL film in (b).

In order to further illustrate thickness overtaking as a result of different exposure time (Figure 3.3), TEM micrographs of microtomed 3 and 5 $(PEI/PAA)_2PEI/MMT$ HL films (where thickness difference is more pronounced) are shown in Figure 3.4. The clay is easily resolved (dark lines) thanks to its high electron density in comparison to the polymer (bright regions). Individual clay platelets (1 nm thick, ~100 nm in diameter, white star in Figure 3.4) are deposited parallel to the substrate in films fabricated with both short and long exposure times. It should be noted that the waviness of the film is most probably due to sectioning. For 3 HL films, the one prepared with 5 s exposures

has greater overall thickness. The 5 HL films are quite the opposite, as the sample prepared with 1 min exposures is noticeably thicker. Both results agree well with the ellipsometry measurements in Figure 3.3b. It is possible to resolves individual clay deposition (Figure 3.4 top panel) and increased clay-to-clay spacing from the third to the fifth HL, which line up well with ellipsometric thickness measurements (Figure 3.3b). The close to perfect matching between the ellipsometry and TEM measurements allows superposition of both in Figure 3.3b. These TEM images also show that in some cases clay platelets do not fully cover the polymer (black arrow in Figure 3.4). For films with equal number of clay layers, larger overall thickness implies larger clay spacing, which facilitates the perpendicular wiggling of gas molecules with respect to the diffusion direction and consequently increases the diffusion path and gas barrier behavior[16, 36, 90].

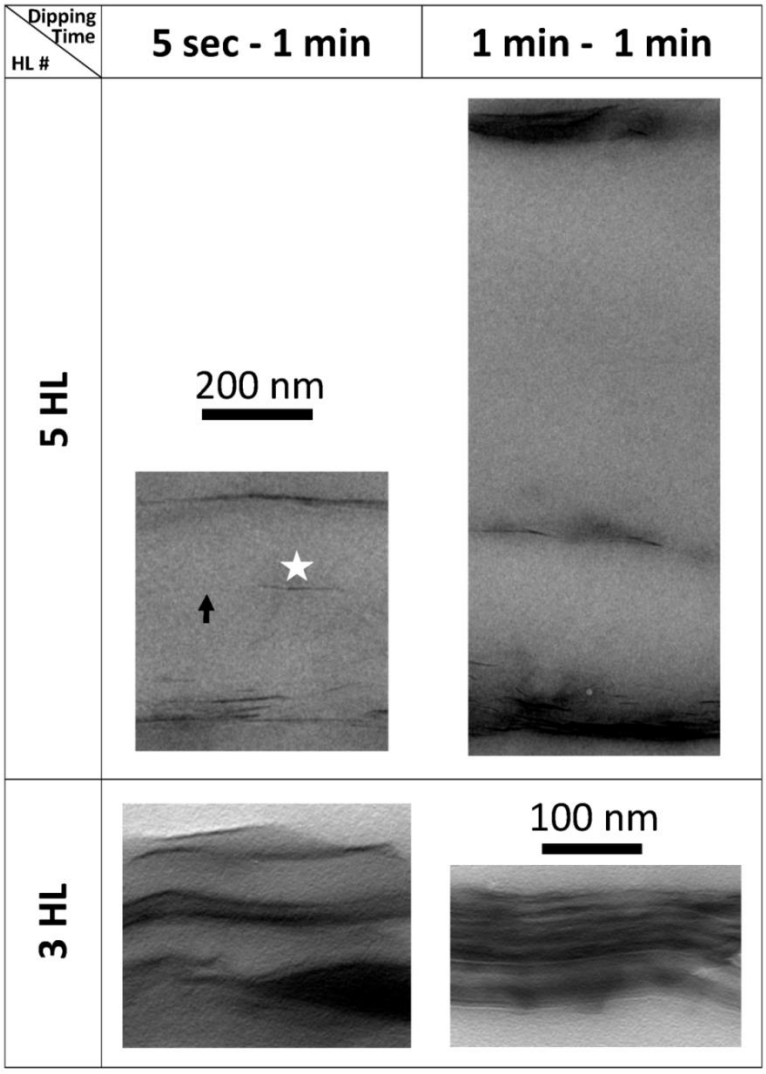

Figure 3.4. TEM cross-sectional images of 3 and 5 hexalayer films deposited using 5 s and 1 min polyelectrolyte exposure time. Arrow - partial clay coverage; star - individual clay platelet (~100 nm in diameter). The growth direction is from bottom to top.

The mass of PEI/PAA/PEI/MMT layers, with different dipping time, was measured with QCM and shown in Figure 3.5. Similar to the trend observed for thickness in Figure 3.3a, both films have linear and exponential growth regions, with 5 s dipping producing more mass before 9 QL. Density of these quadlayer films is

calculated by dividing mass by film thickness and area of film deposited on crystal. It should be noted that small errors in film mass and thickness can be compounded to produce much greater scattering in density. Moreover, the density of films prepared with 1 min dipping shows more variation due to longer interdiffusion time, which could magnify film thickness deviation and ultimately lead to larger density variation. As can be seen in Figure 5b, short dipping time creates films with a lower initial density, but it increases with increasing number of quadlayers (up to 4 QL). The opposite is true for the film with 1 min dipping times, which has higher density initially but decreases with increasing number of quadlayers (and then oscillates around 1.25 g/cm^3 after 4 QL). Although dipping time results in different initial densities, this difference gradually disappears as the number of quadlayers deposited increases.

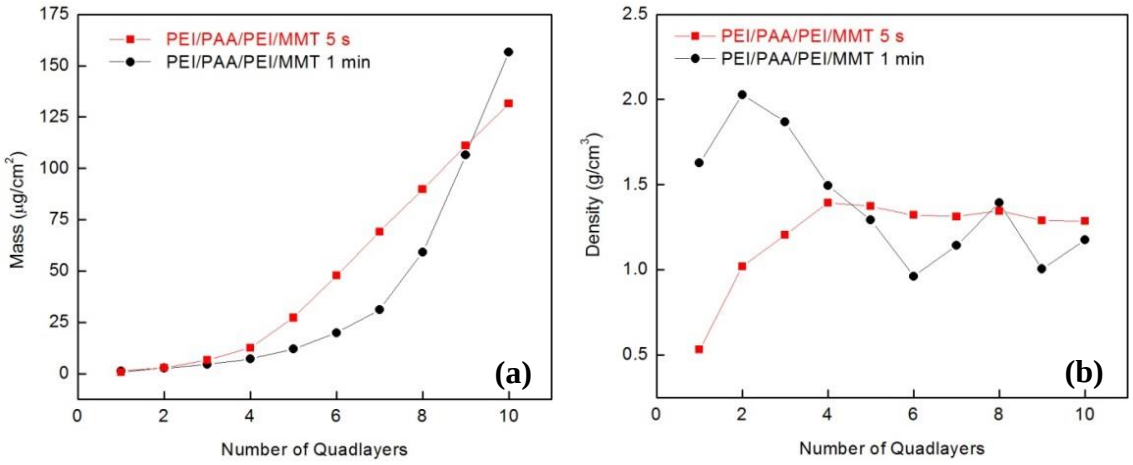

Figure 3.5. Mass (a) and density (b) of films prepared using different dipping time as a function of quadlayers deposited.

3.3.2 Influence of Clay Size on Film Growth

In order to further confirm the role of clay in this process, QL films with different types of clay were prepared. Each clay type has a thickness of about 1 nm, and the average diameters of LAP, MMT and VMT are 25, 200, and 1100 nm, respectively.[30, 125] As shown in Figure 3.6, the overtaking in film thickness happens the earliest in the PEI/PAA/PEI/LAP film (at 7 QL). After switching to the larger diameter MMT, the overtaking in film thickness is postponed to 9 QL (Figure 3.3a). VMT based films further extend the number of layers needed for the longer dip time to overtake 5 s dips in thickness (at 10 QL). Detailed growth curves for LAP and VMT quadlayers can be found in Figure 3.7. VMT has the largest diameter and is therefore most effective in suppressing polyelectrolyte interdiffusion. These results suggest that the extent of thickness postponement can be tailored by changing the clay/polymer concentration ratio and/or clay aspect ratio. It is also known that clay aspect ratio influences barrier properties of these thin films, with greater diameter producing lower transmission rate for a given number of layers.

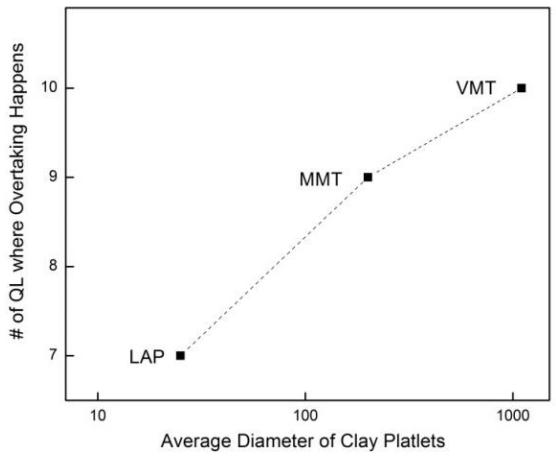

Figure 3.6. Number of quadlayer where overtaking happens as a function of clay diameter.

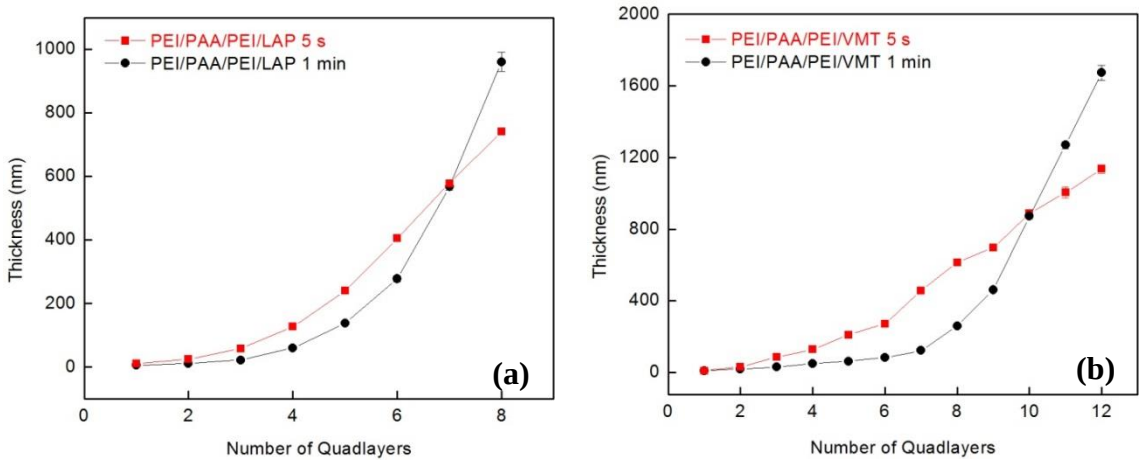

Figure 3.7. Film thickness as a function of quadlayers deposited with laponite (a) or vermiculite (b) clay.

The influence of dipping time on thickness, oxygen transmission rate and permeability of 3 QL films, prepared with three different clays, is shown in Figure 3.8 and Table 1. It is interesting to note that regardless of clay type, short dip time always leads to lower OTR, which is directly linked to film thickness. As can be seen in Figures

3.3a and 3.6, shorter deposition time always generates a thicker film for at least the first 7 QL. All films used for OTR testing were three quadlayers, so those made with 5 s exposures are thicker than those prepared with 1 min. With all of the films having the same number of clay layers, larger film thickness means larger average clay spacing and an elongated diffusion path for gas. In addition to exposure time, the diameter of clay also plays an important role on the OTR of these thin films. As can be seen for the films prepared with 5 s dips, larger diameter clays generate films with better oxygen barrier (Figure 3.8). VMT has the largest average diameter and the lowest OTR in films prepared with 5 s exposures, but this is not the case for VMT-based films prepared using 1 minute dipping. This unexpected increase in OTR may originate from desorption of polyelectrolytes. Desorption of low molecular weight polyelectrolytes from the film surface could create voids and reduce the number of available bonding sites (discussed in more detail in the next section). These surface defects may not cause a problem for subsequent deposition of polyelectrolytes due to the relatively coiled conformation and inherent flexibility of polyelectrolyte chains, but they may diminish the adsorption of clay. It is likely that the larger the clay platelets, the higher the negative impact on adsorption. Successful adsorption of larger clay platelets may require the establishment of many bonds with the underlying surface, leading to the largest negative impact on VMT.

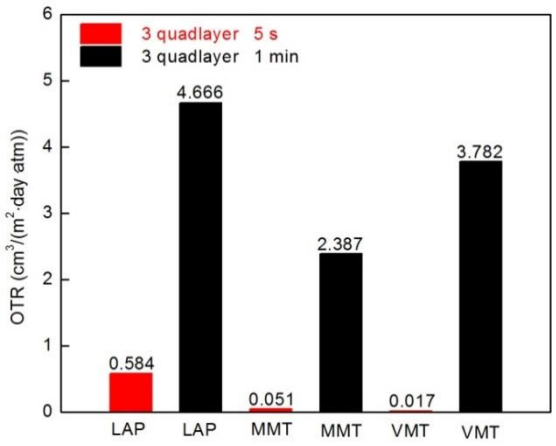

Figure 3.8. Oxygen transmission rate of three quadlayer films fabricated with LAP, MMT, and VMT using 5 s and 1min dip times.

Table 3.2. Properties of three quadlayer films fabricated with various diameter clays and exposure times.

3 QL film recipe	film thickness (nm)	OTR ($cm^3/(m^2 \cdot day \cdot atm)$)	permeability ($\times 10^{-16}$ $cm^3 \cdot cm/(cm^2 \cdot s \cdot Pa)$)	
			film[a]	total
PEI/PAA/PEI/LAP 5 s	58.08	0.584	0.00083	1.19
PEI/PAA/PEI/MMT 5 s	55.09	0.051	0.000064	0.10
PEI/PAA/PEI/VMT 5 s	85.06	0.017	0.000033	0.034
PEI/PAA/PEI/LAP 1min	22.24	4.666	0.0052	9.54
PEI/PAA/PEI/MMT 1min	24.12	2.387	0.0018	4.88
PEI/PAA/PEI/VMT 1min	30.71	3.782	0.0047	7.74

[a] Film permeability was decoupled from the total permeability using a previously described method.

3.3.3 Growth Mechanism for Clay-Polymer Assemblies

It has been shown that shorter exposure time deposits a thicker (Figure 3.3) and heavier (Figure 3.5a) film in the first few layers. This result seems counterintuitive at first glance, because it has been generally accepted that the adsorption of polyelectrolyte at each deposition step is kinetically irreversible.[67, 104, 145] Several studies have suggested that the adsorption process requires 10-20 min to reach saturation.[142, 147-148, 155] Based on the aforementioned assumptions, typical dipping times continue to be set between 5 and 20 min.[156-159] Although these assumptions work well for strong polyelectrolyte assemblies, they are unreliable for weak polyelectrolytes. Unlike with strong polyelectrolytes, the linkage between two weak polyelectrolytes (or weak-strong polyelectrolytes combinations) cannot be considered "frozen". It has been demonstrated that it is possible for polyelectrolytes that were already integrated into a multilayer assembly to be exchanged by polyelectrolytes in solution, breaking and reforming ionic crosslinks between them in the process.[31, 67, 160] The active nature of these linkages is also exemplified in the desorption of polyelectrolyte from these assemblies.[93-95] When weak polyelectrolyte chains are adsorbed onto an oppositely charged substrate, the individual chains are only weakly bound. Increasing the exposure time of this step only induces more relaxation of polymer chains.[161] The difference between long and short dipping time will not show up until another layer of oppositely charged polyelectrolyte is added. Incoming polyelectrolyte chains will initially adhere to the surface and then form either soluble complexes in solution or a multilayer on the surface. If the enthalpic gain from electrostatic interactions is small, the formation of soluble complexes in solution

will be more favorable based on entropic considerations.[162-163] In this case, the best way to minimize desorption is to reduce deposition time. It has already been shown that thicker all-polymer LbL assemblies can be produced if shorter dipping time is used to minimize desorption of polyelectrolytes.[94-95]

Summarizing the above analysis, the hypothesized growth mechanism of these clay-polymer multilayers in the first 3 QL is illustrated in Figure 3.9. The film prepared with 5 s dip times will be thicker and heavier because there is not enough time for the polyelectrolytes to relax into a more extended conformation or desorb from the surface. In contrast, films prepared with 1 min deposition steps are thinner and lighter. There is no desorption of polycations in the first layer, but the film prepared with longer deposition time is slightly thinner due to the longer time for the polycation chain to relax. Upon dipping into the oppositely charged solution, lower molecular weight polycations are more likely to desorb from the surface by interacting with polyanions in solution and forming soluble complexes.[95] In the meantime, polyanions already adsorbed on surface will continue to relax and adopt a more flattened conformation, leading to an even thinner film. The addition of a third polycation layer will be similar to that of the second layer in terms of desorption and relaxation of polyelectrolytes. The addition of a fourth clay layer completes one full quadlayer. With each quadlayer made using 1 min dipping being thinner than that using 5 s dips, the overall thickness of a 3 QL film will be thinner with longer deposition time.

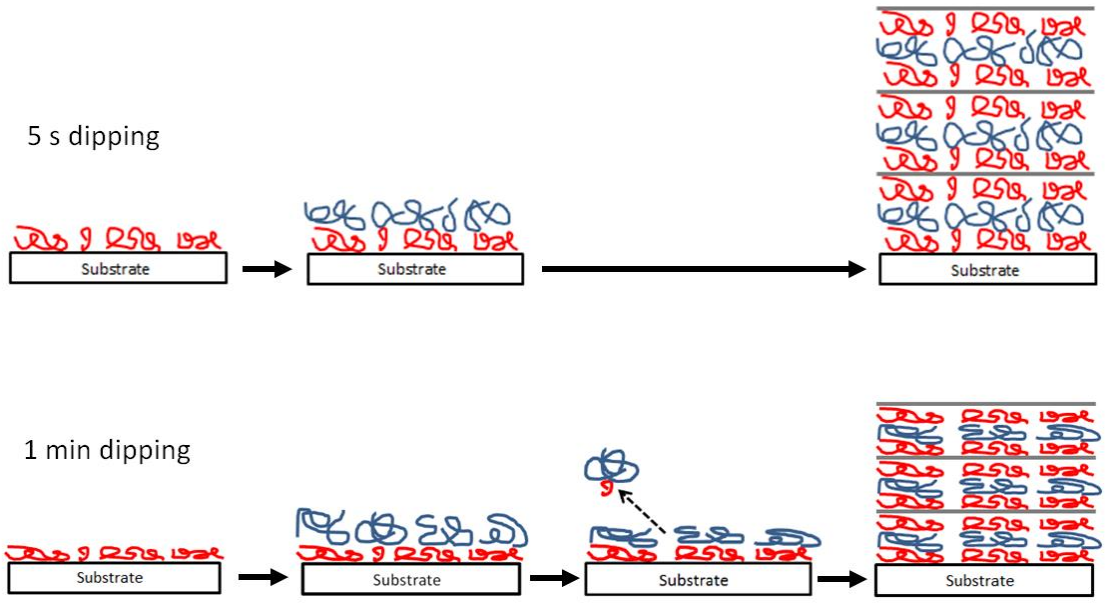

Figure 3.9. Illustration of the layer-by-layer deposition process for three quadlayer films fabricated using 5 s and 1 min deposition times. The red, blue, and gray lines represent polycation, polyanion, and clay, respectively.

It should be noted that the proposed mechanism illustrated in Figure 3.9 describes only the growth of these assemblies in the first few quadlayers, where the influence of polyelectrolyte interdiffusion is not dominant. As these clay-based multilayers get thicker, they will transition to linear growth, where polyelectrolyte interdiffusion will be fully realized and become the predominant force. In the linear growing region, the effect of polyelectrolyte relaxation is negligible because the interdiffusion-driven deposition leads to much greater film thickness and mass.[37, 91, 97] In this regime, polyelectrolyte interdiffusion also eliminates desorption of polyelectrolytes from the assembly.[95] Consequently, every QL fabricated using 1 min deposition is thicker than that made with 5 s exposures in the linear growth region, ultimately causing

the overtaking in film thickness. This relationship between polyelectrolyte interdiffusion and film thickness also explains why the overtaking can be postponed or expedited by altering the clay/polymer concentration ratio and clay diameter, as shown in Figures 3.3 and 3.6. This proposed growth mechanism also agrees with the observed changes in thin film density (Figure 3.5b). In the first few quadlayers, the film prepared with 1 min dipping is more densely packed due to relaxation of polyelectrolytes chains. As more layers are deposited and the polyelectrolyte interdiffusion develops, it begins to dominate the change in film thickness and the packing of the multilayer assembly, eventually eliminating the difference in density beyond 4 QL.

3.4 Conclusions

Layer-by-layer polyelectrolyte deposition time was found to have a significant influence on the growth and gas barrier of clay-polymer assemblies. Regardless of thin film composition, shorter dipping time always produces a thicker film in the first few layers. This unique behavior is due to the differing growth mechanisms in the exponential and linear growing regions. During exponential growth, polyelectrolyte interdiffusion is not fully developed and the growth of the multilayer film is controlled by desorption and relaxation of oppositely charged polyelectrolytes. Films prepared with 5 s dip times are thicker and heavier because there is little time for desorption and relaxation. Linear growth, on the other hand, is primarily controlled by polyelectrolyte interdiffusion, which allows films prepared with 1 min dips to eventually be thicker and heavier. Shorter dipping time turns out to be ideal for clay-polymer assemblies because

the addition of clay suppresses polyelectrolyte interdiffusion and effectively postpones the thickening achieved with longer dips. These results are supported by cross-sectional images and ellipsometric thickness measurements. Altering the clay/polymer concentration ratio and clay diameter provides a way to further tailor the growth and barrier characteristics of multilayer thin films by controlling the extent of polyelectrolyte interdiffusion. The OTR of a film prepared with 5 s dips decreases with increasing clay diameter and films prepared with this short exposure time always have lower OTR than their 1 min counterparts. Short dipping time may even help to reduce the number of layers needed for certain applications, which would reduce processing cost and time. For instance, the MMT-based quadlayer used to require 4 QL with 1 min dipping to achieve an OTR lower than 0.5 $cm^3/(m^2 \cdot day \cdot atm)$.[16] In contrast, this level of oxygen barrier requires only 3 QL with 5 s dips. This finding is very important, because it demonstrates the ability to make useful thin films very quickly, improving the outlook for industrial-scale development of the LbL assembly technique.

CHAPTER IV

FAST SPRAY DEPOSITION OF SUPER GAS BARRIER POLYELECTROLYTE MULTILAYER THIN FILMS*

4.1 Introduction

Layer-by-layer assembly utilizes complementary interactions between components to deposit materials one layer at a time.[18, 28, 91] The deposition of each layer (usually 1-100 nm thick) has been carried out via dipping,[74, 86, 96] spraying,[20, 98, 105] or spinning.[164-166] Dipping is the most popular assembling method due to its simplicity. In fact, most of the early multilayer assemblies were made by hand-dipping a substrate into different polyelectrolyte solutions. Unfortunately, there are inherent drawbacks that limit the application of dip-assisted assembly. Dipping can be relatively slow,[107, 167-168] taking hours or even days to deposit numerous layers. Another potential drawback associated with dipping is cross-contamination of solutions, especially when dip rinsing is employed. The rinsing water can stay relatively pristine for the first few rinses, but accumulating polyelectrolyte will eventually transform the rinse into a dilute solution. Consequently, components from one solution could be carried over to another solution, leading to cross-contamination. Deposited materials can also desorb into dipping solutions by forming soluble polymer complexes with oppositely charged

*Reprinted with permission from Xiang, F. M.; Givens M. T.; Grunlan, J. C., Fast Spray Deposition of Super Gas Barrier Polyelectrolyte Multilayer Thin Films. *Industrial & Engineering Chemistry Research* **2015**, *under review*. – Reproduced by permission of ACS.

polyelectrolytes, leading to further contamination.[94-96] Finally, dipping is challenging for large objects,[109, 168] due to the need for a robot with correspondingly large dimensions, which can be expensive and cumbersome. All of these drawbacks can be eliminated with a spray-assisted process. Several studies have shown that spraying is highly uniform and can produce the same composition as dip coated thin film assemblies.[20, 105, 167]

Despite having clear advantages over dipping, spraying has been unable to replace dipping as the most common method for layer-by-layer deposition, because there is no consensus on the quality of spray-coated films. A major concern is that spray-coated assemblies are thinner than their dip-coated counterparts.[98, 107, 169] Thicker films often correspond to better properties,[16, 37, 78] so there is reduced incentive to switch from dipping to spraying. On the other hand, it has also been shown that spray-assisted multilayer deposition can achieve equal or larger thickness than dip-assisted assemblies.[105-106] The inconsistencies between these studies originate from differing deposition times used. The common deposition time used for spraying was typically a few seconds,[103, 109, 170] while dipping was 5-15 minutes for each layer.[149, 151, 171] Spray coated multilayer assemblies are usually thinner due to less developed polyelectrolyte interdiffusion, which is time dependent and plays a crucial role in film thickness.[67, 91, 172]

In the chapter, the effects of spraying pressure, spraying time, and flow rate on the thickness and roughness of spray-coated polyethylenimine [PEI]/poly(acrylic acid) [PAA] bilayers (BL) were characterized. Spraying time was found to be the dominant factor controlling film roughness and thickness. Thicker films, prepared using longer

spraying time, also exhibited better gas barrier. A sample prepared using the best spraying parameters (50 psi spraying pressure, 0.4 g/s flow rate, and 5 s deposition time) was chosen and then compared with a dip-coated sample fabricated using the same deposition time for each layer. The 7-bilayer spray-coated film was not only thicker and rougher than the dip-coated film, but also exhibited an order of magnitude lower oxygen transmission rate. Further analysis revealed that fast evaporation of excess solution during spraying prevented desorption of loosely bound polymer. This retained material added to thickness and mass accumulated in each layer and ultimately resulted in better gas barrier. This observation that spray-coated films can be thicker and less permeable than dip-coated assemblies is a major breakthrough that should serve to facilitate commercial adoption of this powerful nanocoating technology.

4.2 Experimental Section

4.2.1 Materials

All materials used here were previously described in Chapter III (Section 3.2.1).

4.2.2 Substrates

All substrates used here were previously described in Chapter III (Section 3.2.2).

4.2.3 Dip-Assisted Layer-by-Layer Assembly

The dip-assisted deposition process is identical to that described in Chapter III (Section 3.2.3).

4.2.4 Spray-Assisted Layer-by-Layer Assembly

LbL films were also assembled using an automated spraying system (Svaya Nanotechnologies, Sunnyvale, CA). The distance between the spray nozzle and target is 20 cm. All cleaned substrates were initially sprayed with PEI solution for 30 s and paused for 5 s before being rinsed with deionized water for 10 s, followed by another 10 s pause. This procedure was repeated by an identical spray, pause, rinse, and pause procedure for the PAA solution. After this initial bilayer was deposited, different numbers of layers were added using different spraying parameters, while the rinse and pause times were kept at 10 s and 5 s, respectively. The effect of every parameter was analyzed by varying the value of one parameter while keeping the value of other parameters intact. For example, the influence of varying spraying pressure (30-60 psi) was studied by keeping the spraying time and flow rate at 5 s and 0.4 g/s, respectively. The influence of varying spraying time (1-7 s) was studied by setting the spraying pressure and flow rate at 50 psi and 0.4 g/s, respectively. The influence of varying flow rate (0.2-0.8 g/s) was studied by setting the spraying pressure and spraying time at 50 psi and 5 s, respectively.

4.2.5 Film Characterization

Thin film topography and phase images were collected using a NanoSurf2 Atomic Force Microscope (AFM) (Nanoscience Instruments, Phoenix, AZ). AFM images were obtained in phase contrast mode, with free vibration amplitude of 50 mV, using a conical AFM tip (Aspire, CT170R, Phoenix, AZ) with a radius of 8 nm and resonance frequency of 170 kHz. Area roughness (Ra) of each film was calculated using

a 20 X 20 μm AFM height image. All other characterization was identical to that described in Chapter III (Section 3.2.4).

4.3 Results and Discussion

4.3.1 Influence of Spraying Parameters on Film Thickness and Roughness

The influence of varying key spraying parameters on the thickness of PEI/PAA assemblies was evaluated in an effort to obtain the thickest films. As shown in Figure 4.1, although higher spraying pressure and larger flow rate generates slightly larger thickness, spraying time is most important for controlling film thickness. Increasing the spraying time from 1 to 7 s produces more than 100% increase in film thickness (from 292 to 683 nm). The relationship between spraying time and film thickness can be explained by the two growth regimes shown in Figure 4.1b. Similar to dip-coated assemblies,[37] spray-coated thin films grow non-linearly at first (< 5 BL), with each layer being relatively thin. In the second regime, the film growth becomes linear, and the thickness of each layer is much greater. For the 538 nm thick 7 BL PEI/PAA assembly shown in Figure 4.1b, more than 85% of the film thickness (461 nm) was accumulated in the second regime. Multilayer growth in the second regime is known to be controlled by the extent of polyelectrolyte interdiffusion,[67, 91, 172] which is highly time-dependent. Longer spraying time enables more polyelectrolyte interdiffusion, which helps each layer to grow thicker in this second growth regime (ultimately leading to a larger total film thickness). It should be noted that the thickness of a spray-assisted 7 BL PEI/PAA

assembly (538 nm) is greater than that of its dip-assisted counterpart (365 nm) prepared using the same 5 s deposition time.

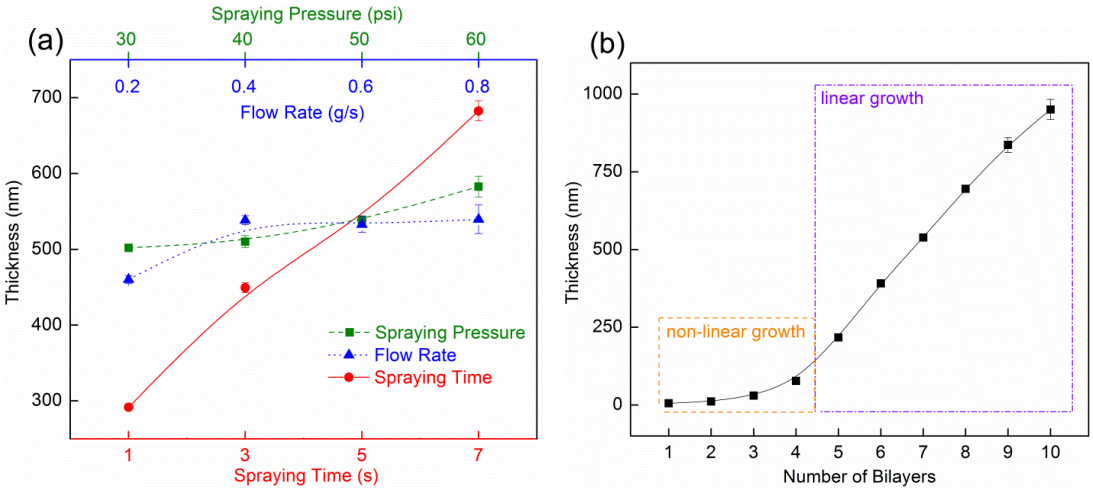

Figure 4.1. Film thickness of spray-coated 7 BL PEI/PAA assemblies as a function of varying spraying pressure, flow rate, and spraying time (a). Thickness of film with optimized spraying parameters (50 psi, 0.4 g/s, 5 s) as a function of PEI/PAA bilayers deposited (b). [Lines were added to guide the eye]

In addition to thickness, another important trait of spray-coated multilayers is surface roughness. Spray-coated thin films were found to have similar or higher surface roughness than dipped films.[98, 105, 107] In this study, the influence of spraying pressure, spraying time, and flow rate on the roughness of 7 BL PEI/PAA assembly were evaluated. The average roughness values shown in Figure 4.2 were calculated using 20 X 20 µm AFM height images (Figure 4.3a, c, e, g, i-n). It can be seen that the influence of the spraying parameters on roughness are very similar to their influence on thickness. Spraying time produces the most significant change in film roughness. It should be noted that the surface roughness remained nearly constant when varying spraying pressure and

flow rate, suggesting that the splash of water droplets upon reaching the substrate surface was negligible in this study. Surface roughness of a sprayed 7BL PEI/PAA assembly (21 nm) is greater than its dipped counterpart (5 nm) prepared using the same 5 s deposition time.

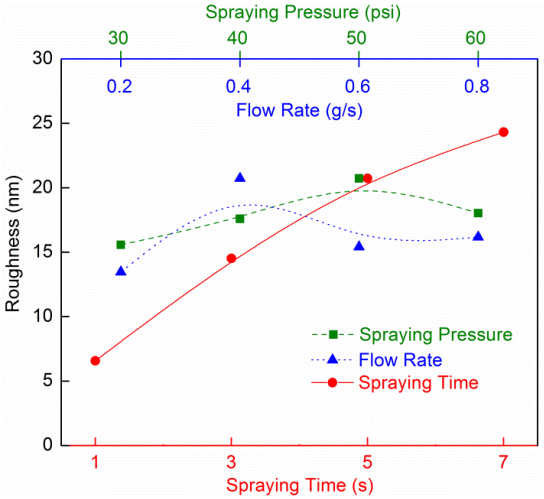

Figure 4. 2. Surface roughness of spray-coated 7 bilayer polyethylenimine/poly(acrylic acid) assemblies as a function of varying spraying pressure, flow rate, and spraying time. [Lines were added to guide the eye]

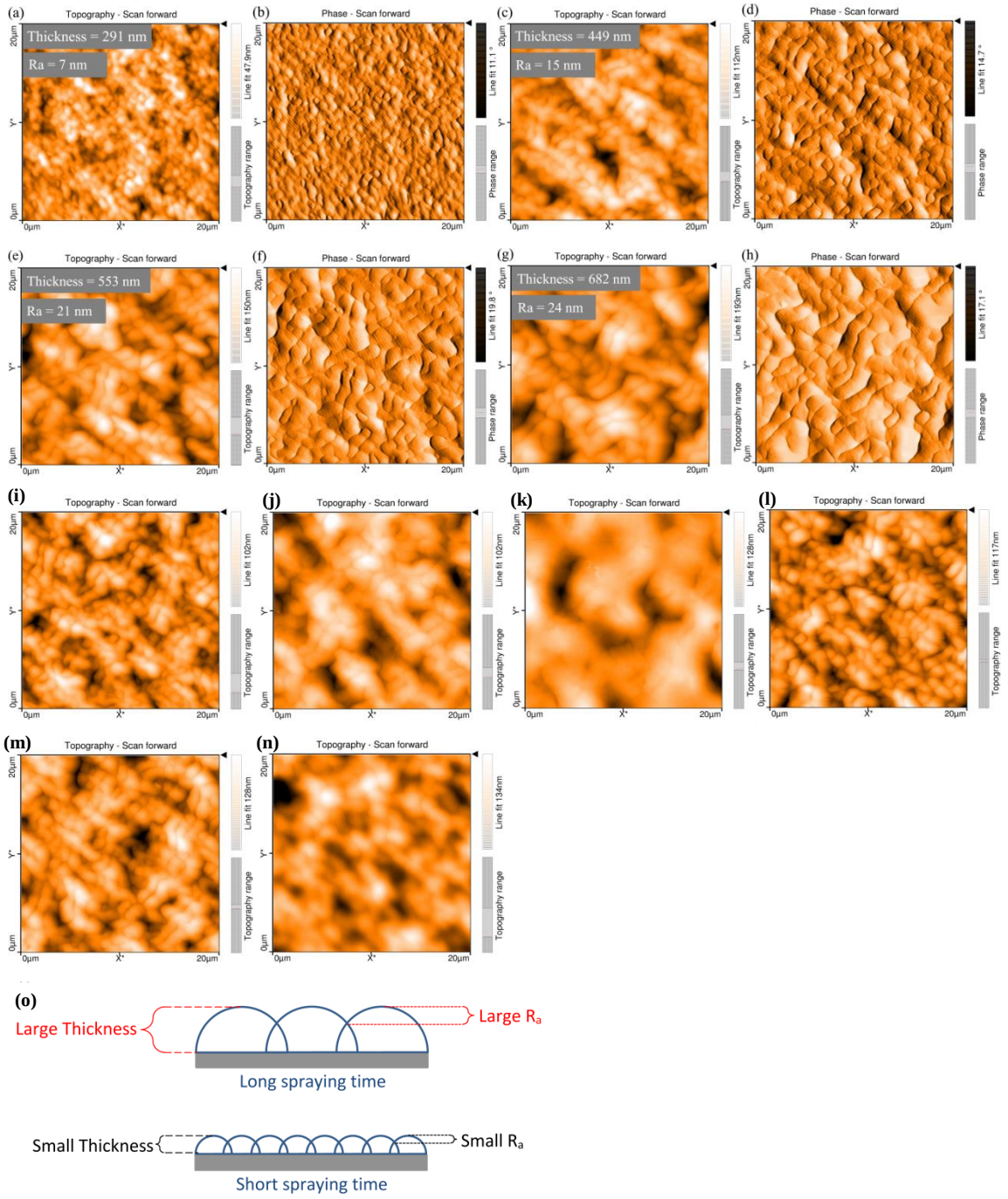

Figure 4.3. AFM topography (a, c, e, g, i-n) and phase (b, d, f, h) images of 7 BL PEI/PAA films prepared with 1 (a, b), 3 (c, d), 5 (e, f), 7 seconds (g, h) spraying time, 0.2 (i), 0.6 (j), 0.8 g/s (k) flow rate, and 30 (l), 40 (m), 60 psi (n) spraying pressure. Schematic side view of film growth highlights how larger islands correspond to greater thickness and roughness in spray-assisted assemblies (o).

The similar influences of varying spraying parameters on deposited film thickness and roughness is explained in Figure 4.3o, which describes the unique growth mechanism of layer-by-layer assembly. During the initial stage of film growth (1st regime in Figure 4.1b), the substrate is covered by islands rather than by a uniform film.[91] These islands grow laterally as more layers are added and subsequently connect with each other, eventually resulting in uniform coverage. As can be seen in Figure 4.3a and 3b, the islands associated with 1 s spraying time are significantly smaller than on films prepared using longer spray time (Figure 4.3c - h). Increasing the spraying time prolongs the deposition time, enabling more polyelectrolyte interdiffusion and larger island growth. The growth of islands is three dimensional, so those with larger horizontal diameter also have greater thickness overall. As shown in Figure 4.3e, a thicker film also exhibits greater variation over its surface, which ultimately leads to larger roughness.

4.3.2 Gas Barrier of Spray-Coated Multilayer Assemblies

The most important factors that control gas barrier of multilayer thin films are composition,[141, 173] intermolecular bonding,[37, 76] and thickness.[74, 174] All films studied here are comprised of polyethylenimine and poly(acrylic acid), assembled at the same pH, so the composition and intermolecular bonding are expected to be very similar.[105, 167] It is not surprising that oxygen transmission rate (OTR) of PEI/PAA films prepared using varying parameters was found to be closely related to their thickness, as shown in Figure 4.4. Spraying pressure appears to have little impact on gas barrier, while flow rate and spraying time have a significant influence. A 7 BL PEI/PAA film deposited with 0.2 g/s flow rate exhibits the highest OTR (i.e., worst gas barrier), possibly due to

insufficient material depositing on the PET substrate. Increasing the flow rate to 0.4 g/s results in a noticeable improvement, but further increasing the flow rate does not produce better gas barrier. The influence of flow rate on gas barrier mirrors its influence on film thickness (Figure 4.1a). Spraying time appears to be the most effective parameter for altering gas barrier. The OTR of 7BL PEI/PAA can be reduced from 0.54 to 0.07 $cm^3/(m^2 \cdot day \cdot atm)$ by increasing the spraying time from 1 to 7 s. Increasing the spraying time from 5 to 7 s only leads to slightly improved gas barrier (from 0.08 to 0.07 $cm^3/(m^2 \cdot day \cdot atm)$), so 5 s was chosen as the best value to save time and materials. A multilayer film prepared with the best spraying parameters (50 psi, 0.4 g/s, 5 s) was compared with a dip-coated assembly prepared using the same deposition time. It was interesting to see that the spray-coated sample had an order of magnitude lower OTR (0.08 $cm^3/(m^2 \cdot day \cdot atm)$) than the dip-coated film (0.91 $cm^3/(m^2 \cdot day \cdot atm)$). This result contradicts a well-accepted belief that spraying leads to thinner films with worse properties, and could potentially expand the use of spray-assisted layer-by-layer assembly.

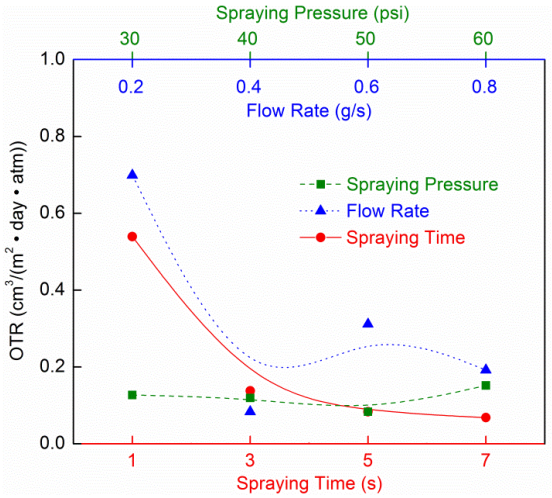

Figure 4.4. Oxygen transmission rate of spray-coated 7 bilayer PEI/PAA assemblies as a function of varying spraying pressure, flow rate, and spraying time. [Lines were added to guide the eye]

4.3.3 Spraying Deposition Mechanism

In an effort to better understand the behavior of spray-coated thin films, various traits of PEI/PAA prepared using different deposition methods were compared. Spray and dip-coated multilayer thin films exhibit similar thickness in the first few bilayers (< 5 BL), as shown in Figure 4.5a. Adding more layers leads to a noticeable difference in thickness. At 7 BL, the thickness of the spray-coated film (538 nm) is much larger than that of the dip-coated film (365 nm). A similar trend is observed for the mass of these assemblies, as shown in Figure 4.5b. Spray-assisted assembly accumulates more mass after the first few bilayers are deposited. With known thickness and mass, film density can be derived, as shown in Figure 4.5c. The density of spray and dip-coated films oscillates between 0.8 and 2 g/cm^3 initially, before remaining almost constant beyond 5

bilayers. PEI/PAA prepared using dip-assisted assembly (~ 1.8 g/ cm^3) is modestly denser than films made using spray-assisted assembly (~ 1.5 g/ cm^3).

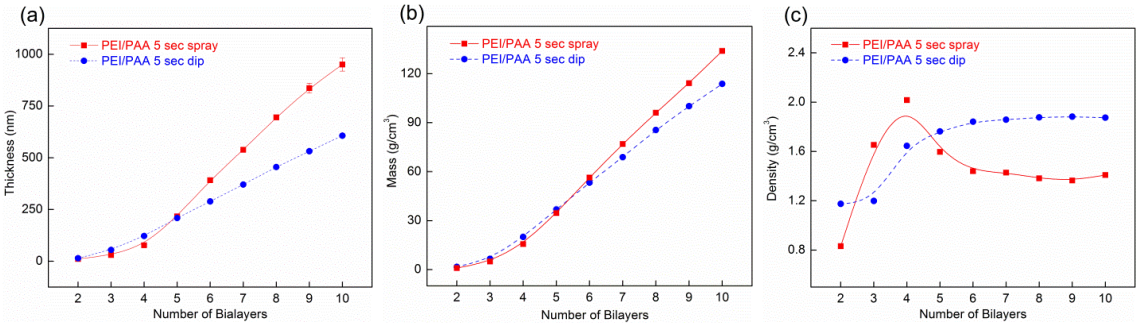

Figure 4.5. Thickness (a), mass (b), and density (c) of spray and dip-coated PEI/PAA multilayer thin films prepared using 5 s deposition time. [Lines were added to guide the eye]

The differences observed between spray and dip-coated thin films can be explained by differences between the two deposition mechanisms, as shown in Figure 4.6. With spraying, polymer solutions are typically deposited onto a vertically-positioned substrate. The polymer solutions consists of very fine droplets, which either leads to the formation of a very thin layer of solution or quickly evaporates upon reaching the surface.[98, 175] Additionally, the vertical position of the substrate allows for excess solution to be rapidly drained, further facilitating the evaporation of polyelectrolyte solutions on the substrate surface. In the dipping process, a substrate is continuously soaked in a given polyelectrolyte solution. Loosely bound polyelectrolytes tend to form soluble complexes with the oppositely charged polyelectrolyte in the surrounding solution, leading to desorption of loosely bound material.[94-96] This complexation and

desorption is largely avoided with spraying for the reasons just mentioned (i.e., draining and fast evaporation). Better retention of polyelectrolytes makes spray-coated films significantly thicker than their dip-coated counterparts (Figure 4.5a), which is also indirectly confirmed by the larger islands observed in the corresponding AFM phase images in Figure 4.6.

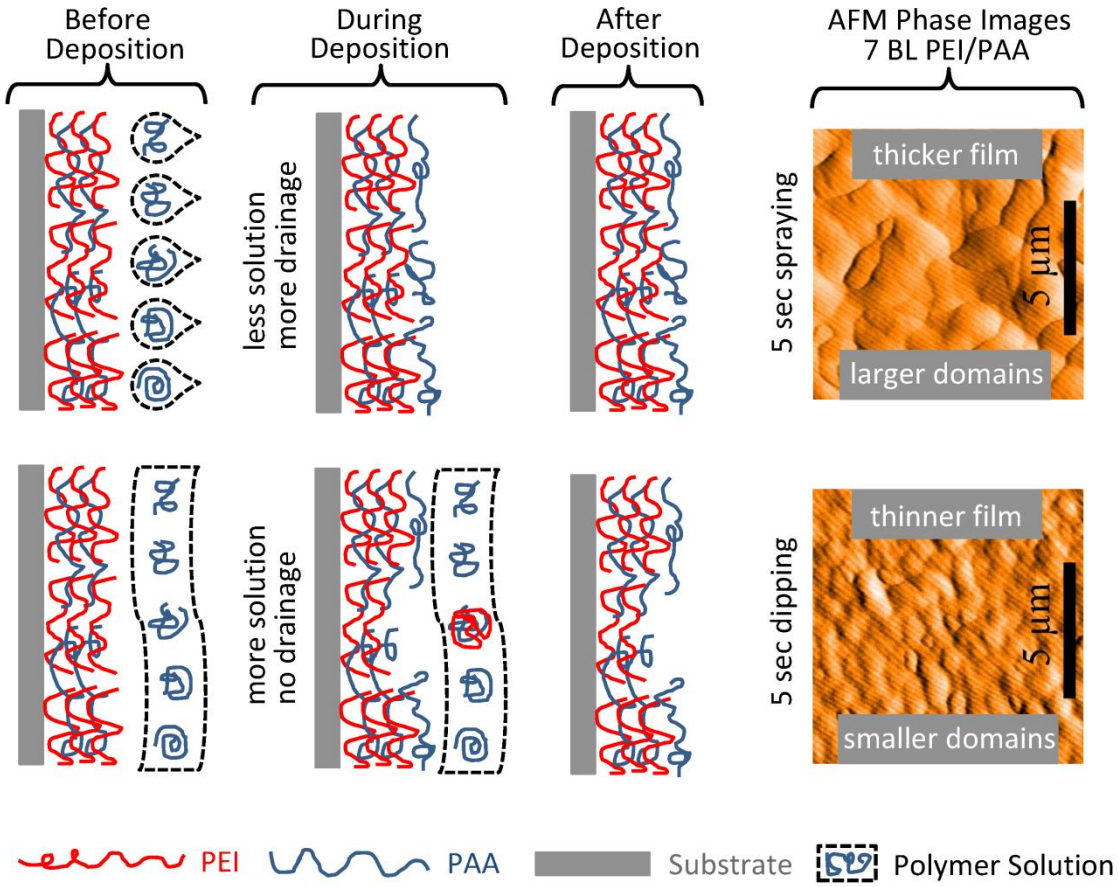

Figure 4.6. Schematic showing the differences between spraying (top) and dipping (bottom) deposition of polyelectrolytes. AFM images were used to support the schematic concepts.

This proposed growth mechanism also explains the density difference between films deposited via spraying or dipping (Figure 4.6). Loosely bound polymer chains can be more effectively removed in the dipping process, which results in a thinner yet more compact assembly. The gas barrier of conventional polymeric films depends primarily on the density of the polymer, because the bonding between polymers chains is Van der Waals. On the contrary, polymer chains are bonded by much stronger bonds (ionic, hydrogen, etc.) in layer-by-layer assembly. As a result, the gas barrier of LbL thin films is a function of both density and number of internal bonds. Since layer-by-layer assemblies prepared using loosely bonded components are known to have a diffused internal structure,[49, 66, 111] the spray-coated thin film with more loosely-bonded polyelectrolytes should have higher level of polymer interdiffusion than that in a dip-coated thin film. This diffused structure could help to establish more electrostatic bonds between polymer chains, leading to better gas barrier.[37] The combination of larger film thickness and more electrostatic bonds should be more than enough to offset the slightly lower density on gas barrier, allowing spray-coated films to display lower oxygen permeability for a given number of deposited layers.

4.4 Conclusions

Layer-by-layer deposition of polyethylenimine and poly(acrylic acid) was performed with spraying and dipping. Spray-assisted film thickness was found to be independent of spraying pressure, but strongly influenced by flow rate and spray time. Insufficient flow rate (0.2 g/s) resulted in reduced film thickness and lower gas barrier.

Increasing the flow rate to 0.4 g/s increased thickness and reduced oxygen transmission rate. It was interesting to note that thicker, rougher films with better gas barrier were also obtained using longer spraying time, but the benefits diminished beyond 5s. A 7 BL PEI/PAA film prepared using the best spraying parameters (50 psi, 0.4 g/s, 5 s) resulted in a thickness of 538 nm and an OTR of 0.08 $cm^3/(m^2 \cdot day \cdot atm)$. Preparing the same 7 BL film with dipping produced a thinner film with an order of magnitude greater OTR. Further analysis revealed that spraying effectively eliminates excess polyelectrolyte solution near the assembly surface, leading to desorption of previously deposited yet loosely attached polymer. Better retention of deposited material results in a slightly less compact but thicker assembly. The combination of larger thickness and more electrostatic bonds makes the spray-coated film a better gas barrier for a given number of deposited layers. This demonstration of fast deposition and better thin film properties from spray-assisted layer-by-layer assembly is a significant breakthrough. Spraying of a continuously moving substrate is a likely method of using LbL deposited thin films commercially.

CHAPTER V

SUPER STRETCHY POLYMER MULTILAYER THIN FILMS WITH TUNABLE GAS BARRIER*

5.1 Introduction

Multilayer thin film assemblies are well known for their ability to provide high barrier to gases,[16, 37, 75, 176-178] but they are typically very stiff (as high as 106 GPa),[37, 90, 179] making them unsuitable for high strain applications. For example, extensive mud-cracking was observed on the post-stretched surface of a 125 nm thick polyethylenimine/montmorillonite clay assembly, whose oxygen transmission rate (OTR) increased more than 40x after 10% stretching.[110] The brittleness of existing gas barrier thin films originates from their composition and bonding type. LbL films assembled with clay are highly brittle due to the inherent rigidity of clay platelets[180] and clay concentrations (exceeding 70 wt%).[90] Even without clay present, multilayer thin films assembled using electrostatic bonding are also very stiff, because movement of polymer chains is restricted by the strong and numerous ionic crosslinks between them.[37, 67] Hydrogen bonding features smaller bond strength and looser crosslinking density,[28, 114-115, 171] relative to ionic bonding, allowing for easier polymer chain

*Parts of this chapter are reprinted with permission from Xiang, F. M.; Ward, M. S.; Givens, M. T.; Grunlan, J. C., Super Stretchy Polymer Multilayer Thin Film with High Gas Barrier. *ACS Macro Lett.* **2014**, *3*, 1055-1058**.** © 2014 ACS. And from Xiang, F. M.; Ward, M. S.; Givens, M. T.; Grunlan, J. C., Structural tailoring of hydrogen-bonded poly(acrylic acid)/poly(ethylene oxide) multilayer thin films for reduced gas permeability. *Soft Matter*. **2014**, *in press***.** © 2015 Royal Society of Chemistry.

mobility and enhanced thin film ductility. On this basis, it can be concluded that LbL films without rigid nanoparticles (e.g. clay) and electrostatic bonding are more likely to be stretchable. It is for this reason that thin films assembled using poly(acrylic acid) [PAA] and poly(ethylene oxide) [PEO] were studied in an effort to produce a stretchy gas barrier nanocoating for elastomeric substrates.

5.2 Experimental Section

5.2.1 Materials

Some of the materials used here were previously described in Chapter III (Section 3.2.1). N-propanol were purchased from Sigma-Aldrich (Milwaukee, WI). Polyethylene oxide (Mw = 4,000,000 g/mol) was purchased from Polysciences (Warrington, PA). Prior to deposition, the pH of each PEO solution (0.1 wt%), PAA solution (0.1 wt%), and 18 mΩ deionized (DI) rinsing water was altered to the same specified value using 1 M HCl.

5.2.2 Substrates

Most of the substrates used here were previously described in Chapter III (Section 3.2.2). Natural rubber film, with a thickness of 1.58 mm, was purchased from McMaster-Carr and used for oxygen transmission rate testing. The rubber was rinsed with DI water, soaked in n-propanol at 40 °C for 10 min, and rinsed again with n-propanol and DI water before being dried with compressed air. Polypropylene sheets were used as substrates for making free-standing films that were used for DSC and FTIR

testing. Polypropylene sheets were cut to 10 × 3 cm strips, then rinsed with methanol and DI water before deposition.

5.2.3 Layer-by-Layer Deposition

Most of the film preparation conditions are identical to those described in Chapter III (Section 3.2.3). Prior to deposition, All cleaned substrates were initially dipped into a 0.1 wt% PEI solution (unaltered pH ~ 10.5) for 10 min and then rinsed with DI water to generate a primer layer.

5.2.4 Film Characterization

An Instron 4411 tensile tester was used to stretch samples at ambient conditions (23 oC, 45% RH) to different strain levels (25, 50, and 100%). Strain rate was set at 20 inch/min, and each sample was held at a given strain level for 2 min before being released. Surface morphology of 20 BL PAA3/PEO3 coated natural rubber films, before and after stretching, was imaged using a JSM-7500F FESEM (JEOL, Tokyo, Japan). Prior to imaging, each film was coated with 3 nm of platinum/palladium to reduce surface charging. A Bruker Dimension Icon AFM was used to determine the elastic modulus of the thin films. All quantitative nanomechanical property mapping measurements were conducted at ambient conditions (24 oC, 45% RH). The half angle, tip radius, and spring constant of the AFM tip (Tap150A, Bruker) are 18o, 8 nm, and 5 N/m, respectively. The ramp size used for all tests was set at 397.2 nm. 40 BL PAA/PEO thin films assembled at different pH were used to prevent the influence of silicon substrate on test results. The reported modulus of each sample was the average of 20

measurements. All other characterization was identical to that described in Chapter IV (Section 4.2.5).

5.3 Results and Discussion

5.3.1 Influence of Assembling pH on Glass Transition Temperature and Modulus

Multilayer thin films assembled with H-bond donating PAA and H-bond accepting PEO are already known to exhibit excellent ductility. It was reported that a 100 bilayer (BL) free-standing PAA/PEO film was stretched to five times its original length before breaking.[114] Mechanical testing of PAA/PEO thin films, assembled at varying pH, reveals that the softest film can be obtained at pH 3 (referred to as PAA_3/PEO_3). The 20 BL PAA_3/PEO_3 assembly not only exhibits reasonable gas barrier when unstretched, but is capable of preserving much of its gas barrier even after 100% strain. This study marks the first report of a super stretchy gas barrier that can be used in applications requiring a gas barrier coating able to withstand large-strain (>25%), such as inflatable elastomers used in tires and seals.

Figure 5.1a shows how the glass transition temperature (T_g) of 100 BL free-standing PAA/PEO assemblies decreases with increasing deposition pH due to less carboxylic acid dimer and more deprotonated acid groups (detailed information about film buildup and characterization is provided in Experimental Section in Supporting Information).[112, 171] The DSC curves of all samples can be found in Supporting Information (Figure 5.2). This change in T_g results in a corresponding change in room temperature elastic modulus of 40 BL PAA/PEO thin films, also shown in Figure 5.1a,

which was measured using an atomic force microscope (AFM). In this experiment, a standard AFM probe was used to obtain a force-distance curve.[181-182] The elastic modulus was calculated using the retraction curve near the peak force, in conjunction with the Hertz model. A remarkable drop in modulus is observed when the glass transition temperature becomes lower than the testing temperature (23 ^{o}C). The softest PAA/PEO thin films, obtained at pH 3, were used in the following gas barrier and strain testing to minimize the possibility of cracking during stretching. Similar to previous findings,[112] the thickness of PAA/PEO assemblies is found to decrease with increasing pH, as shown in Figure 5.1b. The PAA/PEO assemblies investigated here are thinner than those reported earlier due to shorter deposition time used in this study (1 min instead of 10 min).[112] PAA/PEO thin films assembled beyond pH 3 were not investigated because film growth becomes very inconsistent.[114]

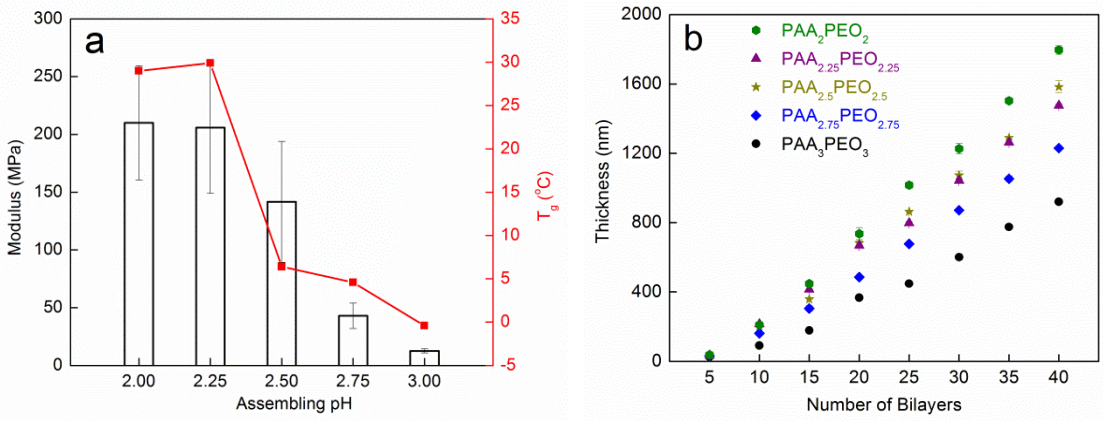

Figure 5.1. Elastic modulus and glass transition temperature as a function of deposition pH for PAA/PEO multilayer thin films (a). Thickness as a function of PAA/PEO bilayers deposited at varying pH (b).

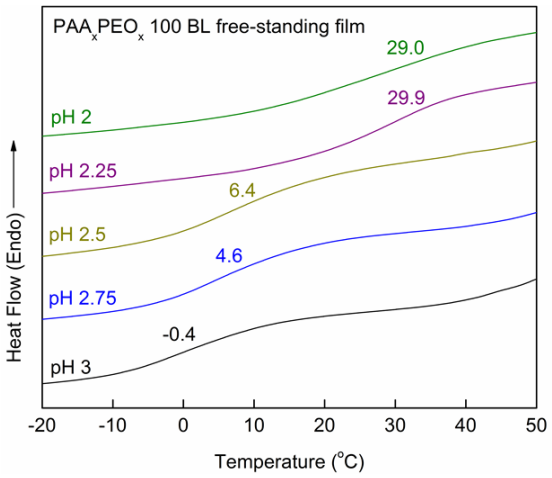

Figure 5.2. DSC curves of 100 BL PAA_3/PEO_3 free-standing films assembled at different deposition pH.

5.3.2 Effect of Stretching on Gas Barrier of PAA/PEO Assembly

Polymer thin films with high gas barrier usually have high cohesive energy density,[118] which prevents gas molecules from moving aside polymer chains.[183-184] Despite being weaker than electrostatic bonding, hydrogen-bonding between polymer chains imparts reasonable gas barrier to the assembly. As shown in Figure 5.3, a 367 nm thick 20 BL PAA_3/PEO_3 nanocoating can reduce the OTR of 1.58 mm thick natural rubber by one order of magnitude (from 840.1 to 87.6 $cm^3/(m^2 \cdot day \cdot atm)$). Although stretching reduces gas barrier in general, increasing the strain level does not lead to larger OTR and barrier remains a factor of five better than uncoated rubber at 100% strain.

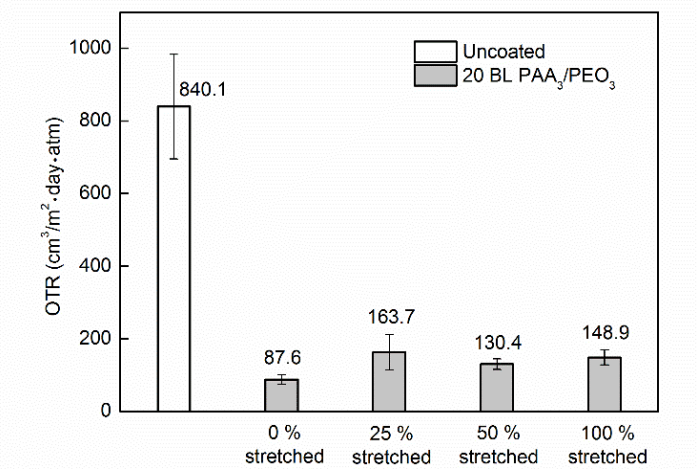

Figure 5.3. Oxygen transmission rate of 1.58 mm natural rubber sheet, coated with 20 BL PAA_3/PEO_3, stretched to varying extents.

5.3.3 Deformation Mechanism of PAA/PEO Assembly

In an effort to better understand the influence of stretching on gas barrier, surface morphology of coated samples before and after stretching was imaged with a field emission scanning electron microscope (FESEM). As shown in Figure 5.4a, the 20 BL PAA_3/PEO_3 nanocoating is quite smooth at 0% strain. Stretching to 25 and 50% strain has little influence on surface morphology, except for the formation of a few shallow lines perpendicular to the stretch direction. These lines become more dense and pronounced when the strain level reaches 100%. When observed at a higher magnification (Figure 5.4e), these lines appear to be creases rather than cracks.

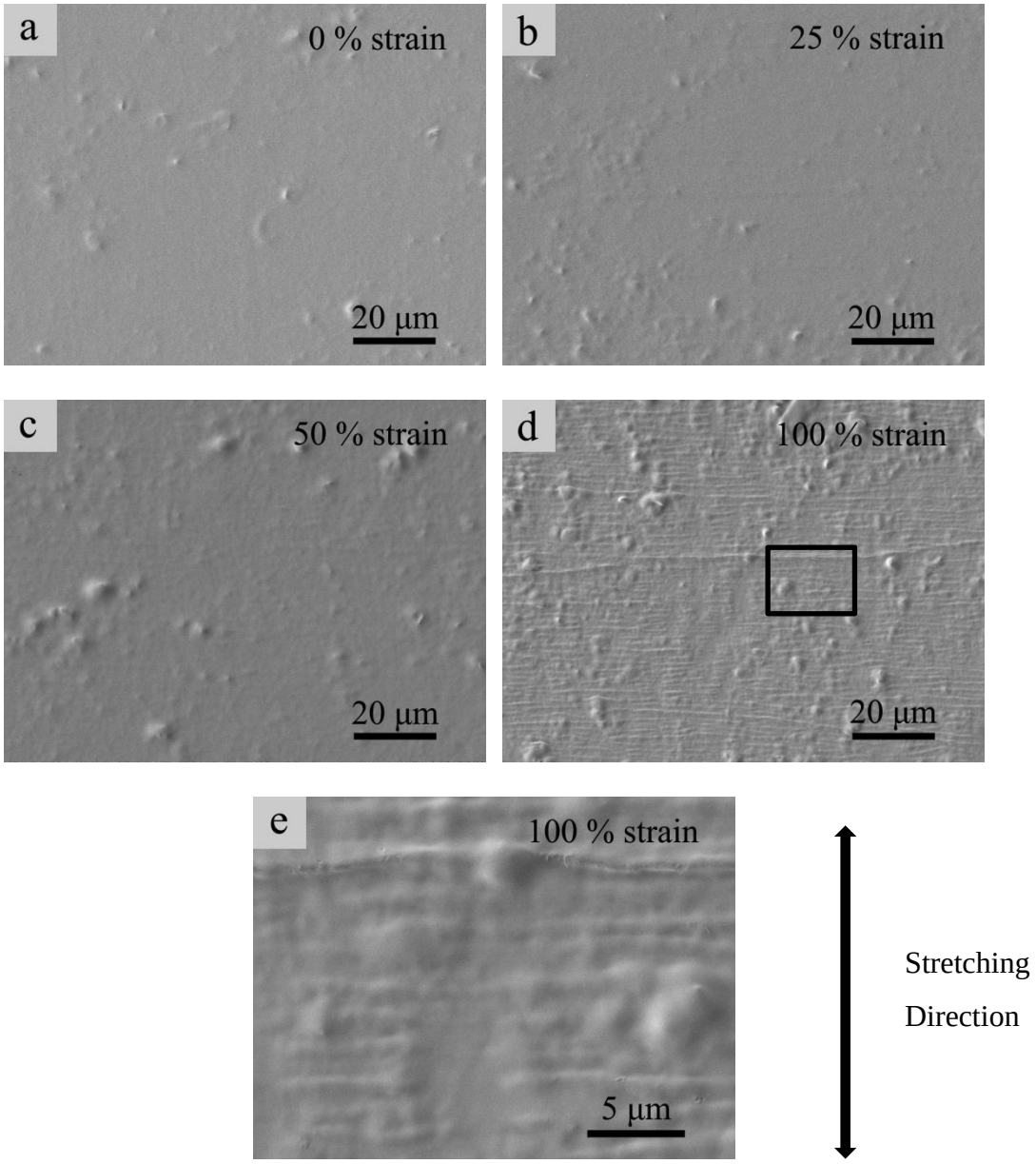

Figure 5.4. FESEM surface images of 20 BL PAA_3/PEO_3 coated rubber after 0 (a), 25 (b), 50 (c), and 100% (d, e) strain [(e) is the magnified image of the area indicated in (d)].

The influence of stretching on structure and morphology can be correlated with the gas barrier of the PAA_3/PEO_3 assembly using the mechanism proposed in Figure 5.5. It was reported that $PAA_{2.5}/PEO_{2.5}$ transformed from elastic to plastic deformation around 10% strain.[114] Since both $PAA_{2.5}/PEO_{2.5}$ and PAA_3/PEO_3 exist in their rubbery state under ambient conditions (23 ^oC, 45% relative humidity (RH)), it is reasonable to assume that both would exhibit similar tensile behavior and become plastically deformed at 25%, as shown schematically in Figure 5.5b. Although plastic deformation has little influence on morphology, it leads to reduced gas barrier, possibly due to thinning of film. Figure 5.5c shows that increasing the strain level to 100% induces plastic deformation at multiple locations. The plastically extended parts of the film fold up after being released, resulting in creases perpendicular to the stretching direction. It is interesting to note that although a remarkable change in surface morphology can be observed after 100% stretching, the OTR of this sample is nearly identical to films tested with lower strain levels. It is believed that smaller, less visible plastic deformation generated at lower strain levels (25 and 50%) reduce the gas barrier of the 20 BL PAA_3/PEO_3 thin film. It is a bit surprising that larger and more visible plastic deformations generated at 100% strain did not further reduce gas barrier. As can be seen in Figure 5.3, the oxygen transmission rate of 25, 50, and 100% strained samples are statistically the same. This result suggests that plastically deformed films have similar gas barrier, regardless of the extent of the damage. There would likely be another drop in barrier upon rupture of the film, but this did not occur up to 100% strain.

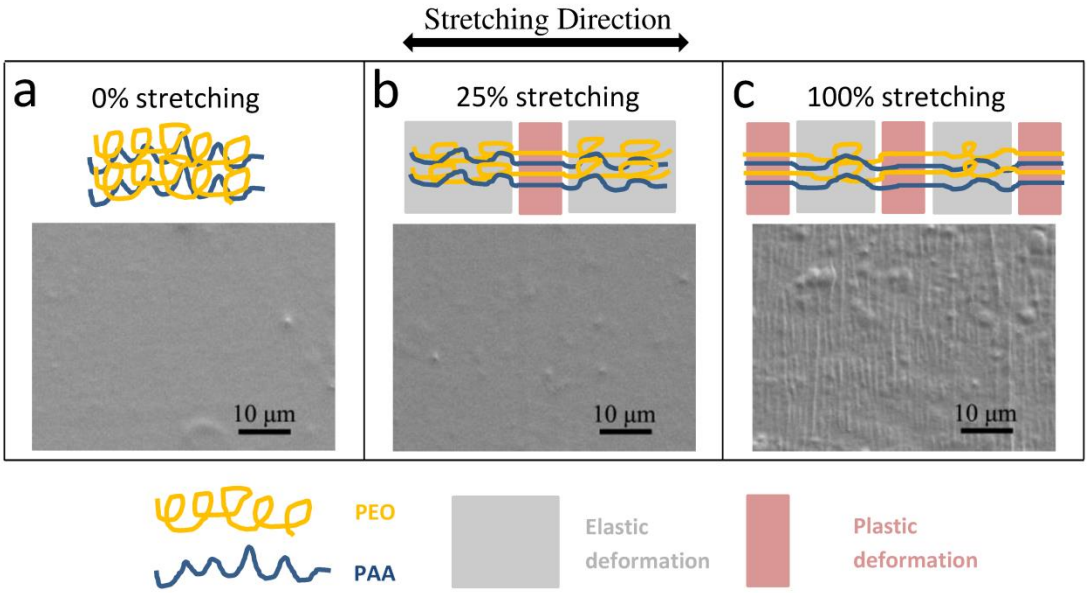

Figure 5.5. Schematic showing the influence of different strain levels 0% (a), 25% (b), 100% (c) on structure and morphology of PAA_3/PEO_3 assembly (FESEM surface images are below each schematic).

As mentioned in the preceding discussions, the greater openness of PAA/PEO hydrogen-bonded assembly reduced its gas barrier relative to its electrostatically-bonded counterpart. In an effort to improve the gas barrier of H-bonded multilayer films, oxygen permeability of PAA/PEO thin films is studied as a function of assembling pH. It is found that the permeability first decreases (pH< 2.75) and then increases (pH> 2.75) with increasing pH. PAA/PEO thin films assembled at pH 2.75 exhibit the lowest permeability due to suppressed COOH dimerization and acid ionization, leading to the establishment of the greatest number of intermolecular hydrogen bonds between PAA and PEO. This preferential bonding between H-bond donor and H-bond acceptor also leads to a more homogeneous morphology with smaller dispersed PEO domains. Moreover, the fundamental knowledge about bonding preference, phase morphology and

gas barrier of PAA/PEO assemblies provides an understanding of the structure-property relationships in hydrogen-bonded assemblies.

5.3.4 Effect of PAA Ionization on Multilayer Film Growth

Layer-by-layer assembly of PAA/PEO thin films is driven by hydrogen bonding between carboxylic acid groups of PAA (as H-bond donors) and ether groups of PEO (as H-bond acceptors).[112] Although the ability of PEO to act as a hydrogen bond acceptor is unaffected by solution pH due to its non-ionic nature, the capability of PAA to act as hydrogen bond donor is highly dependent on assembling pH.[28, 115] As shown in Figure 5.6, with only 5% of COOH groups charged at pH 3.5,[185] the repulsive force between COO^- groups is large enough to prevent the growth of the PAA/PEO assembly.[112] Decreasing assembling pH leads to greater film thickness, due to protonation of COO^- groups, which reduces the intensity of the repulsive force and provides more H-bond donor sites. The influence of pH on film thickness becomes negligible at pH $\leq$ 2.5 due to complete protonation of carboxylic acid groups on PAA. At pH between 2.5 and 3.5 there is a modulation window,[112] in which PAA is partially ionized.

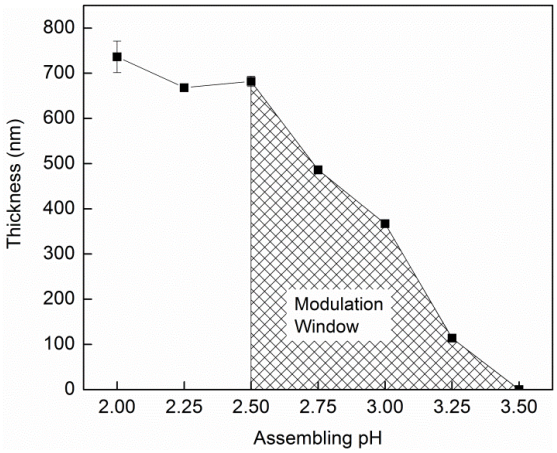

Figure 5.6. Thickness of 20-BL PAA/PEO thin films as a function of assembling pH.

5.3.5. Intermolecular Interactions and Thin Film Composition

Poly(acrylic acid) can form either intramolecular hydrogen bonds with itself, through COOH dimerization, or form intermolecular H-bonds with PEO.[114] The ratio of intra- to inter molecular bond can be quantified using FTIR. The two absorption peaks located at ~1710 and ~1740 cm^{-1} correspond to COOH groups bonded by intra- and intermolecular hydrogen bonds, respectively.[186] As can be qualitatively observed in Figure 5.7a, the peak corresponding to intermolecular bonded COOH at 1733 cm^{-1} grows at the expense of the other peak located at 1705 cm^{-1}, indicating more PAA bonds with PEO as pH increases. Spectral deconvolution of all samples is provided in Supporting Information (Figure 5.8). The percentage of intermolecular H-bonded COOH was calculated using the method developed by Coleman: intramolecular H-bonded COOH = $(area_{1705}/(area_{1705}/a_r + area_{1733}))$.[187] The absorptivity ratio (a_r) was assumed to be 1.6.[171] As can be seen in Figure 5.7b, the percentage of intermolecular hydrogen bonding increases with pH (from 2 to 3), which agrees well with previous findings.[114, 188]

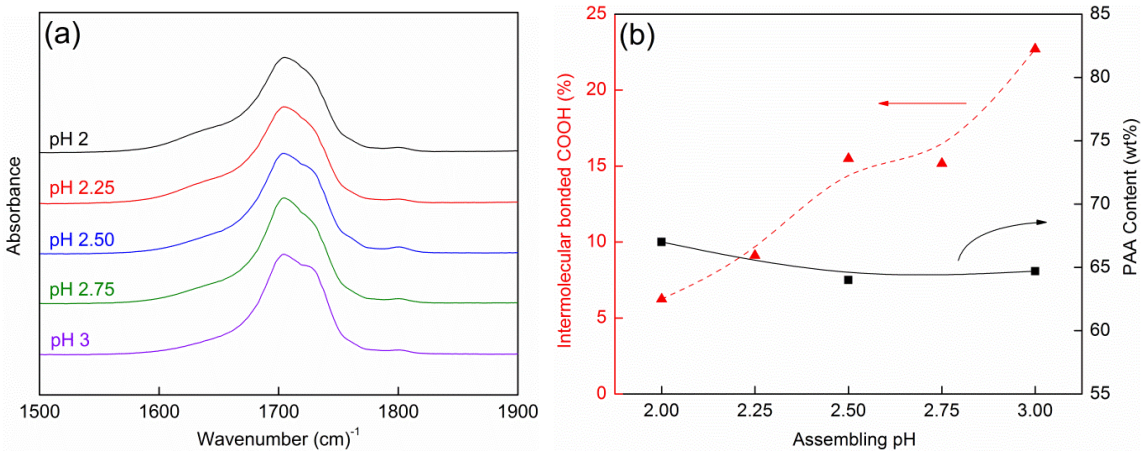

Figure 5.7. FTIR spectra of the COOH region of PAA/PEO multilayer thin films assembled at varying pH (a). Percentage of intramolecular-bonded COOH [triangles], and PAA content [squares] in the film, as a function of pH (b). [Lines were added to guide the eye]

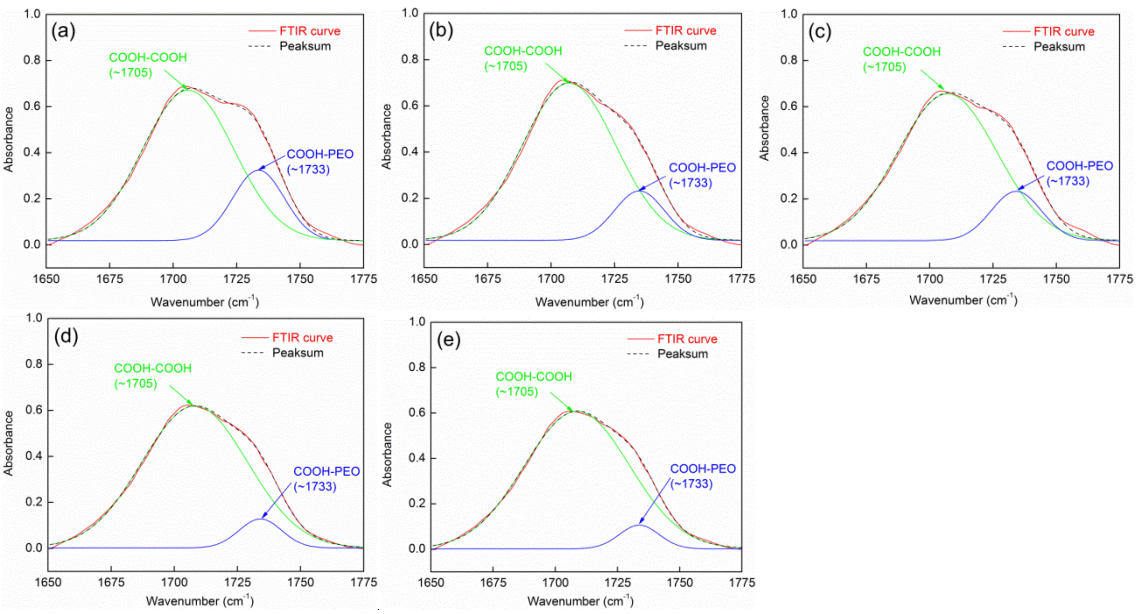

Figure 5. 8. FTIR spectra (red solid curve) of the carboxylic acid region of (PAA/PEO) multilayers assembled at pH 3 (a), 2.75 (b), 2.5 (c), 2.25 (d), 2(e). The contributions from intramolecular hydrogen bonding (green curve, ~1705 cm^{-1}) and intermolecular hydrogen bonding (blue curve, ~1733 cm^{-1}) were calculated assuming the summation of two Gaussian peaks. The peak summation was presented as black dashed curve.

It is interesting to note that the remarkable change in PAA bonding preference does not alter film composition, as proposed in other studies. In fact, according to quartz crystal microbalance (QCM) measurements, PAA content remains around 65 wt% over the entire pH range (Figure 5.7b). This result differs from the findings of previous studies, which suggested that PAA content increased with decreasing pH.[114, 171] According to the proposed hypothesis in these earlier studies, PAA's tendency to bond with itself at lower pH reduces its ability to bond with PEO. Consequently, more PAA was incorporated into the thin film assembly to bond with PEO (to offset its low bonding efficiency), leading to increased PAA content. It should be noted that although elemental analysis and thermogravimetric analysis were used to confirm this concept, the results were inconclusive.[114, 171] This inability of the old hypothesis to explain the constant content of PAA at different pH provides motivation to propose a new model that describes internal structure and intermolecular interactions of the PAA/PEO assemblies, which are closely related to the oxygen permeability of these multilayer thin films.

5.3.6. Thin Film Crystallinity

Figure 5.9 shows the second heating scan for 100 BL freestanding PAA/PEO films cycled between -40 and 80 ^{o}C. A single glass transition temperature can be observed for all samples, indicating a macroscopically homogeneous structure within the assembly. A high-temperature melting peak around 66.2 ^{o}C can be observed in all samples (associated with PEO). An additional low-temperature melting peak around 51.5 ^{o}C appears in samples assembled at higher pH (2.75 and 3). This low temperature peak grows at the expense of the high-temperature melting peak with increasing pH.

Variation in the melting peak of PEO is believed to originate from microscopic phase separation within the macroscopically homogeneous PAA/PEO assembly.[189] The emergence of a low-temperature melting peak corresponds to thinner crystals that formed in smaller PEO domains. Based on this finding, it is assumed that the size of PEO domains become smaller at higher pH.

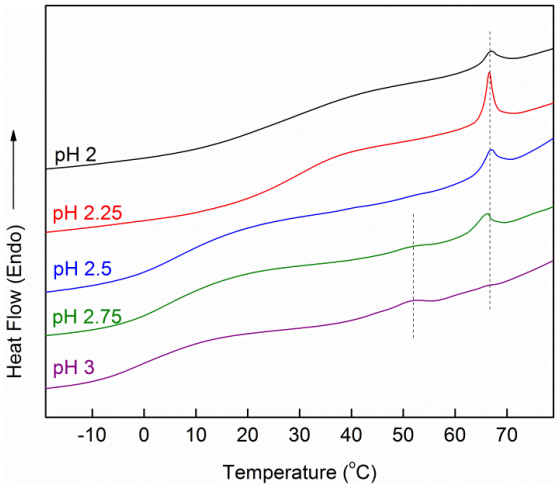

Figure 5.9. Heating curves for PAA/PEO free-standing films assembled at varying pH.

Polymer crystallinity plays an important role in gas barrier due to the impermeable nature of most polymer crystals, and PEO is known to be semi-crystalline in hydrogen-bonded multilayer assemblies.[189] It is for these reasons that the crystallinity of PEO within PAA/PEO multilayer assemblies is analyzed. The enthalpy of melting for each sample was calculated using the heating curves shown in Figure 5.9. The crystallinity (X_c) of PEO is calculated based on the following equation:

$$X_c(\%) = \frac{\Delta H}{\Delta H^o \times \Phi} \times 100\%$$

where ΔH is the enthalpy of melting of PEO in the LbL film and ΔH° is enthalpy of melting of 100% crystalline PEO (188 J/g).[190] Assuming the weight fraction (Φ) of PEO is 35 wt% within the assembly (according to QCM results shown in Figure 5.7b), the crystallinity of PEO within the assembly ranges between 1 and 2 %, as shown in Figure 5.10. It should be noted that the crystallinity of PEO in PAA/PEO assemblies is smaller than that in PMAA/PEO assemblies (6.2-21.7%).[189] This higher crystallinity may originate from the higher tendency of PMAA to form COOH dimer than PAA, thus leaving more unbonded PEO to crystallize.

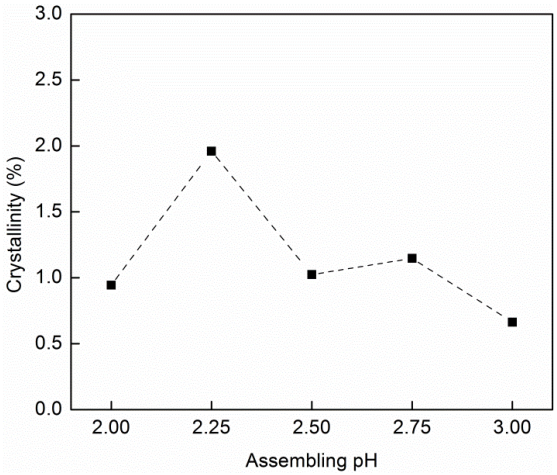

Figure 5.10. Crystallinity of PEO component in 100 BL PAA/PEO free-standing films assembled at varying pH.

5.3.7. Gas Barrier of Hydrogen-Bonded Assemblies

Changes in intermolecular interaction and phase morphology with varying pH have a direct impact on the oxygen permeability of 20 BL PAA/PEO assemblies, as can be seen in Figure 5.11. Film permeability was decoupled from the total permeability using a previously described method.[191] PAA/PEO thin films with the highest oxygen permeability are obtained at pH 2 and 2.25. A slight decrease in permeability can be seen for the film assembled at pH 2.5. The lowest oxygen permeability can be achieved by setting the assembling pH at 2.75, while further increasing the assembling pH to 3 increases permeability. A 50% reduction in oxygen permeability (from 8.1 to 4.1 $x10^{-5}$ $cm^3 \cdot m/(m^2 \cdot day \cdot atm)$) is achieved by changing the assembling pH from 2.25 to 2.75. This lowest permeability value is 5 orders of magnitude better than that of natural rubber (1.32 $cm^3 \cdot m/(m^2 \cdot day \cdot atm)$). A similar trend can be observed in oxygen transmission rate (OTR) of PAA/PEO coated natural rubber films. A natural rubber plaque coated with 20 PAA/PEO bilayers also exhibits the lowest OTR (40.3 $cm^3/(m^2 \cdot day \cdot atm)$), which is 20X smaller than that of the rubber substrate (840.1 $cm^3/(m^2 \cdot day \cdot atm)$).

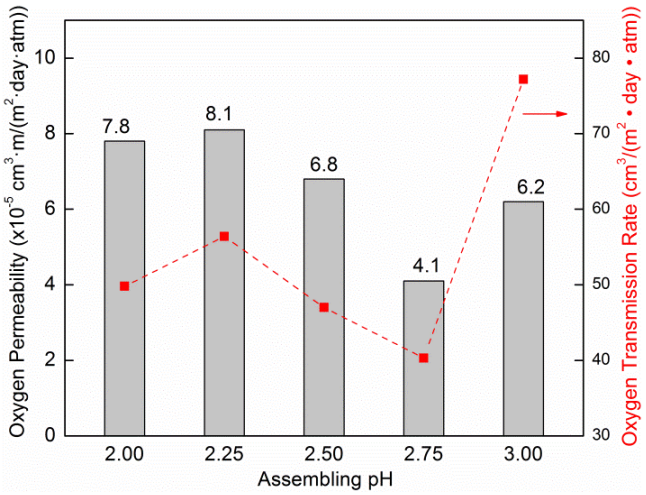

Figure 5.11. Oxygen permeability [bars] and oxygen transmission rate [squares] of 20 bilayer PAA/PEO thin films assembled at varying pH.

5.3.8. PAA/PEO Structure-Property Analysis

Gas barrier of all-polymer LbL assemblies depends on several factors. One of the most important of these factors is crystallinity. Neat PEO is a semicrystalline material whose crystallinity can be as high as 77%.[192] Crystallinity is significantly suppressed in the PAA/PEO assembly, due to interdiffusion of polymer chains.[119] Knowing that PEO makes up only 35 wt% of the assembly, the overall crystallinity of PAA/PEO films is around 0.5%, which is too low to have a noticeable influence on oxygen permeability. Consequently, PAA/PEO thin films are treated as amorphous assemblies to simplify the following discussion.

In amorphous polymeric materials, gas barrier is highly dependent on intermolecular interactions.[37, 193-195] As reflected in the growth of PAA/PEO (Figure 5.6), formation of hydrogen bonds between PAA and PEO is partly suppressed due to partial

ionization of PAA between pH 2.5 and 3.5, leading to thinner multilayer assemblies. As pH decreases within this range, more intermolecular H-bonding is established between these two polymers, which results in lower permeability when the assembling pH decreases from 3 to 2.75.

Besides degree of ionization, the bonding preference of PAA also plays an important role on the intermolecular interactions. Polyacrylic acid can form either intra- or intermolecular hydrogen bonding, but the intramolecular bonds are not very helpful for improving gas barrier. For example, PAA chains can hydrogen-bond with each other in the neat polymer, but even a relatively thick (2.3 μm) PAA film only exhibits marginally improved gas barrier over a polyethylene substrate.[196] On the other hand, bonding between different polymer components within LbL assemblies is known to improve gas barrier of the thin film whether it is ionic or hydrogen bonding.[37, 197] These bonds act as crosslinks within thin films, preventing gas molecule from pushing aside polymer chains to speed diffusion.[198-199] This evidence suggests that intermolecular hydrogen bonding between PAA and PEO is more effective at improving gas barrier of the PAA/PEO multilayer assemblies. As pH increases from 2 to 2.75, more intermolecular hydrogen bonding can be established, as shown in Figure 5.7b, leading to reduced oxygen permeability.

The bonding preference of PAA not only controls oxygen permeability, but also influences the size of dispersed PEO domains. At low pH ($\leq$ 2.5), there are very few intermolecular bonds between PAA and PEO. Consequently, poly(ethylene oxide) chains can exist as larger PEO domains rather than forming a more homogeneous,

interpenetrating complex with PAA. Thicker PEO crystals can be formed within these larger domains, leading to the high-temperature melting peak observed in Figure 5.9. Increasing pH above 2.5 leads to more H-bonding between PAA and PEO, which increases interdiffusion of polymer chains and results in smaller PEO domains. Thinner PEO crystals generated in these small PEO phases corresponds to the low-temperature melting peak in Figure 5.9.

There is an important relationship between the bonding preference of PAA and the size of PEO domains. Smaller PEO domains can be obtained by enhancing the interaction between the dispersed phase (i.e., PEO) and matrix (i.e., PAA or PAA/PEO complex) with more intermolecular hydrogen bonding.[200-202] With the help of smaller PEO domains, it is easier for PAA to form more intermolecular bonds with PEO at the interfaces. If the total volume of PEO is constant as pH increases, smaller PEO domains will produce more specific interfacial area, which can be used to establish more hydrogen bonds. If the total volume of PEO is reduced as pH increases, more PEO becomes part of the matrix, where PAA and PEO are homogeneously mixed through interdiffusion. This leads to even more intermolecular bonds within the PAA/PEO assembly. No matter which case is true, smaller PEO domains always create more intermolecular hydrogen bonds between PAA and PEO within the assembly. When taken together, it can be concluded that both smaller PEO phase and more intermolecular hydrogen bonding leads to better gas barrier.

The influence of pH on phase morphology and bonding is summarized schematically in Figure 5.12. It can be seen that increasing the assembling pH from low

(pH 2) to medium (pH 2.75) leads to more intermolecular hydrogen bonding and smaller PEO domains due to reduced COOH dimer content. Further increasing the assembling pH to 3 results in fewer hydrogen bonds, which is caused by ionization of COOH groups. PAA/PEO multilayer thin films assembled at pH 2.75 feature the most highly H-bond networked structure, because the adverse impacts of both PAA ionization and COOH dimerization are minimized.

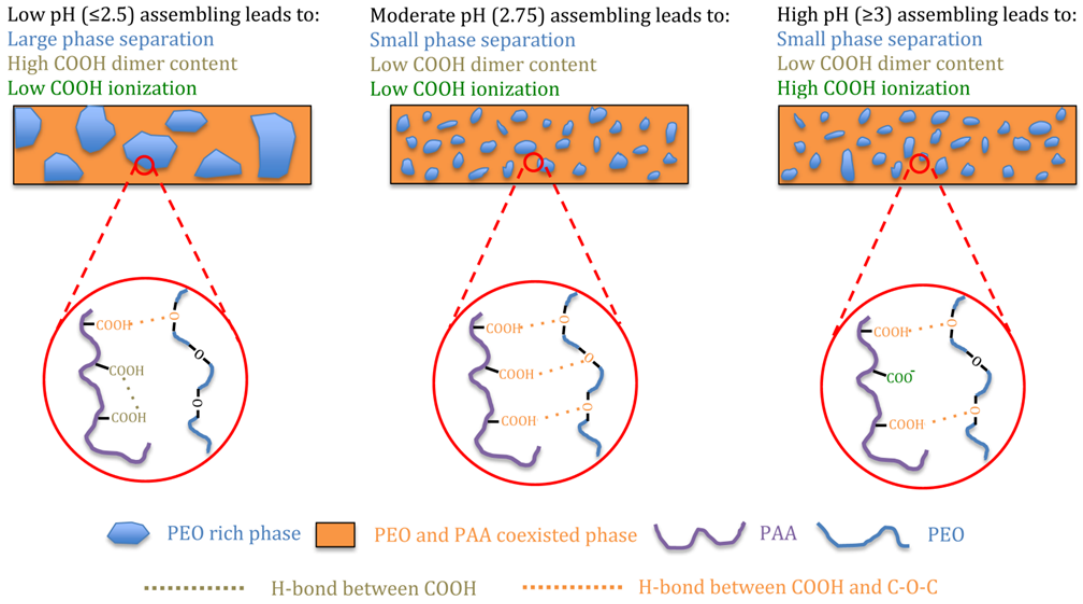

Figure 5.12. Schematic of internal structures and intermolecular interactions of PAA/PEO assemblies in varying pH regimes.

5.4 Conclusions

In conclusion, by assembling hydrogen-bond donating PAA with hydrogen-bond accepting PEO, ductile thin film assemblies can be obtained due to the absence of strong electrostatic bonding. The softest PAA/PEO assembly is obtained at pH 3, and a 367 nm

thick 20 BL PAA3/PEO3 nanocoating reduces the oxygen transmission rate of 1.58 mm thick natural rubber by one order of magnitude when unstretched. Thanks to its excellent ductility, plastic deformation of the PAA3/PEO3 assembly is distributed to multiple locations and kept at a relatively low level to prevent strain-induced cracking. It is for this reason that the negative impact of plastic deformation on gas barrier can be minimized, enabling this thin film to maintain a 5x reduction in rubber OTR even after 100% stretching. It is possible that the gas barrier of PAA3/PEO3 may be reduced after cyclic loading due to accumulated plastic deformation. LbL assembly with larger elastic deformation capability would alleviate this potential problem. Lower Tg assemblies are currently being developed for this purpose.

Moreover, oxygen permeability of PAA/PEO multilayer thin films was studied as a function of assembling pH. A 50% reduction in oxygen permeability was achieved by adjusting solution pH from 2.25 to 2.75. This reduced permeability was found to be a result of optimized intermolecular interactions. Increasing the assembling pH reduces the COOH dimerization and promotes the formation of intermolecular hydrogen bonding between poly(acrylic acid) and poly(ethylene oxide). Further increasing pH beyond 2.75 leads to excessive ionization that disrupts the formation of intermolecular hydrogen bonds. Although the composition of the PAA/PEO assembly remained the same over the entire pH range (from 2 to 3), smaller PEO domains were obtained at pH 2.75 and 3, which formed thinner crystals (as evidenced by a low-temperature melting peak). The size of PEO domains is linked to the extent of intermolecular bonding. Smaller PEO domains and greater intermolecular hydrogen bonding simultaneously contribute to

better gas barrier. Assembling multilayer films at pH 2.75 will minimize the negative impacts of PAA ionization, COOH dimerization, and phase separation, leading to the lowest oxygen permeability. This unique combination of gas barrier, with previously established stretchability,[76, 114] makes these thin films very useful for imparting protection to elastomeric substrates (e.g. tires, bladders, etc.).

CHAPTER VI

CONCLUSIONS AND FUTURE WORK

6.1 Assembly and Property of Multilayer Thin Films

The focus of this dissertation was to optimize the layer-by-layer assembly process and to improve the stretchability of multilayer gas barrier thin films. By varying assembling parameters, such as deposition time and technique, desorption of polyelectrolytes during each assembling step can be significantly suppressed. As a result, thicker multilayer thin films with better gas barrier can be obtained using less time and/or in conjunction with spray coating, improving the outlook for industrial application of LbL technology. In addition to improving the assembling process, stretchy gas barrier assemblies were developed using an all-polymer composition and hydrogen bonding. The H-bonded network imparts reasonable gas barrier to the final assembly, while the lower bond strength and crosslinking density enable the resultant multilayer films to be elastic. This work lays the foundation for the use of layer-by-layer assembled gas barrier thin films in industrial scale manufacturing, as well as on stretchy substrates.

6.1.1 Influence of Deposition Time on Gas Barrier Films

Multilayer thin films with polymer layers sandwiched between clay sheets were produced using different deposition times. By changing the number of PEI/PAA bilayers deposited between clay sheets, the spacing can be precisely controlled. Specifically, polymer/clay assemblies with quadlayer, hexalayer, and octalayer structures were fabricated by depositing 1.5, 2.5, and 3.5 PEI/PAA bilayers between anionic clay layers,

respectively. Despite some difference in film structures, shorter deposition time always leads to larger thickness for the first few layers. Additionally, the polymer/clay assemblies with fewer PEI/PAA bilayers tend to postpone the overtaking in thickness (i.e. shorter dipping time no longer leads to larger thickness) due to suppressed polyelectrolyte interdiffusion imposed by higher clay content. The larger film thickness obtained using shorter dipping time was explained by examining the change of PEI/PAA film thickness and weight during deposition. It was found that when a substrate was immersed in polyelectrolyte solutions, deposition and desorption happened simultaneously. While the deposition process was completed in the first few seconds, desorption of polyelectrolytes increased with dipping time. The best way to retain more previously deposited material is to reduce desorption by shortening the deposition time. It is important to note that thicker films prepared using shorter dip times always lead to better gas barrier regardless of clay type, further proving the universality of the proposed mechanism.

6.1.2 Influence of Deposition Method on Gas Barrier Films

The influence of deposition method on the thickness, roughness, and gas barrier of spray-coated PEI/PAA bilayers was investigated. Spraying parameters were initially optimized using varying spraying pressure, spraying time, and flow rate. Spraying time was found to be the most effective parameter in controlling thickness, roughness, and gas barrier of the final assemblies. A sample prepared using optimized spraying parameters was produced and then compared with another dip-coated sample prepared using the same deposition time (5s). Despite the widely accepted consensus, which

suggests that the dip-coated assemblies will be thicker and more impermeable, the opposite was observed here. Experiments revealed that spray-assisted assembly is more effective at retaining previously deposited materials. Further experiments revealed that rapid draining and accelerated evaporation of excess polymer solutions on a thin film surface leads to reduced polyelectrolyte desorption. The larger thickness and mass gained through spraying deposition helps to offset the negative impact of slightly lower density on gas barrier, enabling spray-coated PEI/PAA bilayers to exhibit better gas barrier than its dip-coated counterpart.

6.1.3 Hydrogen-Bonded Stretchy Gas Barrier Thin Films

The ability of hydrogen bonded PAA/PEO bilayers to act as stretchy gas barrier thin films were systematically analyzed by studying the gas barrier and surface morphology of this elastic coating. The thickness, modulus and glass transition temperature of PAA/PEO were tested as a function of assembling pH. Film thickness was found to decrease with increasing pH due to protonation of H-bond donating PAA. Moreover, film modulus was found to decrease with increasing pH, as a result of reduced glass transition temperature. Despite having a relatively weak hydrogen bonded network, PAA/PEO exhibited reasonable gas barrier. A 20-bilayer PAA/PEO thin film reduced the gas barrier of a 1.58 mm thick natural rubber by one order of magnitude. This improved gas barrier could be largely maintained even after 100% stretching due to excellent elasticity. A careful examination of SEM images revealed that crack formation was prevented through evenly distributed plastic deformation. Additionally, the possibility of improving gas barrier of these assemblies using varying pH was also

examined. Films assembled at lower pH ($\leqslant$2.5) feature more intramoleculear H-bonds between PAA, leading to larger PEO domains, less intermolecular H-bonds, and lower gas barrier. Multilayers created at higher pH ($\geqslant$3) are significantly affected by ionization of PAA, which results in a thinner film and less intermolecular H-bonds. The optimal assembling pH for a PAA/PEO gas barrier assembly is near 2.75.

6.2 Future Research Directions

Recent improvements in the preparation and dispersion of water-dispersible nanoplatelets provide new opportunities for creating new functional multilayer assemblies. For example, the incorporation of graphene could impart excellent electrical conductivity, mechanical strength, and gas barrier to multilayer assemblies, allowing them to be used in multiple applications (e.g., electrochromic devices, conductive touchscreens, and fuel cell electrodes). As mentioned in Chapter V, a small yet noticeable reduction in gas barrier can be observed for strained PAA/PEO due to plastic deformation. In order to expand the application of this stretchy gas barrier to cyclic loading, where accumulation of plastic deformation may lead to catastrophic failure, a completely elastic H-bonded assembly is needed. This could be accomplished by eliminating the intramolecular hydrogen bonding network, which is typically found between PAA chains. Additionally, the possibility of using stretchy multilayer thin films as polymer electrolyte is also discussed in the following sections.

6.2.1 Multilayer Thin Films with Pure Graphene

Graphene oxide (GO) is anionic in water due to oxidized surface defects, such as -COOH and -OH. These negatively charged two-dimensional particles are widely used in LbL assembly through alternate deposition with another positively-charged component.[116] It is important to note that despite creating a useful negative surface charge, these oxidation defects also lead to stress concentration, reduced electrical conduction, and enhanced gas diffusion, which undermine the mechanical, electrical, and gas barrier properties of the resulting polymer/GO composites. In order to fully realize the benefit of graphene, it should be used in its non-oxidized form, which has proven to be extremely difficult. Traditional mechanical mixing leads to aggregation and random alignment of nanoplatelets due to low affinity between components and Brownian motion of filler within molten polymer matrix, respectively. Layer-by-layer assembly is a great way to create thin films with controlled multilayer structure, but, very few polymers (if any) will pair with graphene, which is insoluble in water and chemically inert. Fortunately, the insolubility and chemical inactivity can be circumvented by dispersing graphene using a polymeric surfactant, such as polyvinylpyrrolidone (PVP).[81] PVP is known to be able to bond tightly on the graphene surface,[24] imparting water solubility to the PVP-graphene (PVP-G) complex. Additionally, the PVP located on graphene's surface can act as H-bond acceptor, which is able to bond with an H-bond donor, such as PAA. The detailed assembling mechanism is shown in Figure 6.1, and PAA/PVP-G thin films are shown in Figure 6.2. The controlled assembly of graphene shown here is unprecedented. The parallel stacking of

graphene is expected to impart excellent gas barrier to the final assembly. The introduction of carbon nanotubes (stabilized in PAA solution) may help to create a conducting network within this structure, making it an ideal candidate for touchscreens.

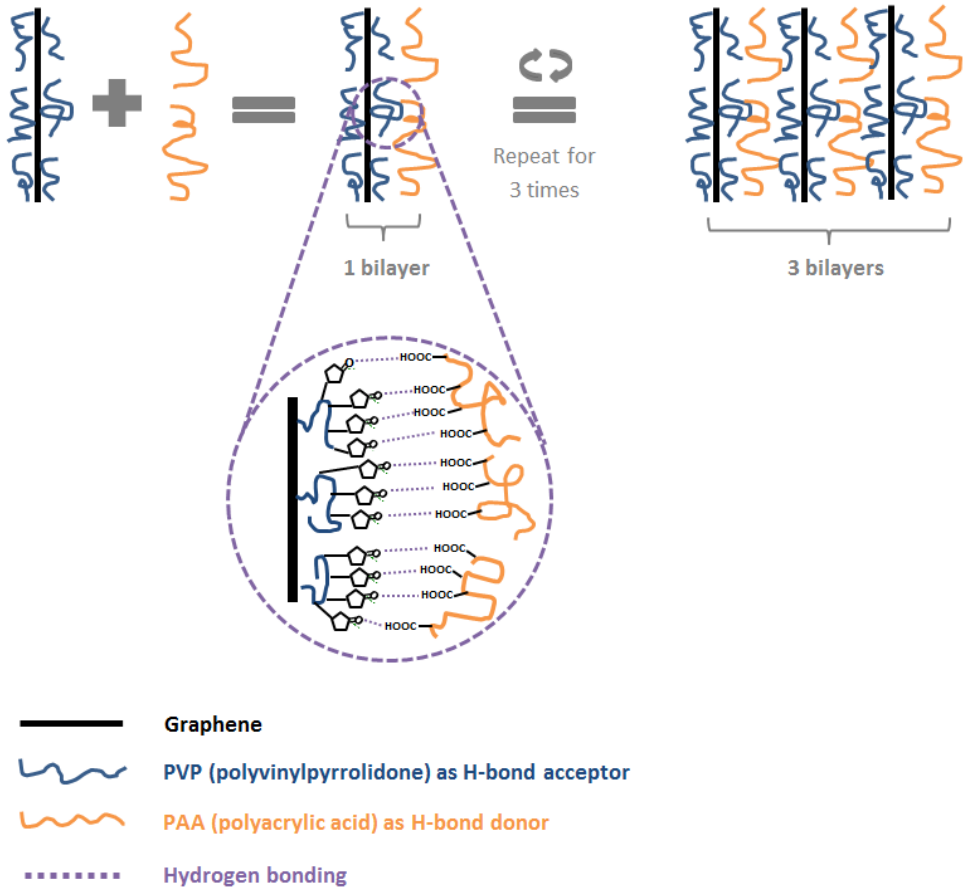

Figure 6.1. Schematic of hydrogen bonding mechanism of PAA/PVP-G assembly.

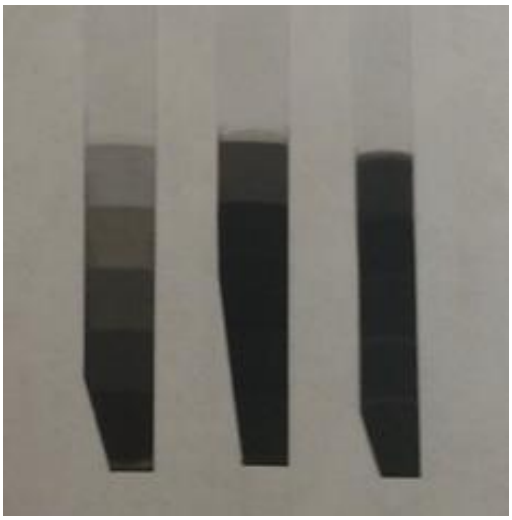

Figure 6.2. LbL graphene assemblies on PET. From left to right: (PAA_3/PVP-G_3), ($PAA_{2.5}$/PVP-$G_{2.5}$), and (PAA_2/PVP-G_2). The subscript of each polymer represents the solution pH used for deposition from water.

6.2.2 Fully Elastomeric LbL Assembly

As mentioned earlier, the plasticity of the PAA/PEO assembly originates from the presence of PAA, which has a very high glass transition temperature (99 ^{o}C) and a strong tendency to bond with itself. The self-bonding of PAA is realized through the intramolecular H-bond generated by COOH dimerization (red circle in Figure 6.3). Since a large portion of this assembly (~65 wt%) consists of PAA, it can be conceived that numerous intramolecular H-bonds can be formed, establishing a relative rigid H-bond network throughout the assembly. This network is believed to be responsible for the plastic deformation that occurs during stretching of PAA/PEO bilayers (Fig. 5.4), which needs to be eliminated to prevent accumulation of plastic deformation during cyclic loadings. It is for this reason that a replacement for PAA is needed to impart full elasticity to the final assembly.

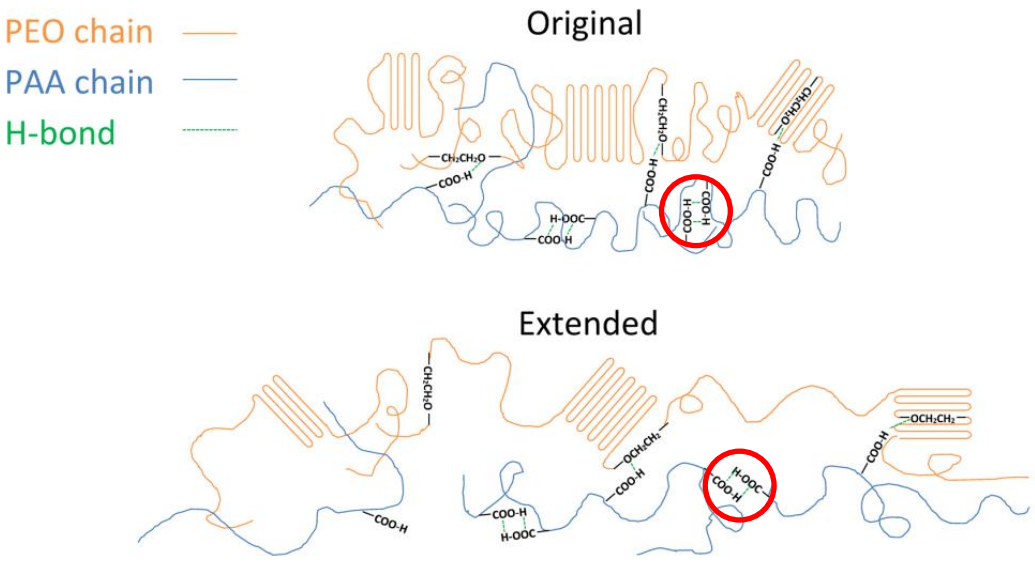

Figure 6.3. Deformation of the H-bonding network within PAA/PEO multilayers before and during stretching.

The use of tannic acid (TA), a macromolecular replacement for PAA that has no glass transition temperature, can successfully prevent the formation of a H-bond network within the final assembly. The elimination of a rigid H-bonded network results in a purely elastic assembly that consists of H-bonding only between TA and PEO. The gas barrier of this assembly can be completely preserved up to 100% strain, as shown in Figure 6.4. The ability of this assembly to prevent crack initiation and plastic deformation is also confirmed by SEM images, as shown in Figure 6.5.

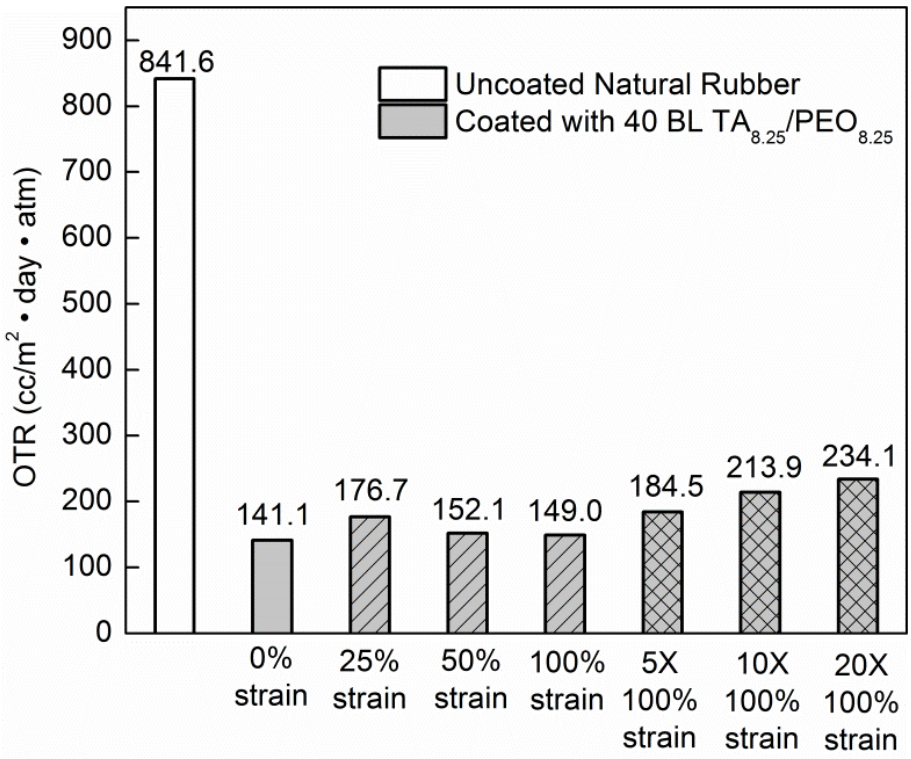

Figure 6.4. OTR of 40 BL $TA_{8.25}/PEO_{8.25}$ coated natural rubber before and after strain.

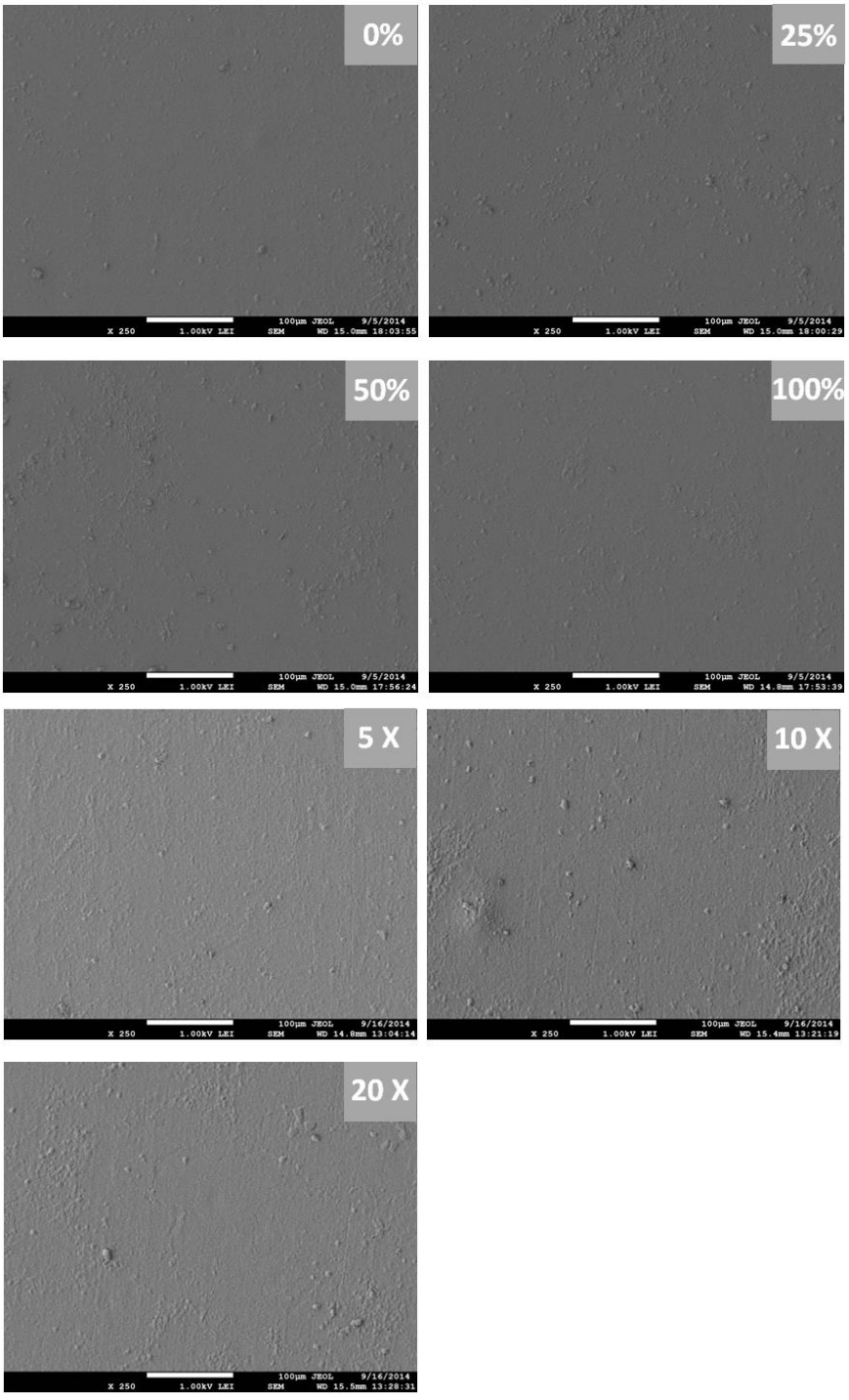

Figure 6.5. FESEM surface images of 40 BL $TA_{8.25}/PEO_{8.25}$ coated rubber after 0, 25, 50, and 100% strain. The lower three images show this film 5× strained to 100%, 10× strained to 100%, and 20× strained to 100%.

6.2.3 Stretchy Ionic Assembly for Polymer Electrolyte

Polymer electrolytes, composed of a salt dispersed in a neutral polymer matrix, are indispensable in all electrochemical devices.[156] There are four major types of polymer electrolytes: solid polymer, polymer gel, polyelectrolyte, and composite polymer. Solid polymer electrolyte is the first and by far the most explored type due to chemical and electrochemical stability, flexibility, and processability. Most solid polymer electrolytes are produced using a solvent evaporation coating technique, which mixes lithium salt with appropriate polymer host such as PEO, poly(vinyl fluoride) (PVDF), polydimethylsiloxane (PDMS), etc. Despite the aforementioned advantages, the application of solid polymer electrolytes is impeded by two major drawbacks: low ionic conductivity (10^{-6}-10^{-8} S/cm) at room temperature and low ion transport number. The low ionic conductivity originates from absence of solvent in the solid polymer matrix. Without the help of solvent, ion transport is solely based on the creation of free volume, which is generated by local segmental motions of polymer chains in the amorphous phase. The low ion transport number originates from the mobility of both anions and cations.

These drawbacks of solid electrolytes can be overcome with the use of polyelectrolytes. Polyelectrolyte assemblies have much higher ion conductivity (as high as 2.12×10^{-3} S/cm)[203] in the presence atmospheric water. Additionally, polyelectrolytes are single ion conductors and their cation transference number is close to 1.0, which is one of the most important requirements for electrochemical applications.[156] Despite being advantageus over common solid polymer electrolytes, the application of

polyelectrolytes is still limited by the low ionic conductivity under dry conditions and the inflexibility of polyelectrolyte chains. Based on the above discussion, it can be surmised that higher ionic conductivity could be achieved by enhancing flexibility of polymer chains. A stretchy Q-plus/PAA bilayer fabricated using electrostatic bonding can be created for this purpose. Q-plus is a quaternized polydimethylsiloxane, which features a super flexible PDMS backbone, with a quaternized alkyamido dimethylamine functional group, as shown in Figure 6.6.

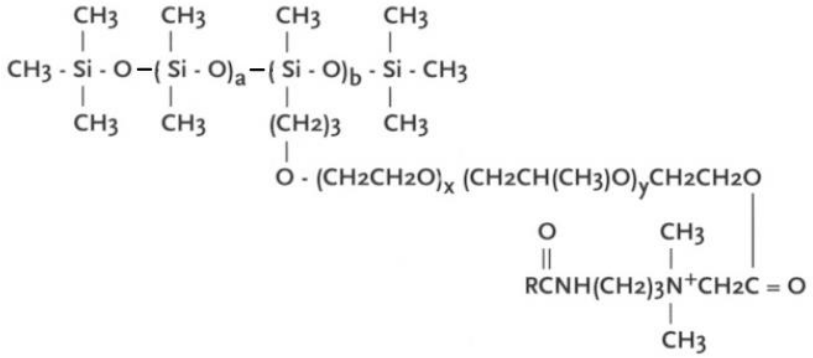

Figure 6.6. Chemical structure of Q-plus.[204]

The use of Q-plus brings several benefits. First, Q-plus chains are highly flexible, which contributes to the flexibility of the whole assembly. Secondly, there is only one functional group per Q-plus chain. This leads to low crosslinking density within the film, which further facilitates the movement of chain segments and the transport of ions. Finally, when paired with PAA using layer-by-layer assembly, the intramolecular bonding within PAA can be suppressed with the help of polymer interdiffusion, which

offset the negative impact of COOH dimerization on PAA chain flexibility. The low glass transition temperature of PDMS helps the resulting PAA/Q-plus free-standing film exhibit extremely low glass transition temperature (-24.8 ^{o}C), as can be seen in Figure 6.7a. The FTIR spectrum of this assembly shows a COO^- peak at 1551 (Fig. 6.7b), confirming the electrostatic nature of this assembly. It should be noted that PAA/PEO hydrogen bonded assembly does not have a peak around 1550, even if it is assembled at pH ≥ 3. This Q-plus/PAA bilayer assembly is the first stretchy thin film that are made using electrostatic bonding.

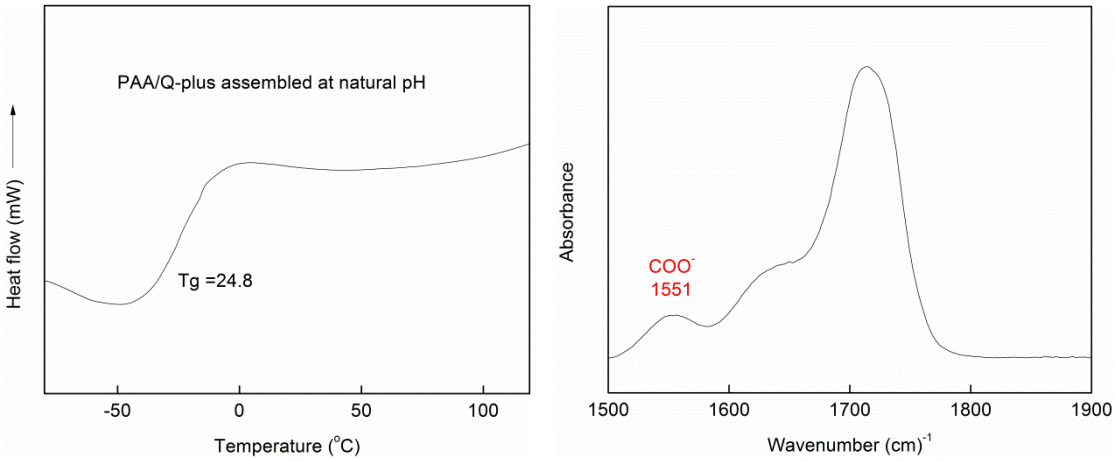

Figure 6.7. DSC and FTIR of a Q-plus/PAA film assembled at unaltered pH.

REFERENCES

1. Duncan, T. V. Applications of nanotechnology in food packaging and food safety: Barrier materials, antimicrobials and sensors. *J. Colloid Interface Sci.* **2011,** *363*, 1-24.

2. Lange, J.; Wyser, Y. Recent innovations in barrier technologies for plastic packaging—a review. *Packaging Technology and Science* **2003,** *16*, 149-158.

3. Jin-Seong, P.; Heeyeop, C.; Ho Kyoon, C.; Sang In, L. Thin film encapsulation for flexible AM-OLED: a review. *Semicond. Sci. Technol.* **2011,** *26*, 034001.

4. Mittal, V. Polymer Layered Silicate Nanocomposites: A Review. *Materials* **2009,** *2*, 992-1057.

5. Zeng, K.; Bai, Y. Improve the gas barrier property of PET film with montmorillonite by in situ interlayer polymerization. *Mater. Lett.* **2005,** *59*, 3348-3351.

6. Hu, Y.; Prattipati, V.; Mehta, S.; Schiraldi, D.; Hiltner, A.; Baer, E. Improving gas barrier of PET by blending with aromatic polyamides. *Polymer* **2005,** *46*, 2685-2698.

7. MacDonald, W. A. Engineered films for display technologies. *J. Mater. Chem.* **2004,** *14*, 4-10.

8. Jacquelot, E.; Espuche, E.; Gerard, J. F.; Duchet, J.; Mazabraud, P. Morphology and gas barrier properties of polyethylene-based nanocomposites. *J. Polym. Sci., Part B: Polym. Phys.* **2006,** *44*, 431-440.

9. Möller, M. W.; Lunkenbein, T.; Kalo, H.; Schieder, M.; Kunz, D. A.; Breu, J. Barrier Properties of Synthetic Clay with a Kilo-Aspect Ratio. *Adv. Mater.* **2010,** *22*, 5245-5249.

10. Cussler, E. L.; Hughes, S. E.; Ward, W. J.; Aris, R. Barrier Membranes. *J. Membr. Sci.* **1988,** *38*, 161-174.

11. Herrera-Alonso, J. M.; Sedlakova, Z.; Marand, E. Gas barrier properties of nanocomposites based on in situ polymerized poly(n-butyl methacrylate) in the presence of surface modified montmorillonite. *J. Membr. Sci.* **2010,** *349*, 251-257.

12. Picard, E.; Gauthier, H.; Gerard, J. F.; Espuche, E. Influence of the intercalated cations on the surface energy of montmorillonites: Consequences for the morphology

and gas barrier properties of polyethylene/montmorillonites nanocomposites. *J. Colloid Interface Sci.* **2007,** *307*, 364-376.

13. Fornes, T. D.; Yoon, P. J.; Keskkula, H.; Paul, D. R. Nylon 6 nanocomposites: the effect of matrix molecular weight. *Polymer* **2001,** *42*, 09929-09940.

14. Müller, G.; Baudrand, D. W.; Jarrett, G.; Draper, C. R. *Plating on plastics: a practical handbook*; Robert Draper1971.

15. Tjong, S. Structural and mechanical properties of polymer nanocomposites. *Materials Science and Engineering: R: Reports* **2006,** *53*, 73-197.

16. Priolo, M. A.; Gamboa, D.; Holder, K. M.; Grunlan, J. C. Super Gas Barrier of Transparent Polymer−Clay Multilayer Ultrathin Films. *Nano Lett.* **2010,** *10*, 4970-4974.

17. Decher, G.; Hong, J.-D. Buildup of ultrathin multilayer films by a self-assembly process, 1 consecutive adsorption of anionic and cationic bipolar amphiphiles on charged surfaces. *Makromol. Chem. Macromol. Symp.* **1991,** *46*, 321-327.

18. Decher, G. Fuzzy nanoassemblies: Toward layered polymeric multicomposites. *Science* **1997,** *277*, 1232-1237.

19. Lösche, M.; Schmitt, J.; Decher, G.; Bouwman, W. G.; Kjaer, K. Detailed structure of molecularly thin polyelectrolyte multilayer films on solid substrates as revealed by neutron reflectometry. *Macromolecules* **1998,** *31*, 8893-8906.

20. Schaaf, P.; Voegel, J. C.; Jierry, L.; Boulmedais, F. Spray ‐ Assisted Polyelectrolyte Multilayer Buildup: from Step ‐ by ‐ Step to Single ‐ Step Polyelectrolyte Film Constructions. *Adv. Mater.* **2012,** *24*, 1001-1016.

21. Crouzier, T.; Picart, C. Ion Pairing and Hydration in Polyelectrolyte Multilayer Films Containing Polysaccharides. *Biomacromolecules* **2009,** *10*, 433-442.

22. Stockton, W. B.; Rubner, M. F. Molecular-Level Processing of Conjugated Polymers. 4. Layer-by-Layer Manipulation of Polyaniline via Hydrogen-Bonding Interactions. *Macromolecules* **1997,** *30*, 2717-2725.

23. Erel-Unal, I.; Sukhishvili, S. A. Hydrogen-bonded multilayers of a neutral polymer and a polyphenol. *Macromolecules* **2008,** *41*, 3962-3970.

24. Wajid, A. S.; Das, S.; Irin, F.; Ahmed, H.; Shelburne, J. L.; Parviz, D.; Fullerton, R. J.; Jankowski, A. F.; Hedden, R. C.; Green, M. J. Polymer-stabilized graphene dispersions at high concentrations in organic solvents for composite production. *Carbon* **2012,** *50*, 526-534.

25. Zhang, Y.; Sunarso, J.; Liu, S.; Wang, R. Current status and development of membranes for CO< sub> 2</sub>/CH< sub> 4</sub> separation: A review. *International Journal of Greenhouse Gas Control* **2013,** *12*, 84-107.

26. Liebig, J. Ueber Versilberung und Vergoldung von Glas. *Justus Liebigs Ann. Chem.* **1856,** *98*, 132-139.

27. Laufer, G.; Priolo, M. A.; Kirkland, C.; Grunlan, J. C. High oxygen barrier, clay and chitosan-based multilayer thin films: an environmentally friendly foil replacement. *Green Mater.* **2013,** *1*, 4-10.

28. Sukhishvili, S. A.; Granick, S. Layered, erasable polymer multilayers formed by hydrogen-bonded sequential self-assembly. *Macromolecules* **2002,** *35*, 301-310.

29. Sheng, K.; Bai, H.; Sun, Y.; Li, C.; Shi, G. Layer-by-layer assembly of graphene/polyaniline multilayer films and their application for electrochromic devices. *Polymer* **2011,** *52*, 5567-5572.

30. Yang, Y. H.; Malek, F. A.; Grunlan, J. C. Influence of Deposition Time on Layer-by-Layer Growth of Clay-Based Thin Films. *Ind. Eng. Chem. Res.* **2010,** *49*, 8501-8509.

31. Lavalle, P.; Vivet, V.; Jessel, N.; Decher, G.; Voegel, J. C.; Mesini, P. J.; Schaaf, P. Direct evidence for vertical diffusion and exchange processes of polyanions and polycations in polyelectrolyte multilayer films. *Macromolecules* **2004,** *37*, 1159-1162.

32. Ladam, G.; Schaad, P.; Voegel, J. C.; Schaaf, P.; Decher, G.; Cuisinier, F. In situ determination of the structural properties of initially deposited polyelectrolyte multilayers. *Langmuir* **2000,** *16*, 1249-1255.

33. Decher, G.; Schmitt, J. Fine-tuning of the film thickness of ultrathin multilayer films composed of consecutively alternating layers of anionic and cationic polyelectrolytes. In *Trends in Colloid and Interface Science VI*; Springer, 1992, pp 160-164.

34. Ariga, K.; Hill, J. P.; Ji, Q. M. Layer-by-layer assembly as a versatile bottom-up nanofabrication technique for exploratory research and realistic application. *Phys. Chem. Chem. Phys.* **2007,** *9*, 2319-2340.

35. Affinito, J. D.; Gross, M. E.; Coronado, C. A.; Graff, G. L.; Greenwell, I. N.; Martin, P. M. A new method for fabricating transparent barrier layers. *Thin Solid Films* **1996,** *290–291*, 63-67.

36. Priolo, M. A.; Holder, K. M.; Greenlee, S. M.; Stevens, B. E.; Grunlan, J. C. Precisely Tuning the Clay Spacing in Nanobrick Wall Gas Barrier Thin Films. *Chem. Mater.* **2013,** *25*, 1649-1655.

37. Yang, Y. H.; Haile, M.; Park, Y. T.; Malek, F. A.; Grunlan, J. C. Super Gas Barrier of All-Polymer Multilayer Thin Films. *Macromolecules* **2011,** *44*, 1450-1459.

38. Gunders, D. Wasted: How America is losing up to 40 percent of its food from farm to fork to landfill. *Natural Resources Defense Council Issue Paper. August. This report was made possible through the generous support of The California Endowment* **2012**.

39. Faisant, J.; Ait-Kadi, A.; Bousmina, M.; Deschenes, L. Morphology, thermomechanical and barrier properties of polypropylene-ethylene vinyl alcohol blends. *Polymer* **1998,** *39*, 533-545.

40. Czeremuszkin, G.; Latreche, M.; Wertheimer, M.; da Silva Sobrinho, A. Ultrathin silicon-compound barrier coatings for polymeric packaging materials: an industrial perspective. *Plasmas Polym.* **2001,** *6*, 107-120.

41. Fierro, J. L. G. *Metal oxides : chemistry and applications*; Taylor & Francis: Boca Raton, FL, 2006. p xxi, 783 p.

42. Graff, G. L.; Burrows, P. E.; Williford, R. E.; Praino, R. F. Barrier layer technology for flexible displays. *Flexible Flat Panel Displays* **2005**, 57-77.

43. Yoo, B. M.; Shin, H. J.; Yoon, H. W.; Park, H. B. Graphene and graphene oxide and their uses in barrier polymers. *J. Appl. Polym. Sci.* **2014,** *131*.

44. Zeman, S.; Kubík, L. Permeability of polymeric packaging materials. *Technical Sciences/University of Warmia and Mazury in Olsztyn* **2007**, 26-34.

45. Xiang, F.; Shi, Y.; Li, X.; Huang, T.; Chen, C.; Peng, Y.; Wang, Y. Cocontinuous morphology of immiscible high density polyethylene/polyamide 6 blend induced by multiwalled carbon nanotubes network. *Eur. Polym. J.* **2012,** *48*, 350-361.

46. Ray, S. S.; Okamoto, M. Polymer/layered silicate nanocomposites: a review from preparation to processing. *Prog. Polym. Sci.* **2003,** *28*, 1539-1641.

47. Yeo, J. H.; Lee, C. H.; Park, C. S.; Lee, K. J.; Nam, J. D.; Kim, S. W. Rheological, morphological, mechanical, and barrier properties of PP/EVOH blends. *Adv. Polym. Tech.* **2001,** *20*, 191-201.

48. Wang, H.; Keum, J. K.; Hiltner, A.; Baer, E.; Freeman, B.; Rozanski, A.; Galeski, A. Confined Crystallization of Polyethylene Oxide in Nanolayer Assemblies. *Science* **2009,** *323*, 757-760.

49. Lavalle, P.; Picart, C.; Mutterer, J.; Gergely, C.; Reiss, H.; Voegel, J.-C.; Senger, B.; Schaaf, P. Modeling the Buildup of Polyelectrolyte Multilayer Films Having Exponential Growth ✗ . *The Journal of Physical Chemistry B* **2003,** *108*, 635-648.

50. Gao, F. Clay/polymer composites: the story. *Mater. Today* **2004,** *7*, 50-55.

51. Kim, H.; Miura, Y.; Macosko, C. W. Graphene/Polyurethane Nanocomposites for Improved Gas Barrier and Electrical Conductivity. *Chem. Mater.* **2010,** *22*, 3441-3450.

52. Cho, J.; Paul, D. Nylon 6 nanocomposites by melt compounding. *Polymer* **2001,** *42*, 1083-1094.

53. Fornes, T.; Paul, D. Modeling properties of nylon 6/clay nanocomposites using composite theories. *Polymer* **2003,** *44*, 4993-5013.

54. Fornes, T.; Yoon, P.; Hunter, D.; Keskkula, H.; Paul, D. Effect of organoclay structure on nylon 6 nanocomposite morphology and properties. *Polymer* **2002,** *43*, 5915-5933.

55. Yariv, S.; Cross, H. *Organo-clay complexes and interactions*; CRC Press2001.

56. Li, P.; White, K. L.; Lin, C.-H.; Kim, D.; Muliana, A.; Krishnamoorti, R.; Nishimura, R.; Sue, H.-J. Mechanical Reinforcement of Epoxy with Self-Assembled Synthetic Clay in Smectic Order. *ACS Appl. Mater. Interfaces* **2014,** *6*, 10188-10195.

57. Lansbury, R. C. Method of vacuum metallizing thermoplastic polymeric film and resulting product. Google Patents, 1973.

58. Bishop, C. *Roll-to-roll vacuum deposition of barrier coatings*; John Wiley & Sons2010; Vol. 46.

59. Ing, S.; Davern, W. Glow discharge formation of silicon oxide and the deposition of silicon oxide thin film capacitors by glow discharge techniques. *J. Electrochem. Soc.* **1965,** *112*, 284-288.

60. Erlat, A.; Spontak, R.; Clarke, R.; Robinson, T.; Haaland, P.; Tropsha, Y.; Harvey, N.; Vogler, E. SiOx gas barrier coatings on polymer substrates: morphology and gas transport considerations. *The Journal of Physical Chemistry B* **1999,** *103*, 6047-6055.

61. Inagaki, N.; Tasaka, S.; Nakajima, T. Preparation of oxygen gas barrier polypropylene films by deposition of SiOx films plasma‐polymerized from mixture of tetramethoxysilane and oxygen. *J. Appl. Polym. Sci.* **2000,** *78*, 2389-2397.

62. Inagaki, N.; Tasaka, S.; Hiramatsu, H. Preparation of oxygen gas barrier poly (ethylene terephthalate) films by deposition of silicon oxide films plasma‐polymerized from a mixture of tetramethoxysilane and oxygen. *J. Appl. Polym. Sci.* **1999,** *71*, 2091-2100.

63. da Silva Sobrinho, A. S.; Czeremuszkin, G.; Latreche, M.; Wertheimer, M. R. Defect-permeation correlation for ultrathin transparent barrier coatings on polymers. *Journal of Vacuum Science & Technology A: Vacuum, Surfaces, and Films* **2000,** *18*, 149-157.

64. Chwang, A. B.; Rothman, M. A.; Mao, S. Y.; Hewitt, R. H.; Weaver, M. S.; Silvernail, J. A.; Rajan, K.; Hack, M.; Brown, J. J.; Chu, X. Thin film encapsulated flexible organic electroluminescent displays. *Appl. Phys. Lett.* **2003,** *83*, 413-415.

65. Iler, R. Multilayers of colloidal particles. *J. Colloid Interface Sci.* **1966,** *21*, 569-594.

66. Schmitt, J.; Gruenewald, T.; Decher, G.; Pershan, P. S.; Kjaer, K.; Loesche, M. Internal structure of layer-by-layer adsorbed polyelectrolyte films: a neutron and x-ray reflectivity study. *Macromolecules* **1993,** *26*, 7058-7063.

67. Zacharia, N. S.; Modestino, M.; Hammond, P. T. Factors influencing the interdiffusion of weak polycations in multilayers. *Macromolecules* **2007,** *40*, 9523-9528.

68. Ariga, K.; Ji, Q. M.; Hill, J. P.; Bando, Y.; Aono, M. Forming nanomaterials as layered functional structures toward materials nanoarchitectonics. *Npg Asia Mater.* **2012,** *4*.

69. Dvoracek, C. M.; Sukhonosova, G.; Benedik, M. J.; Grunlan, J. C. Antimicrobial Behavior of Polyelectrolyte− Surfactant Thin Film Assemblies. *Langmuir* **2009,** *25*, 10322-10328.

70. Grunlan, J. C.; Choi, J. K.; Lin, A. Antimicrobial behavior of polyelectrolyte multilayer films containing cetrimide and silver. *Biomacromolecules* **2005,** *6*, 1149-1153.

71. Hammond, P. T. Building biomedical materials layer-by-layer. *Mater. Today* **2012,** *15*, 196-206.

72. Morton, S. W.; Poon, Z.; Hammond, P. T. The architecture and biological performance of drug-loaded LbL nanoparticles. *Biomaterials* **2013,** *34*, 5328-5335.

73. De Cock, L. J.; De Koker, S.; De Geest, B. G.; Grooten, J.; Vervaet, C.; Remon, J. P.; Sukhorukov, G. B.; Antipina, M. N. Polymeric Multilayer Capsules in Drug Delivery. *Angew. Chem. Int. Ed.* **2010,** *49*, 6954-6973.

74. Hagen, D. A.; Foster, B.; Stevens, B.; Grunlan, J. C. Shift-Time Polyelectrolyte Multilayer Assembly: Fast Film Growth and High Gas Barrier with Fewer Layers by Adjusting Deposition Time. *ACS Macro Lett.* **2014,** *3*, 663-666.

75. Stevens, B.; Dessiatova, E.; Hagen, D. A.; Todd, A. D.; Bielawski, C. W.; Grunlan, J. C. Low-Temperature Thermal Reduction of Graphene Oxide Nanobrick Walls: Unique Combination of High Gas Barrier and Low Resistivity in Fully Organic Polyelectrolyte Multilayer Thin Films. *ACS Appl. Mater. Interfaces* **2014,** *6*, 9942-9945.

76. Xiang, F.; Ward, S. M.; Givens, T. M.; Grunlan, J. C. Super Stretchy Polymer Multilayer Thin Film with High Gas Barrier. *ACS Macro Lett.* **2014,** *3*, 1055-1058.

77. Laufer, G.; Kirkland, C.; Morgan, A. B.; Grunlan, J. C. Intumescent Multilayer Nanocoating, Made with Renewable Polyelectrolytes, for Flame-Retardant Cotton. *Biomacromolecules* **2012,** *13*, 2843-2848.

78. Li, Y.-C.; Mannen, S.; Morgan, A. B.; Chang, S.; Yang, Y.-H.; Condon, B.; Grunlan, J. C. Intumescent All-Polymer Multilayer Nanocoating Capable of Extinguishing Flame on Fabric. *Adv. Mater.* **2011,** *23*, 3926-3931.

79. Laufer, G.; Kirkland, C.; Morgan, A. B.; Grunlan, J. C. Exceptionally Flame Retardant Sulfur-Based Multilayer Nanocoating for Polyurethane Prepared from Aqueous Polyelectrolyte Solutions. *ACS Macro Lett.* **2013,** *2*, 361-365.

80. Mendelsohn, J.; Barrett, C. J.; Chan, V.; Pal, A.; Mayes, A.; Rubner, M. Fabrication of microporous thin films from polyelectrolyte multilayers. *Langmuir* **2000,** *16*, 5017-5023.

81. Parviz, D.; Das, S.; Ahmed, H. T.; Irin, F.; Bhattacharia, S.; Green, M. J. Dispersions of non-covalently functionalized graphene with minimal stabilizer. *ACS Nano* **2012,** *6*, 8857-8867.

82. Suzuki, I.; Egawa, Y.; Mizukawa, Y.; Hoshi, T.; Anzai, J.-i. Construction of positively-charged layered assemblies assisted by cyclodextrin complexation. *Chem. Commun.* **2002**, 164-165.

83. Ejima, H.; Richardson, J. J.; Liang, K.; Best, J. P.; van Koeverden, M. P.; Such, G. K.; Cui, J.; Caruso, F. One-step assembly of coordination complexes for versatile film and particle engineering. *Science* **2013,** *341*, 154-157.

84. Broderick, A. H.; Manna, U.; Lynn, D. M. Covalent Layer-by-Layer Assembly of Water-Permeable and Water-Impermeable Polymer Multilayers on Highly Water-Soluble and Water-Sensitive Substrates. *Chem. Mater.* **2012,** *24*, 1786-1795.

85. Borges, J. o.; Mano, J. o. F. Molecular interactions driving the layer-by-layer assembly of multilayers. *Chem. Rev.* **2014,** *114*, 8883-8942.

86. Kim, D.; Tzeng, P.; Barnett, K. J.; Yang, Y.-H.; Wilhite, B. A.; Grunlan, J. C. Highly Size-Selective Ionically Crosslinked Multilayer Polymer Films for Light Gas Separation. *Adv. Mater.* **2014,** *26*, 746-751.

87. Celia, E.; Darmanin, T.; Taffin de Givenchy, E.; Amigoni, S.; Guittard, F. Recent advances in designing superhydrophobic surfaces. *J. Colloid Interface Sci.* **2013,** *402*, 1-18.

88. Caruso, F.; Caruso, R. A.; Möhwald, H. Nanoengineering of Inorganic and Hybrid Hollow Spheres by Colloidal Templating. *Science* **1998,** *282*, 1111-1114.

89. Zhang, L.; Li, Y.; Sun, J.; Shen, J. Mechanically Stable Antireflection and Antifogging Coatings Fabricated by the Layer-by-Layer Deposition Process and Postcalcination. *Langmuir* **2008,** *24*, 10851-10857.

90. Priolo, M. A.; Gamboa, D.; Grunlan, J. C. Transparent Clay-Polymer Nano Brick Wall Assemblies with Tailorable Oxygen Barrier. *ACS Appl. Mater. Interfaces* **2010,** *2*, 312-320.

91. Picart, C.; Lavalle, P.; Hubert, P.; Cuisinier, F. J. G.; Decher, G.; Schaaf, P.; Voegel, J. C. Buildup mechanism for poly(L-lysine)/hyaluronic acid films onto a solid surface. *Langmuir* **2001,** *17*, 7414-7424.

92. Croll, T. I.; O'Connor, A. J.; Stevens, G. W.; Cooper-White, J. J. A blank slate? Layer-by-layer deposition of hyaluronic acid and chitosan onto various surfaces. *Biomacromolecules* **2006,** *7*, 1610-1622.

93. Hoogeveen, N. G.; Stuart, M. A. C.; Fleer, G. J.; Bohmer, M. R. Formation and stability of multilayers of polyelectrolytes. *Langmuir* **1996,** *12*, 3675-3681.

94. Izumrudov, V.; Kharlampieva, E.; Sukhishvili, S. A. Salt-induced multilayer growth: Correlation with phase separation in solution. *Macromolecules* **2004,** *37*, 8400-8406.

95. Sui, Z. J.; Salloum, D.; Schlenoff, J. B. Effect of molecular weight on the construction of polyelectrolyte multilayers: Stripping versus sticking. *Langmuir* **2003,** *19*, 2491-2495.

96. Xiang, F.; Tzeng, P.; Sawyer, J. S.; Regev, O.; Grunlan, J. C. Improving the Gas Barrier Property of Clay–Polymer Multilayer Thin Films Using Shorter Deposition Times. *ACS Appl. Mater. Interfaces* **2014,** *6*, 6040-6048.

97. Podsiadlo, P.; Michel, M.; Lee, J.; Verploegen, E.; Kam, N. W. S.; Ball, V.; Lee, J.; Qi, Y.; Hart, A. J.; Hammond, P. T.; Kotov, N. A. Exponential growth of LBL films with incorporated inorganic sheets. *Nano Lett.* **2008,** *8*, 1762-1770.

98. Izquierdo, A.; Ono, S.; Voegel, J.-C.; Schaaf, P.; Decher, G. Dipping versus spraying: exploring the deposition conditions for speeding up layer-by-layer assembly. *Langmuir* **2005,** *21*, 7558-7567.

99. Cho, J.; Char, K.; Hong, J. D.; Lee, K. B. Fabrication of Highly Ordered Multilayer Films Using a Spin Self-Assembly Method. *Adv. Mater.* **2001,** *13*, 1076-1078.

100. Salomäki, M.; Peltonen, T.; Kankare, J. Multilayer films by spraying on spinning surface — Best of both worlds. *Thin Solid Films* **2012,** *520*, 5550-5556.

101. Winterton, L. C.; Vogt, J.; Lally, J. M.; Stockinger, F. Methods of modifying surface characteristics. Google Patents, 2002.

102. Porcel, C.; Izquierdo, A.; Ball, V.; Decher, G.; Voegel, J.-C.; Schaaf, P. Ultrathin coatings and (poly (glutamic acid)/polyallylamine) films deposited by continuous and simultaneous spraying. *Langmuir* **2005,** *21*, 800-802.

103. Popa, G.; Boulmedais, F.; Zhao, P.; Hemmerlé, J.; Vidal, L.; Mathieu, E.; Félix, O.; Schaaf, P.; Decher, G.; Voegel, J.-C. Nanoscale Precipitation Coating: The Deposition of Inorganic Films through Step-by-Step Spray-Assembly. *ACS Nano* **2010,** *4*, 4792-4798.

104. Bertrand, P.; Jonas, A.; Laschewsky, A.; Legras, R. Ultrathin polymer coatings by complexation of polyelectrolytes at interfaces: suitable materials, structure and properties. *Macromol. Rapid Commun.* **2000,** *21*, 319-348.

105. Schlenoff, J. B.; Dubas, S. T.; Farhat, T. Sprayed polyelectrolyte multilayers. *Langmuir* **2000,** *16*, 9968-9969.

106. Stewart-Clark, S.; Lvov, Y.; Mills, D. Ultrasonic nebulization-assisted layer-by-layer assembly for spray coating of multilayered, multicomponent, bioactive nanostructures. *J. Coat. Technol. Res.* **2011,** *8*, 275-281.

107. Kolasinska, M.; Krastev, R.; Gutberlet, T.; Warszynski, P. Layer-by-Layer Deposition of Polyelectrolytes. Dipping versus Spraying. *Langmuir* **2008,** *25*, 1224-1232.

108. Mateos, A. J.; Cain, A. A.; Grunlan, J. C. Large-Scale Continuous Immersion System for Layer-by-Layer Deposition of Flame Retardant and Conductive Nanocoatings on Fabric. *Ind. Eng. Chem. Res.* **2014,** *53*, 6409-6416.

109. Krogman, K. C.; Lowery, J. L.; Zacharia, N. S.; Rutledge, G. C.; Hammond, P. T. Spraying asymmetry into functional membranes layer-by-layer. *Nat. Mater.* **2009,** *8*, 512-518.

110. Holder, K. M.; Spears, B. R.; Huff, M. E.; Priolo, M. A.; Harth, E.; Grunlan, J. C. Stretchable Gas Barrier Achieved with Partially Hydrogen-Bonded Multilayer Nanocoating. *Macromol. Rapid Commun.* **2014,** *35*, 960-964.

111. Kharlampieva, E.; Kozlovskaya, V.; Sukhishvili, S. A. Layer-by-Layer Hydrogen-Bonded Polymer Films: From Fundamentals to Applications. *Adv. Mater.* **2009,** *21*, 3053-3065.

112. DeLongchamp, D. M.; Hammond, P. T. Highly ion conductive poly (ethylene oxide)-based solid polymer electrolytes from hydrogen bonding layer-by-layer assembly. *Langmuir* **2004,** *20*, 5403-5411.

113. Elsner, N.; Kozlovskaya, V.; Sukhishvili, S. A.; Fery, A. pH-Triggered softening of crosslinked hydrogen-bonded capsules. *Soft Matter* **2006,** *2*, 966-972.

114. Lutkenhaus, J. L.; Hrabak, K. D.; McEnnis, K.; Hammond, P. T. Elastomeric flexible free-standing hydrogen-bonded nanoscale assemblies. *J. Am. Chem. Soc.* **2005,** *127*, 17228-17234.

115. Kharlampieva, E.; Sukhishvili, S. A. Hydrogen‐bonded layer‐by‐layer polymer films. *J. Macromol. Sci. Polymer. Rev.* **2006,** *46*, 377-395.

116. Potts, J. R.; Dreyer, D. R.; Bielawski, C. W.; Ruoff, R. S. Graphene-based polymer nanocomposites. *Polymer* **2011,** *52*, 5-25.

117. DeLongchamp, D. M.; Hammond, P. T. Fast ion conduction in layer-by-layer polymer films. *Chem. Mater.* **2003,** *15*, 1165-1173.

118. Jeffrey, G. A. *An introduction to hydrogen bonding*; Oxford university press New York1997; Vol. 12.

119. Kharlampieva, E.; Kozlovskaya, V.; Ankner, J. F.; Sukhishvili, S. A. Hydrogen-Bonded Polymer Multilayers Probed by Neutron Reflectivity. *Langmuir* **2008,** *24*, 11346-11349.

120. Zeng, G.; Gao, J.; Chen, S.; Chen, H.; Wang, Z.; Zhang, X. Combining hydrogen-bonding complexation in solution and hydrogen-bonding-directed layer-by-

layer assembly for the controlled loading of a small organic molecule into multilayer films. *Langmuir* **2007,** *23*, 11631-11636.

121. Pavlidou, S.; Papaspyrides, C. D. A review on polymer–layered silicate nanocomposites. *Prog. Polym. Sci.* **2008,** *33*, 1119-1198.

122. Ojijo, V.; Sinha Ray, S.; Sadiku, R. Effect of Nanoclay Loading on the Thermal and Mechanical Properties of Biodegradable Polylactide/Poly[(butylene succinate)-co-adipate] Blend Composites. *ACS Appl. Mater. Interfaces* **2012,** *4*, 2395-2405.

123. Phua, S. L.; Yang, L.; Toh, C. L.; Huang, S.; Tsakadze, Z.; Lau, S. K.; Mai, Y.-W.; Lu, X. Reinforcement of Polyether Polyurethane with Dopamine-Modified Clay: The Role of Interfacial Hydrogen Bonding. *ACS Appl. Mater. Interfaces* **2012,** *4*, 4571-4578.

124. Choudalakis, G.; Gotsis, A. D. Permeability of polymer/clay nanocomposites: A review. *Eur. Polym. J.* **2009,** *45*, 967-984.

125. Priolo, M. A.; Holder, K. M.; Greenlee, S. M.; Grunlan, J. C. Transparency, Gas Barrier, and Moisture Resistance of Large-Aspect-Ratio Vermiculite Nanobrick Wall Thin Films. *ACS Appl. Mater. Interfaces* **2012,** *4*, 5529-5533.

126. Najafi, N.; Heuzey, M. C.; Carreau, P. J. Polylactide (PLA)-clay nanocomposites prepared by melt compounding in the presence of a chain extender. *Compos. Sci. Technol.* **2012,** *72*, 608-615.

127. Laufer, G.; Kirkland, C.; Cain, A. A.; Grunlan, J. C. Clay–Chitosan Nanobrick Walls: Completely Renewable Gas Barrier and Flame-Retardant Nanocoatings. *ACS Appl. Mater. Interfaces* **2012,** *4*, 1643-1649.

128. Kiliaris, P.; Papaspyrides, C. D. Polymer/layered silicate (clay) nanocomposites: An overview of flame retardancy. *Prog. Polym. Sci.* **2010,** *35*, 902-958.

129. Zanetti, M.; Kashiwagi, T.; Falqui, L.; Camino, G. Cone Calorimeter Combustion and Gasification Studies of Polymer Layered Silicate Nanocomposites. *Chem. Mater.* **2002,** *14*, 881-887.

130. Gilman, J. W.; Harris, R. H.; Shields, J. R.; Kashiwagi, T.; Morgan, A. B. A study of the flammability reduction mechanism of polystyrene-layered silicate nanocomposite: layered silicate reinforced carbonaceous char. *Polym. Adv. Technol.* **2006,** *17*, 263-271.

131. Yeh, J. M.; Huang, H. Y.; Chen, C. L.; Su, W. F.; Yu, Y. H. Siloxane-modified epoxy resin-clay nanocomposite coatings with advanced anticorrosive properties prepared by a solution dispersion approach. *Surf. Coat. Technol.* **2006,** *200*, 2753-2763.

132. Yasmin, A.; Abot, J. L.; Daniel, I. M. Processing of clay/epoxy nanocomposites by shear mixing. *Scr. Mater.* **2003,** *49*, 81-86.

133. Arroyo, M.; López-Manchado, M. A.; Herrero, B. Organo-montmorillonite as substitute of carbon black in natural rubber compounds. *Polymer* **2003,** *44*, 2447-2453.

134. Zeng, C.; Lee, L. J. Poly(methyl methacrylate) and Polystyrene/Clay Nanocomposites Prepared by in-Situ Polymerization. *Macromolecules* **2001,** *34*, 4098-4103.

135. Ren, C.; Du, X.; Ma, L.; Wang, Y.; Zheng, J.; Tang, T. Preparation of multifunctional supported metallocene catalyst using organic multifunctional modifier for synthesizing polyethylene/clay nanocomposites via in situ intercalative polymerization. *Polymer* **2010,** *51*, 3416-3424.

136. Dennis, H. R.; Hunter, D. L.; Chang, D.; Kim, S.; White, J. L.; Cho, J. W.; Paul, D. R. Effect of melt processing conditions on the extent of exfoliation in organoclay-based nanocomposites. *Polymer* **2001,** *42*, 9513-9522.

137. Medellin-Rodriguez, F. J.; Burger, C.; Hsiao, B. S.; Chu, B.; Vaia, R.; Phillips, S. Time-resolved shear behavior of end-tethered Nylon 6–clay nanocomposites followed by non-isothermal crystallization. *Polymer* **2001,** *42*, 9015-9023.

138. Wang, K.; Liang, S.; Du, R.; Zhang, Q.; Fu, Q. The interplay of thermodynamics and shear on the dispersion of polymer nanocomposite. *Polymer* **2004,** *45*, 7953-7960.

139. Leterrier, Y. Durability of nanosized oxygen-barrier coatings on polymers. *Prog. Mater Sci.* **2003,** *48*, 1-55.

140. Yang, Y.-H.; Bolling, L.; Priolo, M. A.; Grunlan, J. C. Super Gas Barrier and Selectivity of Graphene Oxide-Polymer Multilayer Thin Films. *Adv. Mater.* **2013,** *25*, 503-508.

141. Priolo, M. A.; Holder, K. M.; Gamboa, D.; Grunlan, J. C. Influence of Clay Concentration on the Gas Barrier of Clay–Polymer Nanobrick Wall Thin Film Assemblies. *Langmuir* **2011,** *27*, 12106-12114.

142. Dubas, S. T.; Schlenoff, J. B. Factors controlling the growth of polyelectrolyte multilayers. *Macromolecules* **1999,** *32*, 8153-8160.

143. Advincula, R.; Aust, E.; Meyer, W.; Knoll, W. In situ investigations of polymer self-assembly solution adsorption by surface plasmon spectroscopy. *Langmuir* **1996,** *12*, 3536-3540.

144. Lvov, Y.; Ariga, K.; Onda, M.; Ichinose, I.; Kunitake, T. A careful examination of the adsorption step in the alternate layer-by-layer assembly of linear polyanion and polycation. *Colloids Surf. A* **1999,** *146*, 337-346.

145. Sukhorukov, G. B.; Schmitt, J.; Decher, G. Reversible swelling of polyanion/polycation multilayer films in solutions of different ionic strength. *Ber. Bunsenges. Phys. Chem.* **1996,** *100*, 948-953.

146. von Klitzing, R. Internal structure of polyelectrolyte multilayer assemblies. *Phys. Chem. Chem. Phys.* **2006,** *8*, 5012-5033.

147. Kurth, D. G.; Osterhout, R. In situ analysis of metallosupramolecular coordination polyelectrolyte films by surface plasmon resonance spectroscopy. *Langmuir* **1999,** *15*, 4842-4846.

148. Ariga, K.; Lvov, Y.; Kunitake, T. Assembling alternate dye-polyion molecular films by electrostatic layer-by-layer adsorption. *J. Am. Chem. Soc.* **1997,** *119*, 2224-2231.

149. Schlenoff, J. B.; Dubas, S. T. Mechanism of Polyelectrolyte Multilayer Growth: Charge Overcompensation and Distribution. *Macromolecules* **2001,** *34*, 592-598.

150. Cho, C.; Valverde, L.; Ozin, G. A.; Zacharia, N. S. Reactive Wet Stamping for Patterning of Polyelectrolyte Multilayers. *Langmuir* **2010,** *26*, 13637-13643.

151. Almodovar, J.; Place, L. W.; Gogolski, J.; Erickson, K.; Kipper, M. J. Layer-by-Layer Assembly of Polysaccharide-Based Polyelectrolyte Multilayers: A Spectroscopic Study of Hydrophilicity, Composition, and Ion Pairing. *Biomacromolecules* **2011,** *12*, 2755-2765.

152. Kunz, D. A.; Schmid, J.; Feicht, P.; Erath, J.; Fery, A.; Breu, J. Clay-Based Nanocomposite Coating for Flexible Optoelectronics Applying Commercial Polymers. *ACS Nano* **2013,** *7*, 4275-4280.

153. Gamboa, D.; Priolo, M. A.; Ham, A.; Grunlan, J. C. Note: Influence of rinsing and drying routines on growth of multilayer thin films using automated deposition system. *Rev. Sci. Instrum.* **2010,** *81*, 036103-036103-3.

154. Jang, W. S.; Grunlan, J. C. Robotic dipping system for layer-by-layer assembly of multifunctional thin films. *Rev. Sci. Instrum.* **2005,** *76*, 103904.

155. Motschmann, H.; Stamm, M.; Toprakcioglu, C. Adsorption-Kinetics of Block Copolymers from a Good Solvent - a 2-Stage Process. *Macromolecules* **1991,** *24*, 3681-3688.

156. Nguyen, C. A.; Argun, A. A.; Hammond, P. T.; Lu, X.; Lee, P. S. Layer-by-Layer Assembled Solid Polymer Electrolyte for Electrochromic Devices. *Chem. Mater.* **2011,** *23*, 2142-2149.

157. Peng, C.; Thio, Y. S.; Gerhardt, R. A. Effect of Precursor-Layer Surface Charge on the Layer-by-Layer Assembly of Polyelectrolyte/Nanoparticle Multilayers. *Langmuir* **2011,** *28*, 84-91.

158. Lee, S.-W.; Lee, D. Integrated Study of Water Sorption/Desorption Behavior of Weak Polyelectrolyte Layer-by-Layer Films. *Macromolecules* **2013**.

159. Vidyasagar, A.; Sung, C.; Losensky, K.; Lutkenhaus, J. L. pH-Dependent Thermal Transitions in Hydrated Layer-by-Layer Assemblies Containing Weak Polyelectrolytes. *Macromolecules* **2012,** *45*, 9169-9176.

160. Jomaa, H. W.; Schlenoff, J. B. Accelerated Exchange in Polyelectrolyte Multilayers by "Catalytic" Polyvalent Ion Pairing. *Langmuir* **2005,** *21*, 8081-8084.

161. McAloney, R. A.; Goh, M. C. In situ investigations of polyelectrolyte film formation by second harmonic generation. *J. Phys. Chem. B* **1999,** *103*, 10729-10732.

162. Schoeler, B.; Kumaraswamy, G.; Caruso, F. Investigation of the influence of polyelectrolyte charge density on the growth of multilayer thin films prepared by the layer-by-layer technique. *Macromolecules* **2002,** *35*, 889-897.

163. Dubas, S. T.; Schlenoff, J. B. Polyelectrolyte multilayers containing a weak polyacid: Construction and deconstruction. *Macromolecules* **2001,** *34*, 3736-3740.

164. Jiang, C.; Markutsya, S.; Tsukruk, V. V. Compliant, Robust, and Truly Nanoscale Free-Standing Multilayer Films Fabricated Using Spin-Assisted Layer-by-Layer Assembly. *Adv. Mater.* **2004,** *16*, 157-161.

165. Cranston, E. D.; Gray, D. G. Birefringence in spin-coated films containing cellulose nanocrystals. *Colloids Surf. A* **2008,** *325*, 44-51.

166. Tang, Q.; Tang, Z.; Wu, J.; Lin, J.; Oh, I. Highly conducting multilayer films from graphene nanosheets by a spin self-assembly method. *J. Mater. Chem.* **2011,** *21*, 5378-5385.

167. Krogman, K.; Zacharia, N.; Schroeder, S.; Hammond, P. Automated process for improved uniformity and versatility of layer-by-layer deposition. *Langmuir* **2007,** *23*, 3137-3141.

168. Dierendonck, M.; De Koker, S.; De Rycke, R.; De Geest, B. G. Just spray it - LbL assembly enters a new age. *Soft Matter* **2014,** *10*, 804-807.

169. Shukla, A.; Avadhany, S. N.; Fang, J. C.; Hammond, P. T. Tunable Vancomycin Releasing Surfaces for Biomedical Applications. *Small* **2010,** *6*, 2392-2404.

170. Nogueira, G. M.; Banerjee, D.; Cohen, R. E.; Rubner, M. F. Spray-Layer-by-Layer Assembly Can More Rapidly Produce Optical-Quality Multistack Heterostructures. *Langmuir* **2011,** *27*, 7860-7867.

171. Lutkenhaus, J. L.; McEnnis, K.; Hammond, P. T. Tuning the Glass Transition of and Ion Transport within Hydrogen-Bonded Layer-by-Layer Assemblies. *Macromolecules* **2007,** *40*, 8367-8373.

172. Jomaa, H. W.; Schlenoff, J. B. Salt-Induced Polyelectrolyte Interdiffusion in Multilayered Films: A Neutron Reflectivity Study. *Macromolecules* **2005,** *38*, 8473-8480.

173. Liu, A.; Walther, A.; Ikkala, O.; Belova, L.; Berglund, L. A. Clay Nanopaper with Tough Cellulose Nanofiber Matrix for Fire Retardancy and Gas Barrier Functions. *Biomacromolecules* **2011,** *12*, 633-641.

174. Laachachi, A.; Ball, V.; Apaydin, K.; Toniazzo, V.; Ruch, D. Diffusion of Polyphosphates into (Poly(allylamine)-montmorillonite) Multilayer Films: Flame Retardant-Intumescent Films with Improved Oxygen Barrier. *Langmuir* **2011,** *27*, 13879-13887.

175. Merrill, M. H.; Sun, C. T. Fast, simple and efficient assembly of nanolayered materials and devices. *Nanotechnology* **2009,** *20*, 075606.

176. Svagan, A. J.; Åkesson, A.; Cárdenas, M.; Bulut, S.; Knudsen, J. C.; Risbo, J.; Plackett, D. Transparent Films Based on PLA and Montmorillonite with Tunable Oxygen Barrier Properties. *Biomacromolecules* **2012,** *13*, 397-405.

177. Chen, J.-T.; Fu, Y.-J.; An, Q.-F.; Lo, S.-C.; Huang, S.-H.; Hung, W.-S.; Hu, C.-C.; Lee, K.-R.; Lai, J.-Y. Tuning nanostructure of graphene oxide/polyelectrolyte LbL assemblies by controlling pH of GO suspension to fabricate transparent and super gas barrier films. *Nanoscale* **2013,** *5*, 9081-9088.

178. Aulin, C.; Karabulut, E.; Tran, A.; Wågberg, L.; Lindström, T. Transparent Nanocellulosic Multilayer Thin Films on Polylactic Acid with Tunable Gas Barrier Properties. *ACS Appl. Mater. Interfaces* **2013,** *5*, 7352-7359.

179. Podsiadlo, P.; Kaushik, A. K.; Arruda, E. M.; Waas, A. M.; Shim, B. S.; Xu, J.; Nandivada, H.; Pumplin, B. G.; Lahann, J.; Ramamoorthy, A.; Kotov, N. A. Ultrastrong and Stiff Layered Polymer Nanocomposites. *Science* **2007,** *318*, 80-83.

180. Chen, B.; Evans, J. R. Elastic moduli of clay platelets. *Scr. Mater.* **2006,** *54*, 1581-1585.

181. Adamcik, J.; Lara, C.; Usov, I.; Jeong, J. S.; Ruggeri, F. S.; Dietler, G.; Lashuel, H. A.; Hamley, I. W.; Mezzenga, R. Measurement of intrinsic properties of amyloid fibrils by the peak force QNM method. *Nanoscale* **2012,** *4*, 4426-4429.

182. Pittenger, B.; Erina, N.; Su, C. Quantitative mechanical property mapping at the nanoscale with PeakForce QNM. *Application Note Veeco Instruments Inc* **2010**.

183. Matsuzaki, R.; Keating, T.; Todoroki, A.; Hiraoka, N. Rubber-based strain sensor fabricated using photolithography for intelligent tires. *Sensors and Actuators A: Physical* **2008,** *148*, 1-9.

184. Matsuzaki, R.; Todoroki, A. Wireless strain monitoring of tires using electrical capacitance changes with an oscillating circuit. *Sensors and Actuators A: Physical* **2005,** *119*, 323-331.

185. Smith, K. L.; Winslow, A. E.; Petersen, D. E. Association Reactions for Poly(alkylene Oxides) and Polymeric Poly(carboxylic Acids). *Ind. Eng. Chem.* **1959,** *51*, 1361-1364.

186. Coleman, M. M.; Lee, J. Y.; Serman, C. J.; Wang, Z.; Painter, P. C. Poly(ethylene-co-methacrylic acid)-polyether blends. *Polymer* **1989,** *30*, 1298-1307.

187. Lee, J. Y.; Painter, P. C.; Coleman, M. M. Hydrogen bonding in polymer blends. 3. Blends involving polymers containing methacrylic acid and ether groups. *Macromolecules* **1988,** *21*, 346-354.

188. Coleman, M. M.; Painter, P. C. Hydrogen bonded polymer blends. *Prog. Polym. Sci.* **1995,** *20*, 1-59.

189. Sung, C.; Vidyasagar, A.; Hearn, K.; Lutkenhaus, J. L. Effect of Thickness on the Thermal Properties of Hydrogen-Bonded LbL Assemblies. *Langmuir* **2012,** *28*, 8100-8109.

190. Cimmino, S.; Di Pace, E.; Martuscelli, E.; Silvestre, C. Evaluation of the equilibrium melting temperature and structure analysis of poly(ethylene oxide)/poly(methyl methacrylate) blends. *Macromol. Chem. Phys.* **1990,** *191*, 2447-2454.

191. Jang, W. S.; Rawson, I.; Grunlan, J. C. Layer-by-layer assembly of thin film oxygen barrier. *Thin Solid Films* **2008,** *516*, 4819-4825.

192. Maurya, K. K.; Srivastava, N.; Hashmi, S. A.; Chandra, S. Proton conducting polymer electrolyte: II poly ethylene oxide + NH4l system. *J. Mater. Sci.* **1992,** *27*, 6357-6364.

193. Zhang, Z.; Britt, I. J.; Tung, M. A. Permeation of oxygen and water vapor through EVOH films as influenced by relative humidity. *J. Appl. Polym. Sci.* **2001,** *82*, 1866-1872.

194. McHugh, T. H.; Krochta, J. M. Sorbitol- vs Glycerol-Plasticized Whey Protein Edible Films: Integrated Oxygen Permeability and Tensile Property Evaluation. *J. Agric. Food. Chem.* **1994,** *42*, 841-845.

195. Gontard, N.; Thibault, R.; Cuq, B.; Guilbert, S. Influence of Relative Humidity and Film Composition on Oxygen and Carbon Dioxide Permeabilities of Edible Films. *J. Agric. Food. Chem.* **1996,** *44*, 1064-1069.

196. Ward, L. J.; Schofield, W. C. E.; Badyal, J. P. S.; Goodwin, A. J.; Merlin, P. J. Atmospheric Pressure Plasma Deposition of Structurally Well-Defined Polyacrylic Acid Films. *Chem. Mater.* **2003,** *15*, 1466-1469.

197. Xiang, F.; Ward, S. M.; Givens, T. M.; Grunlan, J. C. Super Stretchy Polymer Multilayer Thin Film with High Gas Barrier. *ACS Macro Lett.* **2014**, 1055-1058.

198. Lagaron, J. M.; Catalá, R.; Gavara, R. Structural characteristics defining high barrier properties in polymeric materials. *Mater. Sci. Technol.* **2004,** *20*, 1-7.

199. Kochumalayil, J. J.; Berglund, L. A. Water-soluble hemicelluloses for high humidity applications - enzymatic modification of xyloglucan for mechanical and oxygen barrier properties. *Green Chemistry* **2014,** *16*, 1904-1910.

200. Zhang, X.; Takegoshi, K.; Hikichi, K. Composition dependence of the miscibility and phase structure of amorphous/crystalline polymer blends as studied by high-resolution solid-state carbon-13 NMR spectroscopy. *Macromolecules* **1992,** *25*, 2336-2340.

201. Avella, M.; Martuscelli, E. Poly-d-(−)(3-hydroxybutyrate)/poly(ethylene oxide) blends: phase diagram, thermal and crystallization behaviour. *Polymer* **1988,** *29*, 1731-1737.

202. Moskala, E. J.; Howe, S. E.; Painter, P. C.; Coleman, M. M. On the role of intermolecular hydrogen bonding in miscible polymer blends. *Macromolecules* **1984,** *17*, 1671-1678.

203. Argun, A. A.; Ashcraft, J. N.; Hammond, P. T. Highly conductive, methanol resistant polyelectrolyte multilayers. *Adv. Mater.* **2008,** *20*, 1539-1543.

204. SilSense® Silicones High Performance Cationics for Versatile, Effective Hair Conditioning. https://www.lubrizol.com/Personal-Care/Documents/Technical-Data-Sheets/TDS-316-SilSense%C2%AE-Silicones.pdf.